Hydroconversion of Furan Derivatives over Bifunctional Metal-Acid Catalysts in the Gas Phase

Hanan Abdulaziz I Althikrallah

Thesis submitted in accordance with the requirements of the University of Liverpool for the degree of Doctor of Philosophy

May 2022

Abstract

Hydroconversion of Furan Derivatives over Bifunctional Metal-Acid Catalysts in the Gas Phase

The conversion of biomass to chemicals and fuels has attracted much academic and industrial interest. Such interest has increased due to the decline of fossil fuel reserves affecting the energy supply. Biomass-derived furanic compounds are a low-cost renewable feedstock that could be applied to produce value-added chemicals, which can boost the supply of green energy. 2,5-Dimethylfuran (DMF) and 2,5-dimethyltetrahydrofuran (DMTHF) are recognised as important intermediates within bio-oil upgrading transformation. However, furanic compounds have a high content of oxygen, which influences their acidity, homogeneity, polarity and heating value. Bifunctional metal-acid catalysts could promote furan ring-opening and oxygen removal in the hydrodeoxygenation (HDO) upgrading process. Nevertheless, the kinetics and mechanism of HDO of furanic compounds, particularly at the gas-solid interface, have not been studied in detail yet. Moreover, to the best of our knowledge, no research has been done on the use of heteropoly acids (HPAs) as catalysts in these reactions so far.

The main purpose of this thesis is to investigate the conversion of DMF and DMTHF as model furanic compounds to produce value-added products at the gas-solid interface under mild conditions via catalytic hydrogenation, hydrogenolysis and hydrodeoxygenation reactions in the presence of bifunctional metal-acid catalysts comprising Pt and cesium salt of Keggin-type tungstophosphoric heteropoly acid $Cs_{2.5}H_{0.5}PW_{12}O_{40}$, hereinafter referred to as CsPW. This cesium salt has a large surface area, high thermal stability (~500 °C decomposition temperature) and high tolerance to water, with proton sites almost as strong

as those in the parent heteropoly acid $H_3PW_{12}O_{40}$. The mechanism and kinetics of these reactions on the catalyst surface were also investigated. All reactions were carried out in a fixed-bed continuous flow reactor using H_2 as a carrier gas at ambient pressure (1 bar) in the temperature range 70–100 °C. Our results demonstrate the high efficiency of bifunctional metal-acid catalysis for the hydroconversion of furanic compounds to alkanes that can be used as fuel components.

Firstly, the hydrogenation and hydrogenolysis reactions of DMF over commercial carbon-supported Pt, Pd, Rh and Ru catalysts were investigated. The efficiency of these reactions in the gas phase (fixed-bed flow reactor) was compared with that in the liquid phase (batch reactor). It was found that the total turnover frequency (TOF) values for all these metals in the gas phase DMF hydroconversion is one order of magnitude greater than those for the liquid phase reaction. This indicates that the gas phase process is more efficient as well as more selective towards furan ring-opening compared to the liquid phase process. Generally, all these catalysts exhibited very high activity, giving >99% DMF conversion at ambient pressure and low temperatures (70–100 °C). Platinum has a greater reaction selectivity for the C−O hydrogenolysis of DMF yielding 2-hexanone, 2-hexanol and hexane in parallel with ring-saturation yielding DMTHF. In contracts, Pd, Rh and Ru catalysts are only active for ring-saturation yielding DMTHF. Furthermore, our results show that the rate constant of furan ring opening is nine times greater than that of furan ring saturation on Pt sites. Kinetic results are consistent with a Langmuir-Hinshelwood type reaction mechanism involving adsorption of DMF and H_2 on Pt sites followed by DMF ring hydrogenation and hydrogenolysis in parallel pathways.

Secondly, the HDO of DMF was studied at the gas-solid interface in the presence of bifunctional metal-acid catalysts comprising Ru, Rh, Pt and Pd metals and the strong Brønsted acid CsPW. Among these catalysts, only Pt was found to be active in the opening

of the furan ring. The bifunctional Pt-CsPW catalyst containing 1% Pt per total catalyst weight, deoxygenated DMF to n-hexane with 100% yield at 90 °C and 1 bar H_2 pressure in a one-step gas phase process. The Pt-CsPW catalyst was much more efficient than the monofunctional Pt catalyst. The HDO of DMF proceeds through a sequence of hydrogenolysis, hydrogenation and dehydration steps catalysed by Pt and proton sites of the bifunctional catalyst. The presence of both Pt and proton sites is essential to efficient HDO reaction. The liquid phase HDO of DMF over Pt-CsPW catalyst in a batch reactor (autoclave) was found to be much less efficient than the gas phase process in the flow reactor.

Thirdly, an insight into the reaction mechanism was gained from investigating the HDO of reaction intermediates, in particular DMTHF, in the presence of bifunctional metal-acid catalyst Pt-CsPW. This catalyst has high deoxygenation activity giving >99% n-hexane selectivity at 71% DMTHF conversion at 100 °C. A reaction network for DMTHF hydrodeoxygenation was proposed based on kinetic studies. The reaction had an activation energy of 78.5 kJ mol^{-1}, zero order in DMTHF and a negative order in the partial pressure of H_2 suggesting competitive adsorption of DMTHF and H_2 on the Pt sites. These results agree with a Langmuir-Hinshelwood mechanism. The TOF values were found to increase two orders of magnitude with increasing Pt particle size in the series of supports: γ-Al_2O_3 < SiO_2 < C. This suggests that the hydrogenolysis of C–O bond in furanic compounds on supported Pt catalysts is a structure-sensitive reaction occurring on ensembles of Pt atoms.

Finally, the effect of Au additives on the performance of Pt-CsPW catalyst was studied. Addition of gold to the Pt-CsPW catalyst increases the turnover rate at Pt sites more than twofold, whereas the Au alone without Pt is not active. The enhancement of catalyst activity is attributed to PtAu alloying, which is supported by STEM-EDX and XRD analysis.

Acknowledgements

I arrived in Liverpool, England in 2016 with a determination to become the best I could be in my chosen field. Many people have helped and guided me during the years of my study.

I would like to express my sincere appreciation to my supervisor, Prof. Ivan V. Kozhevnikov, for his guidance and support during my PhD study. Due to his advice and experience, this work has been completed and I have learned many skills.

Many thanks should be given to Dr. Elena F. Kozhevnikova for her kind assistance in solving multiple technical issues in our group as well as conducting experiments.

PhD projects would be exceptionally hard to complete without the assistance of a great number of technical staffs. I would like to extend my thanks to all members of the technical support team in the Chemistry Department and all members of my group at the University of Liverpool.

Let me also extend my great thanks and love to my parents, my brothers, my sisters and my husband for their support and encouragement.

Finally, thanks are due to King Faisal University for their financial support and to the Saudi Cultural Bureau in London for their financial management.

A new chapter in my life is beginning

This work is dedicated to my family and my children

I hope I've made you proud

Publications and Presentations

Published Papers

[1] H. Althikrallah, C. Kunstmann-Olsen, E.F. Kozhevnikova, I.V. Kozhevnikov, Turnover rate of metal-catalysed hydroconversion of 2,5-dimethylfuran: gas-phase versus liquid phase, Catalysts 10 (2020) 1171.

[2] H. Althikrallah, E.F. Kozhevnikova, I.V. Kozhevnikov, Facile gas phase hydrodeoxygenation of 2,5-dimethylfuran over bifunctional metal-acid catalyst Pt-$Cs_{2.5}H_{0.5}PW_{12}O_{40}$, Chem. Commun. 57 (2021) 227–230.

[3] H. Althikrallah, E.F. Kozhevnikova, I.V. Kozhevnikov, Hydrodeoxygenation of 2,5-dimethyltetrahydrofuran over bifunctional metal-acid catalyst Pt $Cs_{2.5}H_{0.5}PW_{12}O_{40}$ in the gas phase: Kinetics and mechanism, Mol. Catal. 510 (2021) 111711.

[4] H. Althikrallah, E.F. Kozhevnikova, I.V. Kozhevnikov, Hydrodeoxygenation of 2,5-dimethyltetrahydrofuran over bifunctional Pt-$Cs_{2.5}H_{0.5}PW_{12}O_{40}$ in the gas phase: enhancing effect of gold, RSC Adv. 12 (2022) 2287–2291.

Conference Presentations

[1] H. Althikrallah, E.F. Kozhevnikova, I.V. Kozhevnikov, Hydrogenation and hydrogenolysis of 2,5-dimethylfuran over noble metal catalysts in the gas phase,7th EuCheMS Chemistry Congress, Liverpool, August 2018.

[2] H. Althikrallah, E.F. Kozhevnikova, I.V. Kozhevnikov, Conversion of 2,5 dimethylfuran into 2-hexanol under mild conditions using carbon-supported noble metal catalysts in the gas phase, UK Catalysis Conference UKCC2019, Loughborough, January 2019.

[3] H. Althikrallah, E.F. Kozhevnikova, I.V. Kozhevnikov, Hydrogenation and hydrogenolysis of furan derivatives over noble metal catalysts at the gas solid interface, The Analytical Research Forum, London, June 2109.

[4] H. Althikrallah, E.F. Kozhevnikova, I.V. Kozhevnikov, Hydrogenation, hydrogenolysis and hydrodeoxygenation of furan derivatives over noble metal catalysts in the gas phase, Fundamentals and Practice Summer School, Liverpool, July 2019.

[5] H. Althikrallah, E.F. Kozhevnikova, I.V. Kozhevnikov, Gas-phase hydrotreatment reactions of 2,5-dimethylfuran using bifunctional metal-acid catalysts, 5th Edition of Global Conference on Catalysis on Chemical Engineering & Technology, London, September 2019.

[6] H. Althikrallah, E.F. Kozhevnikova, I.V. Kozhevnikov, Reaction mechanism of 2,5-dimethylfuran hydrodeoxygenation over bifunctional catalysts Pt-$Cs_{2.5}H_{0.5}PW_{12}O_{40}$ in the gas solid catalyst, UK Catalysis Conference UKCC2021, Loughborough, January 2021.

[7] H. Althikrallah, E.F. Kozhevnikova, I.V. Kozhevnikov, Kinetic study of furan derivatives hydrodeoxygenation over bifunctional metal-acid catalyst Pt-$Cs_{2.5}H_{0.5}PW_{12}O_{40}$ in the gas Phase, Chemical Science Symposium 2021: Biohybrid Approaches to Sustainable Energy Conversion, London, September 2021.

List of Abbreviations

BET	Brunauer-Emmett-Teller
BHJ	Barrett-Joyner-Halenda
CsPW	Caesium Salt of Tungstophosphoric Acid ($Cs_{2.5}H_{0.5}PW_{12}O_{40}$)
DFT	Density Functional Theory
DMF	2,5-Dimethylfuran
DMTHF	2,5-Dimethyltetrahydrofuran
E-R	Rideal-Eley Mechanism Model
EDX	Energy Dispersive X-ray Emission
FID	Flame Ionisation Detector
GC	Gas Chromatography
GC-MS	Gas Chromatography-Mass Spectroscopy
HPA	Heteropoly Acid
HPW	Tungstophosphoric Acid ($H_3PW_{12}O_{40}$)
HMF	5-Hydroxymethylfurfural
HDO	Hydrodeoxygenation
HZSM-5	Proton Form of ZSM-5 Zeolite
ICP-OES	Inductively Coupled Plasma Optical Emission Spectroscopy
L-H	Langmuir-Hinshelwood Mechanism
MTHF	2-Methyltetrahydrofuran
PGM	Platinum Group Metals
POM	Polyoxometalate
PFR	Plug-Flow Reactor
SEM	Scanning Electron Microscopy

STEM	Scanning Transmission Electron Microscopy
THF	Tetrahydrofuran
TEM	Transmission Electron Microscopy
TPD	Temperature Programmed Desorption
TPR	Temperature-Programmed Reduction
TCD	Thermal Conductivity Detector
TGA	Thermal Gravimetric Analysis
TOR	Turnover Rate
TOF	Turnover Frequency
TOS	Time on Stream
XRD	X-ray Diffraction

List of Contents

List of Figures

List of Schemes

List of Tables

Chapter 1. Introduction

1

This chapter provides background information relevant to the research topic. Section 1.1 describes the current challenges in the global energy supply. Section 1.2 contains a general introduction to heterogeneous catalysis, which includes an overview of multifunctional metal-acid catalysis and a brief discussion of the structures and properties of heteropoly acids (HPAs) and their salts. This is followed by section 1.3, which summarises recent literature on catalytic hydroconversion of furan derivatives. Finally, section 1.4 outlines the objectives and the scope of the work that was performed for this thesis.

1.1. Renewable Energy Perspective

1.1.1. The Energy Challenges

Over the centuries, humans have shifted from the use of one fuel source to another. Initially, the primary fuel source was wood. The use of wood caused massive deforestation in most parts of the world. As the forest cover declined, the focus shifted to use of whale oil resources. At the beginning of the 17th century, whale oil became rare, which prompted the search for a new source of energy. Fossil fuels promoted the industrial revolution in the 18th century. All these fuel sources are non-renewable which forced humans to shift to renewable sources as fossil fuels decline. Chemists have turned their attention towards the use of biomass as a source of sustainable energy. Biological background information regarding the origin of biomass indicates that carbohydrates are the biochemical building blocks of biomass formed by plants through photosynthesis. It is estimated that 200 billion tons of

biomass are produced naturally every year during photosynthesis. Human activities consume only 4% of this biomass, while most of the carbohydrates are wasted [1−3].

Environmentally friendly characteristics are the most critical requirement of new renewable sources of energy. The continuous use of fossil fuels has caused severe damage to the environment from greenhouse gases and other pollutants such as sulphur oxides. Unlike the initial use of wood for energy, the burning of cellulosic and hemicellulosic derivatives is associated with reduced environmental pollution compared with the burning of fossil fuels.

The growing use of renewable sources of energy will lead to reduced or zero emissions of greenhouse gases, which affect the atmosphere [2]. Therefore, with such an abundance of raw biomass, it should be possible to produce an efficient source of energy for the world. This marks a shift back to cellulose as the next generator of energy [1]. However, the delivery of a reliable supply of sustainable energy remains the most significant scientific and technological challenge of the 21st century.

1.1.2. Biomass as a Source of Energy

Biomass represents a class of organic material that is derived from plants and animals, especially vegetable oils and animal fats have great potential to produce biodiesel. Biomass feedstock can be grouped into three general classes: starchy feedstocks (including sugars), triglyceride feedstocks, and lignocellulosic feedstocks. The cheapest and most abundant source of biomass is lignocellulose, which is a renewable carbon source composed of three main groups of natural polymeric materials: cellulose (around 50% on dry basis), hemicellulose (10–30% in woods and 20-40% in herbaceous biomass on dry basis) and lignin (20–40% in woods and 10–40% in herbaceous biomass on dry basis). This is a promising raw material for the production of transportation bio-oils by liquefaction, pyrolysis and hydrolysis treatment.

Use of biomass as fuel offers great advantages to the environment compared with use of fossil fuels. Therefore, biofuels may offer a critical remedy to the issues that are related to global climate change which are caused by the burning of fossil fuels such as coal, petrol and oil [2,4]. In support of this, Kurchania [5] indicated that the world demand for gas and oil could be met through efficient utilisation of about 6% of the global production of biomass.

Biomass-derived compounds are often over functionalised due to high oxygen content, which influences the polarity, viscosity, homogeneity, acidity and heating value of the bio-oil produced [6]. The transformation of biomass to biofuels requires application of techniques that include biological, physical and thermochemical conversion. Among them, the most promising for commercial use appears to be thermochemical processes, which use heat and chemical catalysts to decompose biomass into high-value products. According to Jahirul et al. [7], the pyrolysis process has received much attention; it involves thermal decomposition of biomass in the absence of oxygen, which guarantees high fuel-to-feed ratios. This decomposition produces methanol, water, insoluble oils, a mixture of gaseous products and a solution of several acids. Thermal decomposition of biomass in the pyrolysis process requires temperatures of between 377 °C and 527 °C to break down organic structures into oligomers and monomers [7,8]. The bio-oils produced in this way lack the quality of automotive fuels and therefore cannot be used in vehicle engines directly.

The conversion of biomass carbon resources to their constituent chemicals requires a different strategy and chemistry from that used for fossil carbon resources (Fig.1.1). The shift to biomass as a source of energy and raw materials would also require an upgrade of critical methods and technologies in order to make the process cost-effective. In essence, these upgraded methods would require the development of effective catalysts to enhance the production of chemicals and energy.

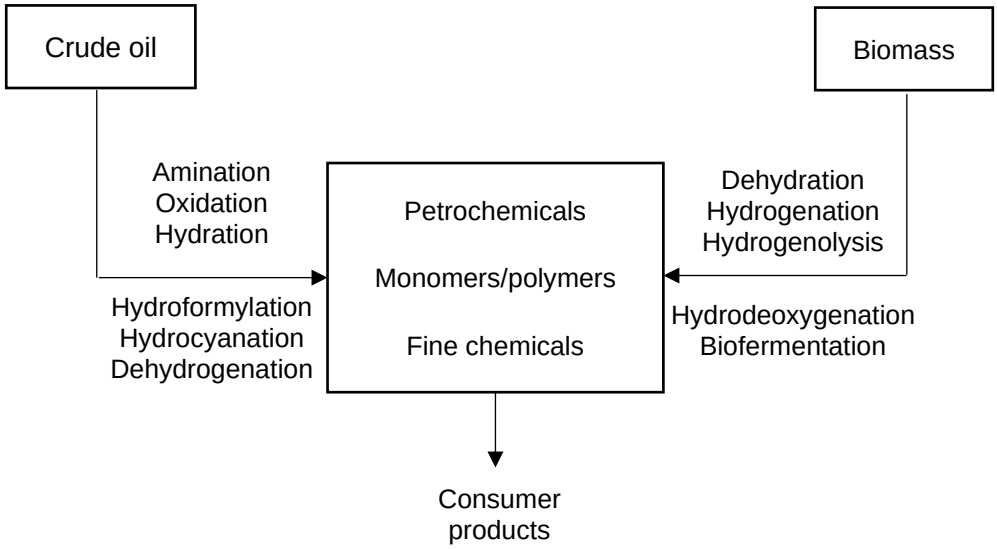

Fig. 1.1 The different reactions that are required to produce value-added chemicals and fuels from crude oil and biomass [5].

For fuel applications, the oxygen content of the bio-oil produced would have to be reduced in order to increase its stability and energy value. One route by which bio-oil can be upgraded is the hydrodeoxygenation (HDO) process to produce a hydrocarbon (Fig. 1.2) [9−11]. However, many HDO processes suffer from low hydrocarbon yields, incomplete elimination of oxygen atoms, severe coke formation and they must be conducted at high reaction temperatures (>400 °C). More active and stable HDO catalysts are required for the complete removal of oxygen atoms at low temperatures.

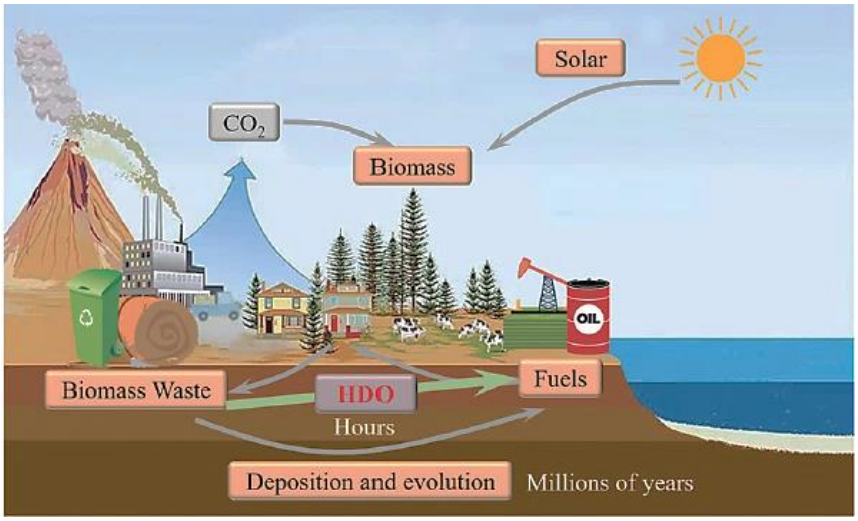

Fig. 1.2 The simplified representation of bio-oil life cycle [11].

1.1.3. Overview of Scientific Problem

In the last few decades, there has been growing interest in green fuels energy in response to increasing environmental concerns and a projected shortage of oil supply. Biomass-derived furanic compounds, which are a family of cellulosic or hemicellulosic platform carbohydrate molecules such as furfural, 2-methylfuran, 2,5-dimethylfuran, etc., have been seen as a potential resource to meet the increasing demand for green energy (Fig. 1.3) [12,13]. Furanic compounds have been widely researched as intermediates in the production of alternative fuels and considered as synthetic chemical building blocks. They are used as resources for liquid alkane fuels, industrial solvents, polymers, pharmacological agents and a variety of useful chemicals e.g., aldehydes, alcohols, acids etc. However, furanic compounds contain high amounts of oxygen and therefore must be upgraded to become energy providers.

Catalytic hydroconversion methods such as hydrogenation, hydrogenolysis and HDO are effective upgrading processes to convert platform furanic compounds to high-value chemicals and green biofuels (petrol, jet fuel, diesel and fuel additives) to provide energy services [14−16]. Hydrogenation involves the addition of H atoms to unsaturated hydrocarbons to saturate double or triple bonds in the molecules. Hydrogenolysis involves the cleavage of a single carbon-carbon or carbon-heteroatom bond. The HDO process comprises a sequence of different reactions such as hydrogenation, hydrogenolysis and dehydration. It leads to the removal of oxygen by cleavage of C−O bonds to form hydrocarbons and environmentally benign water in the presence of H_2. In effect, one molecule of H_2 is used to remove each oxygen atom.

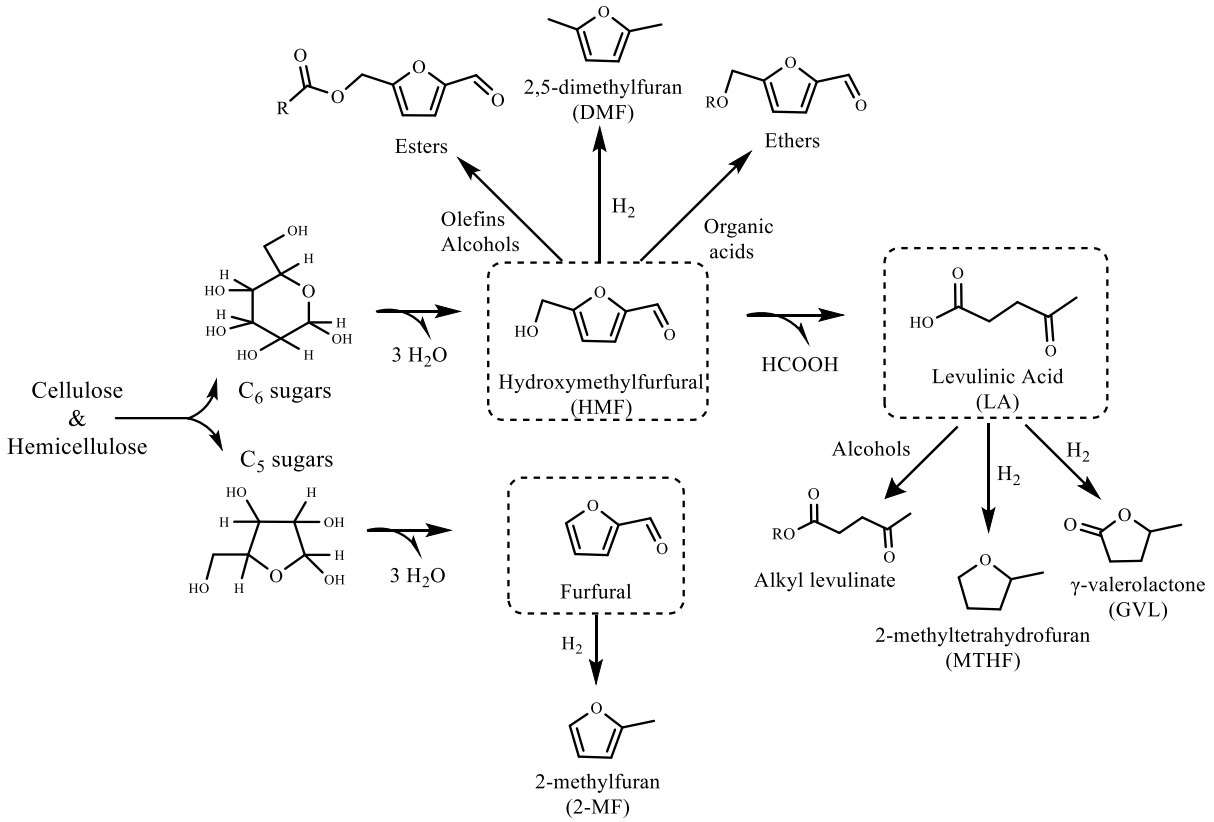

Fig. 1.3 The conversion of biomass-derived cellulosic and hemicellulosic compounds into furanic building blocks for biofuel and fuel additives production (adapted from [13]).

In light of this, despite extensive research in this area, the challenge remains to design more active, selective and sustainable catalysts for the upgrading process. There has been ample research on the liquid phase HDO [15,16]. However, low product yields and severe reaction conditions are serious problems on this route. Moreover, due to the complex chemistry of furanic compounds and the large number of species that are involved, the kinetics and mechanisms of these reactions on the catalyst surface are not understood yet.

1.2. Heterogeneous Catalysis: Definition and Background

Catalysis is an important process that plays a key role in modern chemical and related industries [17−26]. Catalysis has long been used for the large-scale production of chemicals, which was dramatically increased at the beginning of the 20th century. Catalysts enhance the rate of chemical reactions by reducing the activation energy without changing reaction thermodynamics [22,23]. Ideally, the catalysts are not consumed in the reaction because they are regenerated after each catalytic cycle. Consequently, catalysts enhance the sustainability of chemical processes both environmentally and economically as their use decreases the amount of energy input that is required, reduces waste and improves product selectivity, thus amplifying overall economic benefits.

The most important features that determine the efficiency of catalysts are their activity, selectivity and stability [17−20]. Catalyst activity is the ability to accelerate the conversion of reactants into products. It is defined as moles of product formed or reactant converted per unit time and per unit amount of the catalyst. The rate can also be expressed per unit catalyst surface area or per single catalyst active site. The most accurate measure of catalyst activity is the turnover frequency (TOF) or turnover rate (TOR), which is defined as the number of revolutions through which the catalytic cycle passes per unit of time and calculated as the number of molecules converted per active site and per unit time (in $time^{-1}$ units) [26]. Catalyst selectivity is the fraction of the reactant that is converted to the desired product. In most cases, selectivity is defined as the number of moles of the desired product that are formed per the overall number of moles of the reactant converted. Catalyst stability refers to the lifetime of the catalyst and is related to the way in which it becomes deactivated, or its deactivation behaviour. The thermal, mechanical and chemical stabilities of catalysts are the important characteristics that determine the catalyst's life.

Catalysis is categorised into two different types: homogeneous and heterogeneous catalysis. In homogeneous catalysis, the catalyst and the reactants exist in the same, usually liquid, phase. In heterogeneous catalysis, the reactants and the catalyst are in different phases; usually the systems involve a solid catalyst and either liquid or gaseous reactants. The definition of phase in this context is not restricted to solid, liquid and gas, but includes immiscible liquids such as water and oil [28]. Heterogeneous catalysis is more extensively used in industry than homogeneous catalysis due to the ease of separation and recycling of the solid catalyst [22]. The heterogeneous catalytic cycle involves surface reactions that occur in a sequence of elementary steps, as illustrated in Fig. 1.4 [19−26].

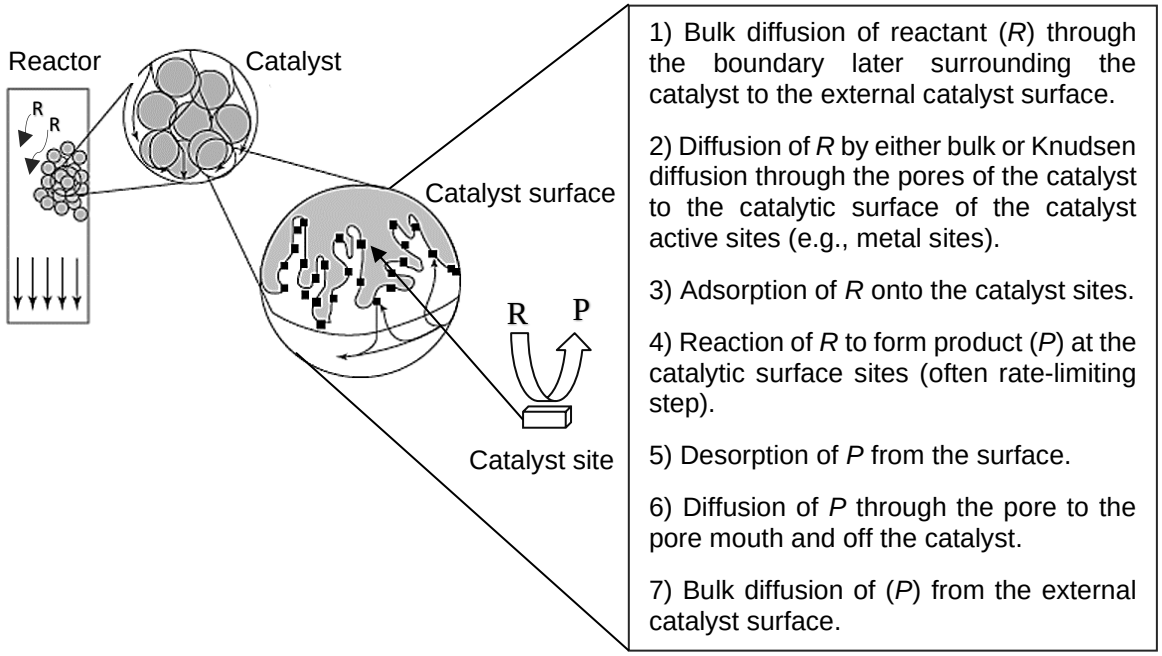

Fig. 1.4 Reaction steps of a heterogeneously catalysed reaction on a solid porous catalyst, where R = reactant and P = product (adapted from [17,19,23]).

The initial stage in a heterogeneous catalytic reaction is the external diffusion of reactants from the bulk fluid phase to the catalyst surface followed by internal diffusion of the reactant molecules through the pores to approach active sites. Adsorption is the next step; it involves the binding of reactant molecules to the active sites within and on the surface of the catalyst. The molecule that binds is called the adsorbate, while the solid surface to which it attaches is called the adsorbent. Two types of adsorption occur: physisorption and chemisorption. As reactant molecules approach the catalyst surface, they are immediately physisorbed at a long distance via van der Waals forces. At a relatively short distance, the molecules interact much more strongly through chemisorption [18,22].

The adsorption stage is followed by surface chemical reactions. The two most typical mechanisms for surface reactions have been recognised (Fig. 1.5). The first is the Langmuir-Hinshelwood mechanism, in which two reactants A and B adsorb close to each other on the catalyst surface, where they react to form product C, which desorbs from the surface. The second mechanism is the Eley-Rideal mechanism, in which reactant A adsorbs to the catalyst and subsequently is attacked by reactant B from the fluid phase to form product C [20,21]. Finally, the product desorbs from the active sites and diffuses out of the catalyst surface. All these steps determine the overall rates of the catalytic reactions.

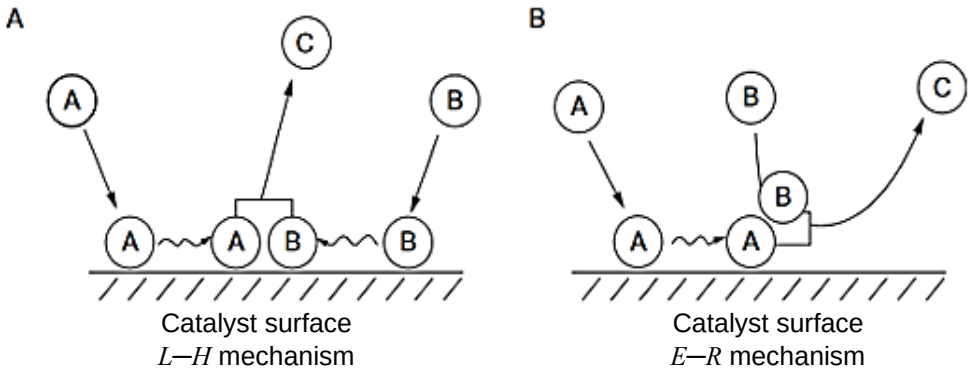

Fig. 1.5 Langmuir–Hinshelwood (L–H) and Eley–Rideal (E–R) mechanisms of reaction on a catalyst [20].

1.2.1. Metal Catalysts

Supported and unsupported metals are important catalysts in many reactions, such as hydrogenation, hydrogenolysis, oxidation, etc. Dissociative adsorption of hydrogen (H_2) to metal sites is the first step in most metal-catalysed hydroconversion reactions that involve H_2. This process involves physical adsorption of the H_2 molecules to the metal surface, dissociation of the H−H bond and formation of a metal-H bond [27─34].

Supported metal catalysts offer several advantages over unsupported catalysts. These are: high metal dispersion; a large accessible surface area of the metal; fewer limitations that are caused by mass and heat transfer; easy metal recovery; metal particle stabilisation; and increased resistance to poisoning. The use of support can provide improved control over reaction selectivity [27,29,30]. Another important property of supported metal catalysts is strong metal-support interaction (SMSI), which can affect the activity and selectivity of supported metal catalysts in hydrotreatment reactions. This strong interaction affects H_2 spillover on the metal sites, whereby H atoms migrate from H−rich to H−poor sites. A variety of support materials is utilised in catalyst preparation, such as active carbons, zeolites and oxides such as silica or alumina [29−31].

Creation of small metal particles on the surface is essential in many chemical reactions for the efficient performance of supported metal catalysts [30−34]. Such particle creation is achieved through use of different preparation methods such as impregnation, ion exchange and co-precipitation [30]. Impregnation is the most common procedure employed for the preparation of supported metal catalysts. It involves the interaction of a metal precursor solution with the support, followed by a reduction reaction under H_2 flow to form metal particles [27,31]. The impregnation method can be classified as wet/diffusional impregnation or dry/incipient impregnation based on the quantity of precursor solution used.

According to Boudart [32], metal-catalysed reactions are structure-sensitive or structure-insensitive, depending on the effect of metal particle size or metal dispersion on TOF. Boudart classified reactions as structure-sensitive if the rate or selectivity of the reaction changed dramatically with metal particle size. In contrast, he termed the reactions as structure-insensitive when particle size did not greatly affect the reaction. For certain reactions, the difference between structure-insensitive and sensitive seems to be related to the nature of the catalyst and the reaction temperature and pressure. In the 1950s, Boreskov and colleagues [34] improved the measurement of the accessible metal surface area of supported metal catalysts by utilisation of selective H_2 adsorption (chemisorption), which enabled them to analyse the impact of the size of platinum particles in Pt catalysts that were used in oxidation reactions. In the 1960s, Boudart and his team [29] made significant contributions to the knowledge of the effects of particle size on the activity and selectivity of supported catalysts.

1.2.2. Heteropoly Acid Catalysts

HPAs and their acidic salts have strong Brønsted acidity, fairly high thermal stability, water tolerance and tuneable redox properties [35−38]. HPAs comprise metal-oxygen polyoxometalate anions and protons (H^+ ions) as counter cations. Polyoxometalate anions are formed by a self-assembly process in solution and can be isolated as HPAs or their salts [37].

There are many structural types of HPAs. The most common is the Keggin structure (Fig. 1.6), which is represented by the formula $(XM_{12}O_{40})^{x-8}$, in which X is the heteroatom or central atom, such as P^{5+}, As^{5+}, Si^{4+}, Ge^{4+} or B^{3+} and M is a metal ion such as molybdenum (VI), tungsten (VI), vanadium (V), niobium (V), tantalum (V), etc. The Keggin unit is composed of a central tetrahedron XO_4 surrounded by 12 metal-oxygen octahedra (WO_6),

as shown in Fig. 1.6 [38,39]. Four types of oxygen atoms exist in the structure; these take the form of 12 terminal M=O_t, 12 edge-sharing angular M−O_{b1}−M, 12 corner-bridging quasi-linear M−O_{b2}−M and four internal X−O_c−M groups [37–38].

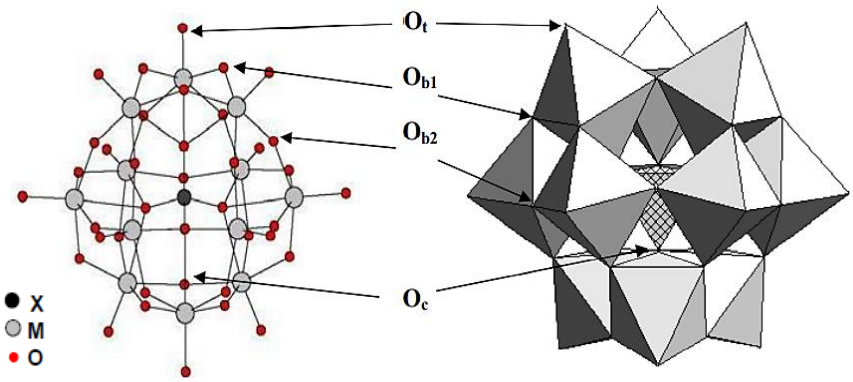

Fig. 1.6 The Keggin structure of the $[XM_{12}O_{40}]^{x-8}$ anion in ball-and-stick (left) and polyhedral (right) representations. Four types of outer oxygen atoms are indicated: terminal (O_t), edge-bridging (O_{b1}), corner-bridging (O_{b2}) and internal (O_c) [38,39].

The acid strength and thermal stability of Keggin HPAs can be estimated from temperature-programmed desorption (TPD) of ammonia from its surface and thermal gravimetric analysis, respectively [37,39]. The acid strength and thermal stability of Keggin HPAs decrease in the following order:

$$H_3PW_{12}O_{40} > H_4SiW_{12}O_{40} > H_3PMo_{12}O_{40} > H_4SiMo_{12}O_{40}$$

There are two types of proton sites within solid HPAs: hydrated and non-hydrated protons. The hydrated protons have high mobility, which results in high conductivity of HPA hydrates [40,41]. The non-hydrated protons are localised on the basic bridging oxygen atoms of the heteropoly anions.

Preparation of heteropoly salts involves replacement of the protons with different metal cations in the parent HPAs. The choice of cation within HPA salts affects their acidity, thermal stability, porosity and solubility [41−45]. Caesium salts of 12-tungstophosphoric acid $Cs_xH_{3-x}PW_{12}O_{40}$ (Cs_xPW), which are synthesized by partial substitution of large

caesium (Cs^+) cations for H^+ of $H_3PW_{12}O_{40}$ (Fig. 1.7), brought about unique changes in the pore structure, surface area and acidity. This exhibits an ideal material as heterogeneous acid catalysts in solid/liquid and solid/gas systems for various kinds of reactions. The Keggin structure forms the primary structure of the catalyst. The arrangement of the primary structure with Cs^+ ions form the secondary structure, which corresponds to micro-crystallites. Aggregates of the micro-crystallites form the tertiary structure (Fig. 1.8) [45,46].

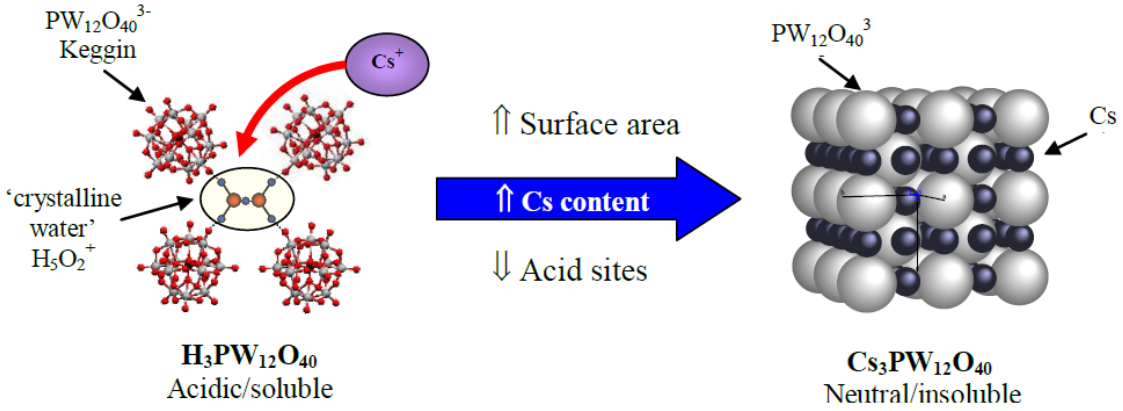

Fig. 1.7 Exchange of Cs ions with $H_3PW_{12}O_{40}$ generates $Cs_xH_{(3-x)}PW_{12}O_{40}$ [42].

According to Okuhara and co-workers [45,46], the surface area and surface acidity of Cs_xPW salts reach a maximum at x = 2.5 (Fig. 1.9). The salt $Cs_{2.5}H_{0.5}PW_{12}O_{40}$ shows strong proton acidity, high surface area (over 100 m^2g^{-1}) and high thermal stability (it decomposes at 500 °C). It is also insoluble in water and organic solvents [44−46], which means that it is suitable for reactions in which water is either the reaction medium or a by-product. The Cs_xPW salts possess bimodal distribution of the pores; mesopores (diameter between 2 nm and 50 nm) as well as micropores (diameter < 2 nm). These salts have high densities of surface proton sites, which makes them very active solid acid catalysts [42−46].

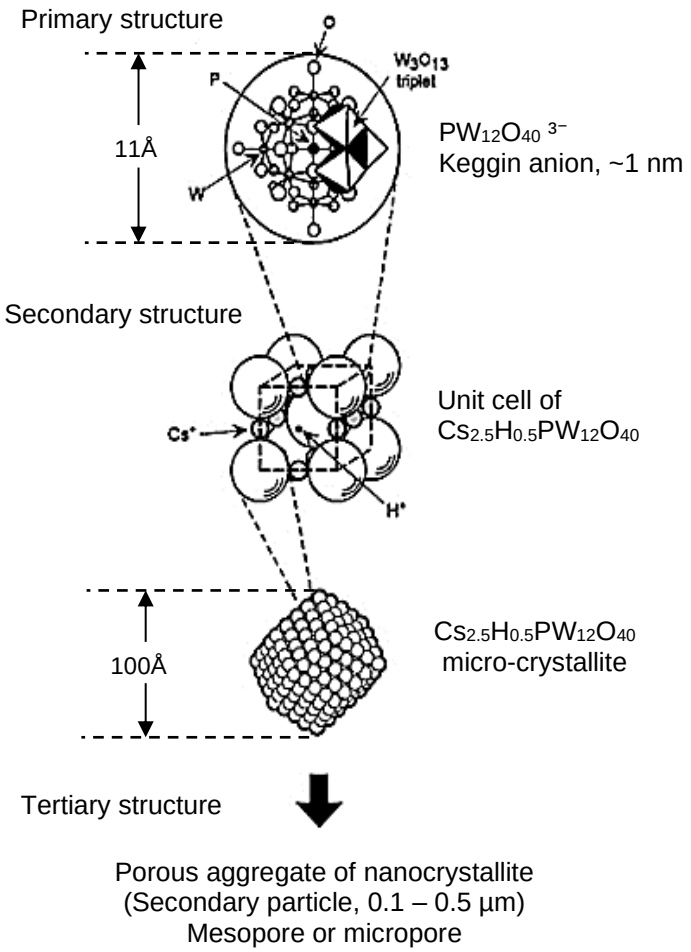

Fig. 1.8 Primary, secondary and tertiary hierarchical structures of $Cs_{2.5}H_{0.5}PW_{12}O_{40}$ [45,46].

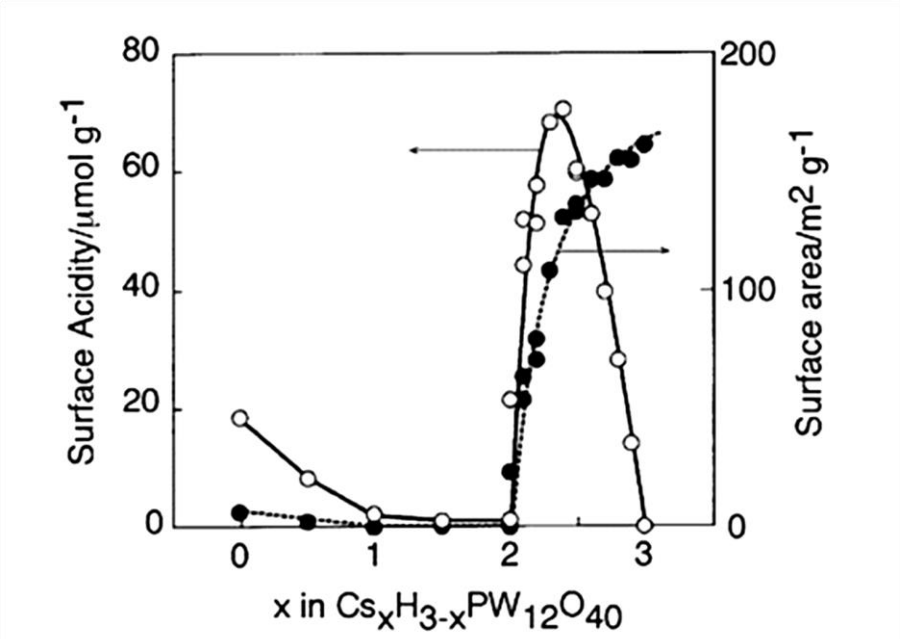

Fig. 1.9 Surface acidity and surface area of $Cs_xH_{3-x}PW_{12}O_{40}$ as a function of Cs content [45,46].

1.2.3. Metal-HPA Multifunctional Catalysts

A multifunctional catalyst contains two or more different active sites that work simultaneously to effect several chemical transformations in a single catalyst bed or one-pot reaction system. Multifunctional catalysts can catalyse cascade reactions without separation of intermediate products. Cascade reactions, also known as domino or tandem reactions, have important advantages over stepwise chemical processes as they pass through a reduced number of intermediate steps and thus offer substantial benefits of reduced cost, time and waste [38,47,48]. Bifunctional metal-acid catalysts, such as Pt/alumina and Pt/zeolite, are widely used in multistep chemical processes [47−53]. Likewise, HPAs have the potential to be used effectively as the acid components of multifunctional catalysts for cascade processes that involve acid and redox catalysis [47]. Currently, there is much attention to the development of bifunctional metal-acid catalysts that incorporate strong acid sites, which exhibit high selectivity towards target products.

1.2.4. Bimetallic Catalysts

Since the late 1960s there has been a strong interest in bimetallic catalysis due to the discovery of the superior properties of the Pt-Sn, Pt-Ir and Pt-Re catalysts in petroleum reforming [54–59]. Considerable progress was achieved both in the characterization of bimetallic surfaces and in the quantum theory of alloys. Supported bimetallic catalysts are widely used for reactions such as reforming, selective oxidation, hydrogenolysis, biomass conversion, etc. In many cases, the addition of another metal to supported metallic nanoparticles produces superior catalytic performance as it alters the structural and chemical properties of the catalytic surface. Moreover, the addition of the second metal can cause an increase in the reaction rate, improve the stability of the catalyst and its selectivity to the desired product [54−62].

Our knowledge about bimetallic catalysis can be summarized as follows [54]:

- The composition of the bimetallic surface can differ substantially from that of the bulk. Chemisorption or the catalytic reaction can induce additional changes in the surface composition.
- The selectivity patterns are mainly determined by the ensemble size effect, but a ligand effect may also occur simultaneously. The ensemble effect is the modification of the geometry of the surface metal atom, which generates highly active surface sites for certain reactions. This activation occurs because the local chemisorption properties are changed by a direct change in the atomic ensemble components in the adsorption site. The ligand effect is thought to modify the catalyst activity as it alters the electronic properties of metal sites, which may affect the strength of the metal-adsorbate interactions [55,56]. The catalytic efficiency is also influenced by the composition of the bimetallic nanoparticles and the relative orientations of the two metals inside the nanoparticles [56].
- Individual surface atoms retain their character in bimetallic catalysts, and their catalytic properties are mainly determined by their nearest neighbours.
- Bimetallic catalysts exhibit higher catalytic activity than either of their constituents because of a lower degree of poisoning. This can result in higher catalyst stability and in a change in reaction selectivity.

In the supported bimetallic catalysts, the following factors should be considered [54]:

(i) ensemble size variation

(ii) particle size effect and dispersion

(iii) matrix effect

(iv) change in hydrogen coverage and in the structure of adsorbed hydrogen

(v) separation of bimetallic into components

(vi) metal-support interaction (MSI)

(vii) suppression of self-poisoning reactions

Two impregnation procedures are commonly used to prepare bimetallic catalysts: co-impregnation and sequential impregnation. In co-impregnation, two metal precursors are mixed before they are impregnated into the catalyst support. In sequential impregnation, the first metal precursor and then the second is impregnated. The difference in the impregnation procedures has a great influence on the catalytic activity. Co-impregnation usually results in the creation of an alloy of mixed metals, whereas sequential impregnation results in a complicated interaction between the mixed metals [60,61].

1.3. Catalytic Hydroconversion of Furanic Compounds

Recently, the conversion of biomass-derived furanic compounds to chemicals and fuels has attracted interest in green chemistry research [4–17]. Selective conversion of furanic derivatives into open-chain compounds such as aldehydes, ketones and alcohols has received much attention in the last few years, due to their wide range of applications in polymer industries to produce polyesters and polyurethanes as well as for the synthesis of fuel components. Heterogeneous bifunctional metal-acid catalysis is a promising method for the hydroconversion (hydrogenation, hydrogenolysis and HDO) of furanic compounds. Use of this method, however, requires increased effort to improve such catalysts in respect of the scope of the substrates, reaction temperature and pressure and H_2 consumption.

The mechanism of hydroconversion of bio-oil remains unclear due to the large number of concurrent reactions that occur throughout the upgrading process. Most studies, therefore, use model compounds to elucidate the mechanism of individual reactions that take place within the process. Use of 2,5-dimethylfuran (DMF) has attracted attention because it can function as a model of biomass-derived furanic compounds. DMF has high energy density (35 M J kg $^{-1}$), a high research octane number (RON, 119), low solubility in water (2.3 g L^{-1}) and relatively low volatility (boiling point ~93 °C); hence it can serve as a potential gasoline alternative as well as a feedstock source to produce value-added chemicals, which can boost the supply of green energy [63].

The next sections (1.3.1 and 1.3.2) discuss the catalytic hydroconversion of furanic compounds. These studies involve ring hydrogenolysis, ring hydrogenation and deoxygenation of furanic compounds.

1.3.1. Hydrogenation and Hydrogenolysis Reactions

It has been reported that supported monometallic Pt group catalysts have high activity and selectivity for the hydroconversion of furans, although some metals require modification in order to enhance their selectivity towards C−O hydrogenation. The catalytic activity and selectivity of these materials strongly depend on the nature of the Pt metals, different supports and reaction conditions [64−70]. In addition, the structure of the reactant itself and how it adsorbs onto the metal surface are significant. Appropriate interaction of the furan ring with the metal surface can enhance the ring-opening reaction, which influences the selectivity for intermediates and desirable products [71].

Aliaga et al. [64] studied the hydrogenation of DMF on carbon-supported noble metal catalysts, in which the metal was Pt, Pd, Rh or Ru. The products were 2,5-dimethyltetrahydrofuran (DMTHF), 2-hexanone, 2-hexanol and n-hexane, as shown in Scheme 1.1. They reported that C_5 and C_6 alcohols were only formed over supported Pt nanoparticles at low temperatures that ranged between 20 °C and 120 °C.

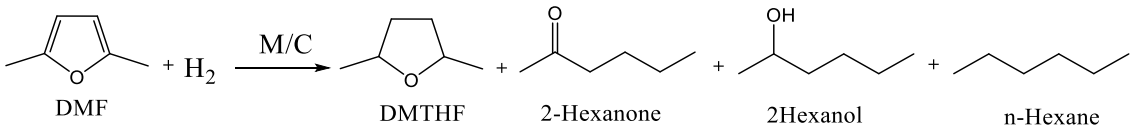

Scheme 1.1 Hydrogenation of DMF over carbon-supported noble metal (M/C) catalysts.

The main products that were observed for Pd/C and Pt/C catalysts were similar to those reported for gas phase hydrogenation of DMF through deuterium labelling studies at 90−220 °C [65]. This study suggested that the reaction proceeded via saturation of the furan ring at low temperatures over Pd/C to give deuterated DMTHF, whereas, at high temperatures, cleavage of the C−O bond occurred to give deuterated ketones for both catalysts. Gilkey et al. [66] also investigated the hydrogenation of DMF over a Ru/C catalyst in liquid phase at

80 °C (Scheme 1.2), which produced a ~97% DMF conversion with high selectivity to DMTHF (~73%) as the main product and the ring-opened products 2-hexanol and 2-hexanone (~19% and ~1% respectively).

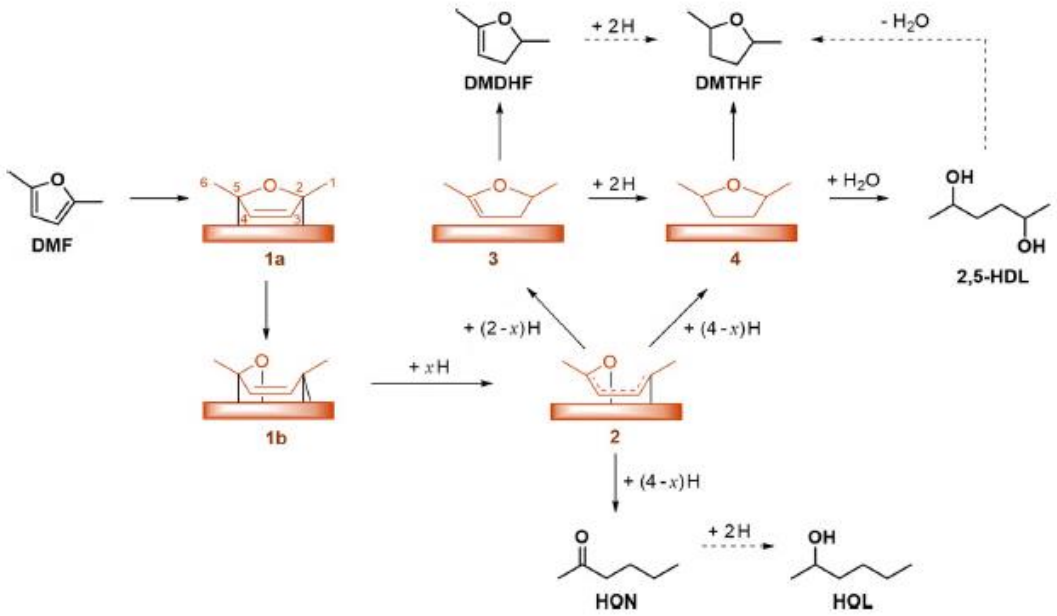

Scheme 1.2 Proposed DMF hydrogenation mechanism over Ru/C. Species drawn in black are bulk species and those drawn in orange are adsorbed to the Ru surface [66].

Among carbon-supported metal catalysts, Pt catalysts appear to show the highest activity and selectivity for the C−O hydrogenolysis. Recently, a kinetic study on hydrogenation and hydrogenolysis of DMF over Pt/C concluded that ring opening was favoured over ring saturation at elevated temperatures and low H_2 pressure; 92% selectivity to 2-hexanone at 100% conversion of DMF was obtained under mild conditions in liquid phase reaction (0.41MPa, 120 °C) [67].

Goto and co-workers [68] continued investigations of the effect of reaction temperature on DMF hydrogenation with Pt supported on a hexagonal boron nitride (h-BN) catalyst in the vapour phase. They showed that the selectivity of this catalyst to ring-opened or ring-saturated products was influenced by the reaction temperature, giving 2-hexanol at low

temperatures and 2-hexanone at high temperatures. This agreed with the findings of Biswas et al. [14]. The proposed reaction network is shown in Scheme 1.3.

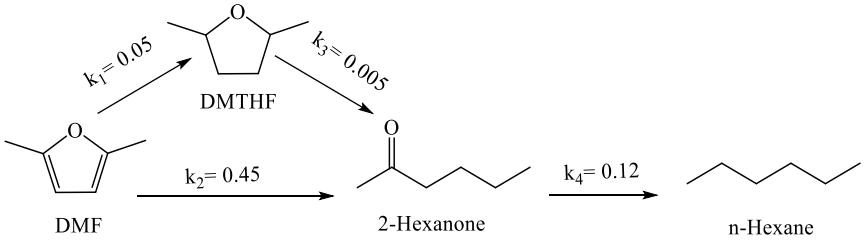

Scheme 1.3 Ring-hydrogenation and ring-opening of DMF using a Pt/h-BN catalyst (rate constants are given in s^{-1}) [68].

With the Pt/h-BN catalyst, the reaction proceeds through two parallel pathways. It produces 2-hexanone either by direct ring-opening (rate constant k_2) or by ring-hydrogenation (rate constant k_1) followed by ring-opening (rate constant k_3). The main product is 2-hexanone; a small amount of 2-hexanone is converted to n-hexane. According to the kinetic results, the rate constant k_2 of direct furan-ring opening is nine times greater than the k_1 of furan-ring saturation [68].

Tong et al. [69] reported direct hydrogenolysis of furans to the corresponding alcohols through use of a Pt catalyst supported on cerium oxide at low temperature (120−180 °C) and at H_2 pressure of 1.5−2MPa to yield hexane-2-ol (69%) as the main product with DMTHF as a by-product (16%). However, Corma et al. [70] reported a 100% yield of 2-hexanone over Pt/C at high temperature (350 °C) through the gas phase hydrogenation of DMF. These examples show that catalyst selection and reaction conditions have strong effect on the reaction pathway and product selectivity.

1.3.2. Hydrodeoxygenation Reaction

Recently, several groups have focused on the direct ring-opening of furans through using catalytic HDO, which is an effective strategy to transform biomass-derived furanic compounds in a controlled manner to chemicals and green fuels. The HDO reactions retain the C−C bond and selectively cleave the C−O bond, which is a more desirable method. Various bifunctional catalysts have been widely used in HDO reactions to produce alkanes. Different supports, active phases and promoters have been employed ([71−79] and references therein). Generally, HDO is conducted under high or atmospheric pressure; the oxygen removal as water (H_2O) is the key in both routes [76,77]. Both routes follow the same procedure, which relies on the H_2 to remove oxygen from the substrate as well as to hydrogenate any unsaturated C−C bonds present. These routes, however, differ in terms of conditions, catalyst type and reaction mechanism, due to the different roles of H_2 in the reactions. Higher catalytic performance of hydrogenation and deoxygenation reactions were observed in the presence of pure H_2 compared to mixed gases or H_2-free as reaction atmosphere [72]. Generally, the overall catalytic HDO mechanism comprises five steps: adsorption, binding, ring-opening, partial hydrogenation and complete deoxygenation.

Solid acid-supported mono- or bi-metallic catalysts have been extensively studied in the performance of HDO on biomass-derived oxygenates [71−136]. A range of metal catalysts has proved successful in HDO reactions [71−109]. For example, noble metal catalysts (Pt, Pd, Ru and Rh), transition metal catalysts (e.g., Ni, Mo, Co, Zn, Ce, Nb, Fe and Cu), as well as traditional hydrotreatment catalysts (NiMo and CoMo) and metal phosphides, such as MoP, WP, CoP and Ni_2P. However, most of these metal catalysts require high H_2 pressure, harsh conditions and they convert aromatic compounds to products with saturated rings. Researchers have reported promising deoxygenation activity of acid-supported noble metal catalysts for whole bio-oils compared with traditional transition-metal catalysts [85,108].

Several HDO studies have involved metal modification with acidic support such as oxide support (e.g., SiO_2-Al_2O_3, ZrO_2, γ-Al_2O_3, zeolite, HPA), metal oxides (e.g., ReO_x, MoO_x or WO_x) and using activated carbon as alternative support in the presence of acid component. It has demonstrated enhanced performance towards C−O hydrogenolysis to form hydrocarbons with >95% selectivity. Hence, acid-supported noble metals are superior catalysts for oxygen removal compared with conventional catalysts under the same conditions, although they are extremely expensive materials.

1.3.2.1. Bifunctional Metal-Acid Catalyst

A vast literature on bifunctional noble metal-acid catalyst systems has shown that strong acid sites with the mesoporous structure are required to facilitate selective HDO of biomass-derived oxygenates to yield the hydrocarbon products [77−109]. As previously discussed, the main role of the metal sites is to dissociate H_2 molecules and provide H atoms for the reaction that occurs in the hydrogenation/hydrogenolysis steps. The acid sites are active in the protonation, deprotonation and dehydration processes. The researchers suggested that increasing the acid strength of these sites reduced activation energy that was required for the opening of the furan ring in the HDO process, which promoted the hydrogenolysis of oxygenated intermediates to produce linear compounds [86]. Similarly, Waidmann et al. found that using acid co-catalysts for the HDO of furan derivatives greatly decreased the reaction temperature to produce alkanes [87]. Moreover, it has been reported that the TOF in HDO reactions is higher when the noble metals are deposited on acidic supports, compared with when non-acidic supports are used, because those on acidic supports have higher activity for C−O bond hydrogenolysis [88]. This can be explained by the synergy between the metal and acid sites. Thus, it is desirable to have a tuneable ratio of Brønsted to Lewis acid sites in the development of more efficient catalysts for HDO of biomass-derived

compounds, where the acidity may enhance the activity of the metal through interface interactions [82−109].

Yan et al. [89] tested several acid-supported monometallic (Ru, Rh, Pd and Pt) catalysts for the one-pot conversion of cellobiose (glucose dimer) to C_6 alcohols. They found that this catalyst was very active and nearly 100% selective for sorbitol under acidic conditions (pH 2). Similarly, Ardiyanti et al. [90] studied a series of catalysts, which consisted of Pd, Pt or Rh supported on zirconia, in the hydrotreatment of lignocellulosic biomass at 350 °C and 20 MPa total pressure over a four-hour reaction time. The researchers found that Pd/ZrO_2 showed the highest activity, which was greater than that of the $CoMo/\gamma\text{-}Al_2O_3$ catalyst. Gates et al. [91] studied the catalytic conversion of furan to aliphatic hydrocarbons in the presence of $Pt/\gamma\text{-}Al_2O_3$ at 300 °C and 1.4 bar of H_2. They suggested that both the acid sites and active metal sites in the presence of H_2 were essential to break the C−O bonds and to remove oxygen to form alkanes and alkenes.

In the same way, the HDO of DMF was investigated by Moreno and co-workers [92] over a $Pt/SiO_2\text{-}Al_2O_3$ catalyst. The mechanism was proposed including ring hydrogenation to DMTHF followed by hydrogenolysis of DMTHF to 2-hexanol and, finally, dehydration-hydrogenation to the final product, *n*-hexane. Lee et al. [93] applied Pt-based mesoporous zeolite catalysts for upgrading dibenzofuran (DBF) under 320 °C and 40 bar. Dibenzofuran conversion of 88.9% with an optimal bi-cyclohexane selectivity of 65.0% was obtained. Likewise, Wang et al. [94] used Pt supported on hierarchical zeolite (HZSM-5) to enhance the HDO of dibenzofuran into bi-cyclohexane at 260 °C under 3 MPa pressure. Cycloalkanes were produced with 86.8% selectivity under high DBF conversion (99.7%) via the partial hydrogenation of the aromatic rings followed by the C−O bond cleavage.

Gilkey et al. [96] found that using Ru/C catalyst for the HDO of DMF in the presence of homogeneous Brønsted acid (sulphuric acid) at 80 °C offered a potentially direct route to linear alcohols and diols. Similarly, the feasibility of a one-pot conversion of cellulose to liquid alkanes was presented by de Beeck et al. [97], who used a biphasic catalytic system at elevated temperatures in the presence of modified Ru/C catalysts with tungstosilicic acid. The reaction proceeded through several steps, in which the acid was primarily responsible for cellulose hydrolysis and dehydration steps (removal of oxygen atoms by C−O hydrogenolysis) while the modified Ru/C selectively hydrogenated intermediates to form liquid alkanes [97].

Based on literature reports, research into the utilization of polyoxometalates as catalysts in both liquid phase and gas phase systems has increased significantly. There have been recent catalytic studies using heteropoly acids in HDO reactions [98−105]. For example, Zhao et al. [98] used different metal modified HPA catalysts for direct synthesis of linear ethyl levulinate from carbohydrates such as cellulose, glucose and fructose. Liu [99] also reported that methyl levulinate can be efficiently produced from fructose over Fe-HPW catalyst, with 74% yield of methyl levulinate obtained at 130 °C. Previously, Kozhevnikov's group have reported that bifunctional catalysts comprising Pt metal on acidic supports such as zeolite HZSM-5 [100] and HPA [101,102] are highly active for HDO of a wide range of aliphatic and aromatic bio-derived oxygenates in the gas phase under mild conditions to yield the corresponding alkanes. Kogan et al. [103] reported the hydrogenation of aromatic ketones by Pd/HPA catalyst supported on alumina or carbon at high temperature and pressure (200 °C and 3 MPa) to produce alkanes. According to Alotaibi et al., the polyoxometalate structure remained unchanged after the reaction as evidenced by IR and XRD [104]. Similarly, Yadav et al. provided XRD evidence that Pd/HPA catalyst was stable in the HDO of 5-hydroxymethylfurfural to produce DMF (1.0 MPa, 90 °C) [105].

The synergistic effect between the noble metal sites and acid sites in bifunctional metal-acid catalysts has been suggested to explain their high activity for direct C−O hydrogenolysis [106−109]. Xue and co-workers [106] employed mesoporous silica SBA-15 catalyst doped with Pd/Nb for the liquid phase HDO of DMTHF to produce selectively hexane at 180 °C and 2 MPa H_2 pressure. Similarly, oxophilic promoter such as NbO_x species in the presence of solid acid sites was thought to be responsible for a synergistic effect in the multifunctional $Pd/NbOPO_4$ catalyst, which resulted in superior catalyst performance in the HDO of furan-derived adducts to liquid alkanes at 170 °C and 2 MPa H_2 [107].

Hibbitts et al. [86] reported that ReO_x−Rh catalyst produced Brønsted acid sites under relatively low H_2 pressure which could promote hydrogenolysis and formation of linear hydrocarbons. Chia et al. [108] studied the hydrogenolysis of tetrahydrofurfuryl alcohol (TFA) to produce 1,5-pentanediol. When a Rh/C catalyst was used, the selectivity to 1,5-pentanediol of 59% at 8.5% TFA conversion was observed at 393K and 34 bar H_2. When MoO_x was added as a promoter, the selectivity to 1,5-pentanediol was increased to 91% and the conversion was increased six-fold. Further, 1,5-pentanediol selectivity of 97% at 47% TFA conversion was achieved by the addition of ReO_x as a co-metal.

In the same way, Xue et al. [109] explored the production of liquid alkanes through catalytic HDO of cellobiose over a Pt-acid catalyst containing NbO_x promoter species at 5 MPa H_2 pressure at 190 °C in cyclohexane as a solvent. The reaction could progress via two routes: hydrogenation of the furanic ring followed by hydrogenolysis to 2-hexanol; or hydrogenolysis to 2-hexanone followed by hydrogenation to 2-hexanol. In both cases, 2-hexanol finally underwent HDO to produce hexane at yields up to 28%. Several other metal/support combinations were tested including Pt/H-ZSM-5, $Pt\text{-}ReO_x/SiO_2$ and $Pt\text{-}ReO_x/C$.

The proposed mechanisms of HDO of biomass-derived furans in both liquid and gas phases usually employ a Langmuir-Hinshelwood-type model [110−118] and consider the surface reaction including furan ring-opening as the rate-determining step. Xia et al. [107,108] found that C−O−C bond cleavage was the rate-determining step in HDO of furans. A Langmuir-Hinshelwood model was used by Lee and Ollis [114] with the assumption of competitive adsorption of the reactant, water and oxygenated intermediate at one site and H_2 adsorption at another site for benzofuran HDO. In the same way, the mechanism of the gas phase HDO reaction of 2-methyl tetrahydrofuran (MTHF), Scheme 1.4, was studied on a silica-supported nickel phosphide catalyst (Ni_2P/SiO_2) at 300 °C and 0.1 MPa pressure of H_2 [115]. The reaction was suggested to proceed via S_N1 or S_N2 nucleophilic substitution, with the S_N2 route preferred. The rate constant was small for the ring-opening step of the reaction, indicating that it was the rate-determining step. A separate kinetic study of benzofuran HDO over NiMo-γAl_2O_3 catalyst by Edelman et al. [116] suggested that a similar reaction pathway was followed, in which hydrogenation of the furan double bond occurred in the first step. The reaction was first-order in the reactant and the surface reaction was suggested to be the rate-controlling step.

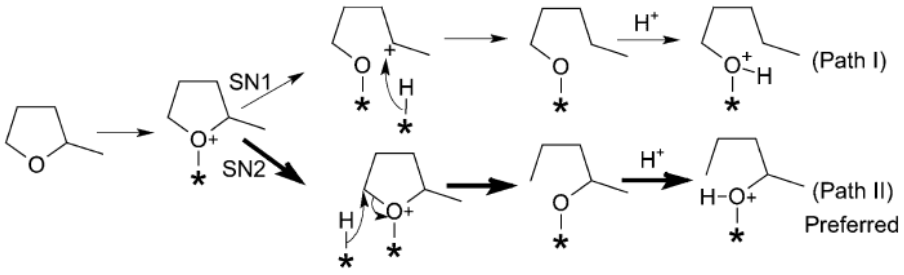

Scheme 1.4 Reaction network of 2-methyltetrahydrofuran HDO on Ni catalysts [115].

Catalyst deactivation is a serious limitation in HDO reactions catalysed by bifunctional metal-acid catalysts [119]. The utilization of strongly acidic catalyst supports may result in the formation of heavy by-products, which can complicate product separation and affect the

yield of the desired products. Thus, the unsaturated oxygenates within bio-oil, especially furans and phenols, interact strongly with Lewis acid sites on the catalyst surface, while Brønsted acid sites provide protons to enhance the formation of carbo-cations, which are precursors of coke. Moreover, catalyst poisoning by water and phosphorus compounds and metal sintering occurs at low H_2 pressure and high temperatures to increase coke formation [120,121]. Factors such as reaction temperature, catalyst acidity, catalyst pore structure and space velocity must be considered in order to minimize catalyst deactivation.

1.3.2.2. Bimetallic Metal-Acid Catalysts

Many studies have reported that bimetallic catalysts show better performance than monometallic catalysts [122−136]. The addition of a second metal may influence both adsorptive and catalytic properties of the first one, which can help to achieve superior catalytic stability and increase catalyst activity and selectivity towards desired products. Pt-based bimetallic catalysts have been the focus of research in recent years to obtain new catalysts that show enhanced selectivity, activity and stability in HDO reactions [123]. Pt and Pd catalysts have been modified by the addition of metals such as Ni, Co, Fe, Zn and Sn in the subsurface to improve performance in hydrogenation and deoxygenation reactions [124−131]. Babu et al. [127] showed that the interaction of Pt with Pd led to electronic modification, which may be the cause of the improved catalytic performance of Pt-Pd catalysts. A similar investigation was carried out on Pt, Pd and alloyed PtPd particles supported on activated carbon for HDO of benzofuran [128]. It was found that HDO activity followed the order PtPd > Pd > Pt. Complete ring hydrogenation was observed before deoxygenation. In contrast, the main route of reaction on Pt/C catalyst involved partial hydrogenation of the furan ring before the hydrogenolysis step.

Dimas-Rivera et al. [129] investigated the role of Pd−Fe/γ-Al_2O_3 (with 0.5 wt% metal content) in the hydrogenation of 2-methylfuran to form the corresponding open-chain C_4−C_5 hydrocarbons and alcohols. The Pd−Fe/γ-Al_2O_3 exhibited a higher conversion rate (31%) at 473K and selectivity for total alcohols of up to 39%, which compared with 5% conversion and 28% alcohol selectivity in the case of Pd/γ-Al_2O_3. It has been reported that the addition of a second metal in bimetallic catalysts can alter the activity and selectivity in ways that depend on the primary metal [130].

Addition of gold as a co-metal has been reported to afford high activity in hydroconversion reactions [132−136]. It should be noted that Au alone does not dissociate H_2; hence it usually shows low activity in hydrotreatment reactions. A carbon-supported PdAu catalyst was employed for the HDO of hydroxymethylfurfural to produce DMF by Nishimura et al. [133]. At 1 bar H_2 pressure and 60 °C, a DMF yield of approximately 100% was achieved. A bimetallic Pd_xAu_y/C catalyst, which was prepared with various Pd/Au molar ratios, showed significantly higher activity than the monometallic Pd/C or Au/C analogues. Charge transfer from Pd to Au is suggested due to PdAu alloy formation. Analysis of the geometric structure showed that gold has fewer near neighbours in the bimetallic catalyst, signifying that gold is enriched. This explains ensemble-size effects on the catalytic performance. Although many studies have proved the effectiveness of supported bimetallic catalysts to upgrade biomass to chemicals and fuels, there remains a lack of knowledge regarding reaction mechanisms, particularly at the gas-solid interface.

1.4. The Scope and Objectives of Thesis

In light of previous research that has been discussed in this chapter, interest has increased in biomass-derived furans as a low-cost renewable feedstock that can be converted to green fuels and value-added chemicals by catalytic hydroconversion. HDO is an effective strategy for the production of fuels from renewable feedstock. Much current research is focused on the HDO of furanic compounds through the utilization of heterogeneous catalysis that employs supported metal catalysts. Complete oxygen removal from furanic compounds over noble metals to produce hydrocarbons requires harsh conditions (200−400 ºC, 7−20 MPa H_2 pressure). Bifunctional metal-acid catalysis has been found to be more efficient than monofunctional metal catalysis for the HDO of organic oxygenates such as ketones, alcohols, phenols, ethers and esters. Previously, bifunctional catalysts that comprise Pt on acidic supports such as zeolites and Keggin-type HPAs have been reported to be highly efficient in the HDO of aliphatic and aromatic ketones in the gas phase. This approach may apply to the HDO of furanic compounds. Previous reports show that in hydroconversion of furanic compounds, Pt is selective to ring-opened products such as ketones and alcohols, whereas Pd, Rh and Ru have high selectivity to ring-saturated tetrahydrofuran derivatives.

The objective of this work was to investigate the HDO of DMF, which was chosen as a model for biomass-derived furanic compounds, in the presence of bifunctional metal-acid catalysts that comprised carbon-supported Pt, Pd, Ru and Rh together with the acidic Cs salt of the Keggin-type tungstophosphoric HPA $Cs_{2.5}H_{0.5}PW_{12}O_{40}$ (CsPW). Attention was focused on the Pt-CsPW catalyst because, among the noble metals, Pt is the most active for furan-ring opening. CsPW is well documented as a solid Brønsted acid catalyst. It has important advantages over the parent HPA $H_3PW_{12}O_{40}$ (HPW), having much larger surface area, higher thermal stability (~500 °C decomposition temperature) and high tolerance to

water, with proton sites almost as strong as those in HPW. The thesis is presented in six chapters as outlined below:

Chapter 1 sets out the background information on heterogeneous catalysis. It includes descriptions of multifunctional catalysis, properties of HPAs and an overview of the catalytic conversion of renewable resources to value-added chemicals and fuels, focused on biomass-derived furanic compounds.

In **Chapter 2,** the experimental techniques that were used in this study are described. They include catalyst preparation, characterisation and testing in a continuous flow fixed-bed reactor.

Chapter 3 presents the results of the kinetic study of hydroconversion of DMF, DMTHF and tetrahydrofuran catalysed by carbon-supported platinum-group metals (Pt, Pd, Rh and Ru) in the gas phase. TOF values are reported and compared with those for the corresponding liquid phase reactions.

Chapter 4 describes the HDO of DMF over bifunctional metal-acid catalysts that comprise carbon-supported Pt and CsPW (Pt-CsPW).

In **Chapter 5,** the kinetics and mechanism of the HDO of DMTHF over bifunctional metal-acid catalyst Pt-CsPW in the gas phase are described.

Chapter 6 describes the effect of gold additives on the activity of the above bifunctional metal-acid catalysts in the HDO of DMTHF.

Finally, **Chapter 7** contains a summary of the results obtained and provides an outlook of possible future research into the HDO of furanic compounds.

References

[1] T. Tong, Q. Xia, X. Liu, Y. Wang, Direct hydrogenolysis of biomass-derived furans over Pt/CeO_2 catalyst with high activity and stability, Catal. Commun. 101 (2017) 129–133.

[2] S. Wang, G. Dai, H. Yang, Z. Luo, Lignocellulosic biomass pyrolysis mechanism: A state-of-the-art review, Prog. Energy Combust. Sci. 62 (2017) 33–86.

[3] M. Akia, F. Yazdani, E. Motaee, D. Han and H. Arandiyan, A review on conversion of biomass to biofuel by nanocatalysts, Biofuel Res. J. 1 (2014) 16–25.

[4] M. Schlaf, Selective deoxygenation of sugar polyols to α, ω-diols and other oxygen content reduced materials—a new challenge to homogeneous ionic hydrogenation and hydrogenolysis catalysis, Dalton Trans. (2006) 4645−4653.

[5] A.K. Kurchania, Biomass energy. In: Biomass conversion, Springer, Berlin, Heidelberg, 2012, pp. 91−93.

[6] A.D. Sutton, F.D. Waldie, R. Wu, M. Schlaf, L.A. 'Pete' Silks, J.C. Gordon, The hydrodeoxygenation of bioderived furans into alkanes, Nat. Chem. 5 (2013) 428−432.

[7] M.I. Jahirul, M. Rasul, A. Chowdhury, N. Ashwath, Biofuels production through biomass pyrolysis–a technological review, Energies 5 (2012) 4952–5001.

[8] G.W. Huber, S. Iborra, A. Corma, Synthesis of transportation fuels from biomass: chemistry, catalysts and engineering, Chem. Rev. 106 (2006) 4044–4098.

[9] J.B. Binder, R.T. Raines, Simple chemical transformation of lignocellulosic biomass into furans for fuels and chemicals. J. Am. Chem. Soc. 131 (2009) 1979–1985.

[10] S. Takkellapati, T. Li, M.A. Gonzalez, An overview of biorefinery-derived platform chemicals from a cellulose and hemicellulose biorefinery, Clean Technol. Environ. Policy 20 (2018) 1615−1630.

[11] L. Qu, X. Jiang, Z. Zhang, X.G. Zhang, G. Song, H. Wang, Y.P. Yuan, Y.L. Chang, A review of hydrodeoxygenation of bio-oil: model compounds, catalysts and equipment, Green Chem. 23 (2021) 9348−9376

[12] C. Baskar, S. Baskar and R.S. Dhillon, Eds., Biomass conversion: The interface of biotechnology, chemistry and materials science, Springer Heidelberg, New York, 2012.

[13] J.A. Melero, J. Iglesias, A. Garcia, Biomass as renewable feedstock in standard refinery units. Feasibility, opportunities and challenges, Energy Environ. Sci. 5 (2012) 7393−7420.

[14] P. Biswas, J.H. Lin, J. Kang, V.V. Guliants, Vapor phase hydrogenation of 2-methylfuran over noble and base metal catalysts, Appl. Catal. A Gen. 475 (2014) 379–385.

[15] E. Furimsky, The mechanism of catalytic hydrodeoxygenation of furan, Appl. Catal. 6 (1983) 159–164.

[16] Y. Rom an-Leshkov, C.J. Barrett, Z.Y. Liu, J.A. Dumesic, Production of dimethylfuran for liquid fuels from biomass-derived carbohydrates, Nature 447 (2007) 982–986.

[17] M.K. Bowker, The Basis and Applications of Heterogeneous Catalysis, Oxford Chemistry Primers, New York, 1998.

[18] G.C. Bond, Heterogeneous catalysis: principles and applications, Clarendon Press, Oxford, 1974.

[19] J.M. Thomas, W.J. Thomas, Principles and practice of heterogeneous catalysis, Wiley, Weinheim, 1996.

[20] M. Misono, Basis of Heterogeneous catalysis in: heterogeneous catalysis of mixed oxides, Elsevier, 176 (2013) 1−23.

[21] J.W.N. Chorkendorff, Concepts of modern catalysis and kinetics, Wiley-VCH, Weinheim, 2003.

[22] R. Prins, A. Wang, X. Li, Introduction to heterogeneous catalysis, World Scientific Publishing, London, 2016.

[23] F. Dumeignil, J.F. Paul, S. Paul, Heterogeneous catalysis with renewed attention: principles, theories and concepts, J. Chem. Educ. 94 (2017) 675–689.

[24] G. Ertl, H. Knözinger, J. Weitkamp, Handbook of heterogeneous catalysis, Wiley-VCH, Weinheim, 1997.

[25] N. Mizuno, M. Misono, Heterogeneous catalysis, Chem. Rev. 98 (1998) 199−218.

[26] M. Boudart, Turnover rates in heterogeneous catalysis, Chem. Rev. 95 (1995) 661−666.

[27] P.N. Rylander, Catalytic hydrogenation over platinum metals, Academic Press, New York, 1967.

[28] G.C. Bond, Metal-catalysed reactions of hydrocarbons, Springer, New York, 2005.

[29] M. Boudart, Catalysis by supported metals, Adv. Catal. 20 (1969) 153–166.

[30] F. Pinna, Supported metal catalysts preparation, Catal. Today 41(1998)129–137.

[31] J.T. Richardson, Principle of catalysts development, Plenum Press, 1989

[32] M. Boudart, Heterogeneous catalysis by metals, J. Mol. Catal. 30 (1985) 27–38.

[33] W.C. Conner, J.L. Falconer, Spillover in heterogeneous catalysis, Chem. Rev. 95 (1995) 759−788.

[34] G.K. Borsekov, M.G. Slinko, V.S. Chesalova, Specific Catalytic activity of platinum. II. Reaction of oxygen interaction with hydrogen, Rus. J. Phys. Chem. A. 30 (1956) 2787.

[35] I.V. Kozhevnikov, Catalysis by heteropoly acids and multicomponent polyoxometalates in liquid phase reactions, Chem. Rev. 98 (1998) 171–198.

[36] S. Soled, S. Miseo, G. Mc Vicker, W. E. Gates, A Gutierrez, J. Paes, Preparation of bulk and supported heteropolyacid salts, Catal. Today 36 (1997) 441.

[37] I.V. Kozhevnikov, Sustainable heterogeneous acid catalysis by heteropoly acids, J. Mol. Catal. A Chem. 262 (2007) 86−92.

[38] I.V. Kozhevnikov, Catalysts for fine chemical synthesis, catalysis by polyoxometalates, Wiley, Chichester, 2002.

[39] Y. Izumi, R. Hasebe, K. Urabe, Catalysis by heterogeneous supported heteropoly acid, J. Catal. 84 (1983) 402−409.

[40] M.J. Janik, R.J. Davis, M. Neurock, A first principles analysis of the location and affinity of protons in the secondary structure of phosphotungstic acid, J Phys. Chem. B 108 (2004) 12292−12300.

[41] M. Misono, Unique acid catalysis of heteropoly compounds (heteropolyoxometalates) in the solid state, Chem. Commun. (2001) 1141−1152.

[42] K. Wilson, A.F. Lee, J.P. Dacquin, Heterogeneous catalysts for converting renewable feedstocks to fuels and chemicals. In Catalysis for Alternative Energy Generation, Springer, New York, NY. (2012) 263−304.

[43] T. Okuhara, Microporous heteropoly compounds and their shape selective catalysis, Appl. Catal. A Gen. 256 (2003) 213–224.

[44] T. Okuhara, N. Mizuno, M. Misono, Catalytic chemistry of heteropoly compounds, Adv. Catal. 41 (1996) 113–252.

[45] S. Soled, S. Miseo, G. McVicker, W.E. Gates, A. Gutierrez, J. Paes, Preparation and catalytic properties of supported heteropolyacid salts, Chem. Eng. J. 64 (1996) 247−254.

[46] T. Okuhara, T. Nishimura, H. Watanabe, K. Na, M. Misono, Novel catalysis of cesium salt of heteropoly acid and its characterization by solid-state NMR, Stud. Surf. Sci. Catal, 90 (1994) 419−428.

[47] T. Okuhara, T. Nakato, Catalysis by porous heteropoly compounds, Catal. Surv. 2 (1998) 31−44.

[48] A. Bruggink, R. Schoevaart, T. Kieboom, Concepts of nature in organic synthesis: cascade catalysis and multistep conversions in concert, Org. Proc. Res. Dev. 7 (2003) 622−640.

[49] J.C. Wasilke, S.J. Obrey, R.T. Baker, G.C. Bazan, Concurrent tandem catalysis, Chem. Rev. 105 (2005) 1001−1020.

[50] A.M. Robinson, J.E. Hensley, J.W. Medlin, Bifunctional catalysts for upgrading of biomass-derived oxygenates: A review, ACS Catal. 6 (2016) 5026–5043.

[51] F. Roessner, U. Roland, J. Mol., Hydrogen spillover in bifunctional catalysis, Catal. A Chem. 112 (1996) 401–412.

[52] O'Driscoll, J.J. Leahy, T. Curtin, The influence of metal selection on catalyst activity for the liquid phase hydrogenation of furfural to furfuryl alcohol, Catal. Today 279 (2017) 194–201.

[53] S. Itagaki, N. Matsuhashi, K. Taniguchi, K. Yamaguchi, N. Mizuno, Efficient hydrodeoxygenation of ketones, phenols and ethers promoted by platinum-heteropolyacid bifunctional catalysts, Chem. Lett. 43 (2014) 1086–1088.

[54] L. Guczi, Z. Schay, Role of bimetallic catalysts in catalytic hydrogenation and hydrogenolysis. Stud. Surf. Sci. Catal. 27 (1986) 313-335.

[55] F. Tao, M.E. Grass, Y. Zhang, D.R. Butcher, F. Aksoy, S. Aloni, V. Altoe, S. Alayoglu, J.R. Renzas, C.K. Tsung, Evolution of structure and chemistry of bimetallic nanoparticle catalysts under reaction conditions. J. Am. Chem. Soc. 132 (2010) 8697–8703.

[56] M. Sankar, N. Dimitratos, P.J. Miedziak, P.P. Wells, C.J. Kiely, G.J. Hutchings, Designing bimetallic catalysts for a green and sustainable future. Chem. Soc. Rev. 41 (2012) 8099–8139.

[57] T. Bligaard, J.K. Nørskov, Ligand effects in heterogeneous catalysis and electrochemistry. Electrochim. Acta 52 (2007) 5512–5516.

[58] J. H. Sinfelt, Bimetallic Catalysts: Discoveries, Concepts and Applications, John Wiely & Sons. Inc., New Yor, 1983.

[59] V. Dal Santo, A. Gallo, A. Naldoni, M. Guidotti, R. Psaro, Bimetallic heterogeneous catalysts for hydrogen production. Catal. Today 197 (2012) 190–205.

[60] D.M. Alonso, S.G. Wettstein, J.A. Dumesic, Bimetallic catalysts for upgrading of biomass to fuels and chemicals, Chem. Soc. Rev. 41 (2012) 8075–8098.

[61] B. Coq, F. Figueras, J. Mol, Bimetallic palladium catalysts: influence of the co-metal on the catalyst performance, J. Mol. Catal. A 173 (2001) 117−134.

[62] F. Gao, W. Goodman, Pd–Au bimetallic catalysts: understanding alloy effects from planar models and (supported) nanoparticles, Chem. Soc. Rev. 41 (2012) 8009−8020.

[63] Y. Qian, L. Zhu, Y. Wang, X. Lu, Recent progress in the development of biofuel 2,5-dimethylfuran, Renew. Sust. Energ. Rev. 41 (2015) 633−646.

[64] C. Aliaga, C.K. Tsung, S. Alayoglu, K. Komvopoulos, P. Yang, G.A. Somorjai, Sum frequency generation vibrational spectroscopy and kinetic study of 2-methylfuran and 2, 5-dimethylfuran hydrogenation over 7 nm platinum cubic nanoparticles, Phys. Chem. C 115 (2011) 8104–8109.

[65] J. Kang, A. Vonderheide, V.V. Guliants, Deuterium-labeling study of the hydrogenation of 2-methylfuran and 2,5-dimethylfuran over carbon supported noble metal catalysts, ChemSusChem 8 (2015) 3044–3047.

[66] M.J. Gilkey, A.V. Mironenko, L. Yang, D.G. Vlachos, B. Xu, Insights into the ring-opening of biomass-derived furanics over carbon-supported ruthenium. ChemSusChem, 9 (2016) 3113−3121.

[67] Y.L. Louie, J. Tang, A.M.L. Hell, A.T. Bell, Kinetics of hydrogenation and hydrogenolysis of 2,5-dimethylfuran over noble metals catalysts under mild conditions, Appl. Catal. B Environ. 202 (2017) 557–568.

[68] H. Goto, A. Takagaki, R. Kikuchi, S.T. Oyama, Hydrogenation of 2,5-dimethylfuran on hexagonal-boron nitride- and silica-supported platinum catalysts, Appl. Catal. A 548 (2017) 122–127.

[69] T. Tong, X. Liu, Y. Guo, M. Norouzi Banis, Y. Hu, Y. Wang, Direct hydrogenolysis of biomass-derived furans over Pt/CeO_2 catalyst with high activity and stability, Catal. Commun. 101 (2017) 129–133.

[70] A. Corma, O. de la Torre, M. Renz, Production of high quality diesel from cellulose and hemicellulose by the sylvan process: catalysts and process variables, Energy Environ. Sci. 5 (2012) 6328.

[71] V. Vorotnikov, D.G. Vlachos, Group additivity and modified linear scaling relations for estimating surface thermochemistry on transition metal surfaces: Application to furanics, J. Phys. Chem. C 119 (2015) 10417−10426.

[72] M. Snåre, I. Kubicková, P. Mäki-Arvela, D. Chichova, K. Eränen, D.Y. Murzin, Catalytic deoxygenation of unsaturated renewable feedstocks for production of diesel fuel hydrocarbons. Fuel 87 (2008) 933−945.

[73] E. Furimsky, Catalytic hydrodeoxygenation, Appl. Catal. A Gen. 199 (2000) 147–190.

[74] Z. He, X. Wang, Hydrodeoxygenation of model compounds and catalytic systems for pyrolysis bio-oils upgrading, Catal. Sustain. Energy 1 (2012) 28−52.

[75] Z. Si, X. Zhang, C. Wang, L. Ma, R. Dong, An overview on catalytic hydrodeoxygenation of pyrolysis oil and its model compounds, Catalysts 7 (2017) 169.

[76] H. Pourzolfaghar, F. Abnisa, W. M. A. Wan Daud and M. K. Aroua, Atmospheric hydrodeoxygenation of bio-oil oxygenated model compounds: A review, J. Anal. Appl. Pyrolysis 133 (2018) 117–127.

[77] S. Kim, E.E. Kwon, Y.T. Kim, S. Jung, H.J. Kim, G.W. Huber, J. Lee, Recent advances in hydrodeoxygenation of biomass-derived oxygenates over heterogeneous catalysts,

Green Chem. 21 (2019) 3715–3743.

[78] S. Dutta, Hydro (deoxygenation) reaction network of lignocellulosic oxygenates, ChemSusChem 13 (2020) 2894−2915.

[79] M. Chia, Y.J. Pagán-Torres, D. Hibbitts, Q. Tan, H.N. Pham, A.K. Datye, M. Neurock, R.J. Davis, J.A. Dumesic, Selective hydrogenolysis of polyols and cyclic ethers over bifunctional surface sites on rhodium–rhenium catalysts, J. Am. Chem. Soc. 133 (2011) 12675−12689.

[80] K. Tomishige, Y. Nakagawa, M. Tamura, Selective hydrogenolysis and hydrogenation using metal catalysts directly modified with metal oxide species, Green Chem. 19 (2017) 2876−2924.

[81] D.Sun, S. Sato, W. Ueda, A. Primo, H. Garcia, A. Corma, Production of C4 and C5 alcohols from biomass-derived materials, Green Chem. 18 (2016) 2579−2597.

[82] P. Bui, J.A. Cecilia, S.T. Oyama, A. Takagaki, A. Infantes-Molina, H. Zhao, D. Li, E. Rodríguez-Castellón, A.J. López, Studies of the synthesis of transition metal phosphides and their activity in the hydrodeoxygenation of a biofuel model compound, J. Catal. 294 (2012) 184−198.

[83] Y. Okamoto, A. Maezawa, T. Imanaka, Active sites of molybdenum sulfide catalysts supported on Al_2O_3 and TiO_2 for hydrodesulfurization and hydrogenation, J. Catal. 120 (1989) 29−45.

[84] J. He, S.P. Burt, M.R. Ball, I. Hermans, J.A. Dumesic, G.W. Huber, Catalytic CO bond hydrogenolysis of tetrahydrofuran-dimethanol over metal supported WOx/TiO_2 catalysts, Appl. Catal. B 258 (2019) 117945.

[85] R.J. Sullivan, E. Latifi, B.K.M. Chung, D.V. Soldatov, M. Schlaf, Hydrodeoxygenation of 2,5-hexanedione and 2,5-dimethylfuran by water, air and acid stable homogeneous ruthenium and iridium catalysts, ACS Catal. 4 (2014) 4116–4128.

[86] D. Hibbitts, Q. Tan and M. Neurock, Acid strength and bifunctional catalytic behavior of alloys comprised of noble metals and oxophilic metal promoters, J. Catal. 315 (2014) 48–58.

[87] C.R. Waidmann, A.W. Pierpont, E.R. Batista, J.C. Gordon, R.L. Martin, R.M. West, R. Wu, Functional group dependence of the acid catalyzed ring opening of biomass derived furan rings: an experimental and theoretical study, Catal. Sci. Technol. 3 (2013) 106−115.

[88] T. Buntara, I. Melián-Cabrera, Q. Tan, J.L.G. Fierro, M. Neurock, J.G. de Vries, H.J. Heeres, Catalyst studies on the ring opening of tetrahydrofuran dimethanol to 1,2,6-hexanetriol, Catal. Today 210 (2013) 106–116.

[89]

[90] A.R. Ardiyanti, A. Gutierrez, M.L. Honkela, A.O. I. Krause, H.J. Heeres, Hydrotreatment of wood-based pyrolysis oil using zirconia-supported mono-and bimetallic (Pt, Pd, Rh) catalysts, Appl. Catal. A Gen. 407 (2011) 56–66.

[91] R.C. Runnebaum, T. Nimmanwudipong, J. Doan, D.E. Block, B.C. Gates, Catalytic conversion of furan to gasoline-range aliphatic hydrocarbons via ring opening and decarbonylation reactions catalyzed by Pt/γ-Al_2O_3, Catal. Lett. 142 (2012) 664-666.

[92] B.M. Moreno, N. Li, J. Lee, G.W. Huber, M. T. Klein, Modeling aqueous-phase hydrodeoxygenation of sorbitol over Pt/SiO_2-Al_2O_3, RSC Adv. 3 (2013) 23769–23784.

[93] H.W. Lee, B.R. Jun, H. Kim, D.H. Kim, J.K Jeon, S.H. Park, C.H. Ko, T.W. Kim, Y.K. Park, Catalytic hydrodeoxygenation of 2-methoxy phenol and dibenzofuran over Pt/mesoporous zeolites, Energy 81 (2015) 33−40.

[94] X. Li, X. Niu, S. Zhu, S. Xu, Z. Wang, X. Zhang, Q. Wang, Highly selective hydrodeoxygenation of dibenzofuran into bicyclohexane over hierarchical Pt/ZSM-5 catalysts, Ind. Eng. Chem. Res. 60 (2021) 2838−2848.

[95] H. Wang, H. Wang, E. Kuhn, M.P. Tucker, B. Yang, Production of jet fuel-range hydrocarbons from hydrodeoxygenation of lignin over super lewis acid combined with metal catalysts, ChemSusChem 11(2018) 285−291.

[96] M.J. Gilkey, D.G. Vlachos, B. Xu, Poisoning of Ru/C by homogeneous Brønsted acids in hydrodeoxygenation of 2, 5-dimethylfuran via catalytic transfer hydrogenation, Appl. Catal. A Gen. 542 (2017) 327–335.

[97] B.O. de Beeck, M. Dusselier, J. Geboers, J. Holsbeek, E. Morré, S. Oswald, L. Giebeler, B.F. Sels, Direct catalytic conversion of cellulose to liquid straight-chain alkanes, Energy Environ. Sci. 8 (2015) 230−240.

[98] S. Zhao, G. Xu, C. Chang, S. Fang, Z. Liu, F. Du, Direct conversion of carbohydrates into ethyl levulinate with potassium phosphotungstate as an efficient catalyst, Catalysts 5 (2015)1897−1910.

[99] Y. Liu, C.L. Liu, H.Z. Wu, W.S. Dong, An Efficient catalyst for the conversion of fructose into methyl levulinate, Catal. Lett. 143 (2013) 1346–1353.

[100] M.A. Alotaibi, E.F. Kozhevnikova, I.V. Kozhevnikov, Hydrogenation of methyl isobutyl ketone over bifunctional Pt–zeolite catalyst, J. Catal. 293 (2012) 141−144.

[101] M.A. Alotaibi, E.F. Kozhevnikova, I.V. Kozhevnikov, Efficient hydrodeoxygenation of biomass-derived ketones over bifunctional Pt-polyoxometalate catalyst, Chem. Commun. 48 (2012) 7194−7196.

[102] K. Alharbi, E.F. Kozhevnikova, I.V. Kozhevnikov, Hydrogenation of ketones over bifunctional Pt-heteropoly acid catalyst in the gas phase, Appl. Catal. A 504 (2015) 457−462.

[103] V. Kogan, Z. Aizenshtat, R. Neumann, Preferential catalytic hydrogenation of aromatic compounds versus ketones with a palladium substituted polyoxometalate as pre-catalyst, New J. Chem. 26 (2002) 272−274.

[104] M.A. Alotaibi, E.F. Kozhevnikova, I.V. Kozhevnikov, Deoxygenation of propionic acid on heteropoly acid and bifunctional metal-loaded heteropoly acid catalysts: Reaction pathways and turnover rates, Appl. Catal. A 447 (2012) 32–40.

[105] A.B. Gawade, M.S. Tiwari, G.D. Yadav, Biobased green process: Selective hydrogenation of 5-hydroxymethylfurfural to 2,5-dimethyl furan under mild conditions using Pd-$Cs_{2.5}H_{0.5}PW_{12}O_{40}$/K-10 clay, ACS Sustain. Chem. Eng. 4 (2016) 4113−4123.

[106] F. Xue, D. Ma, T. Tong, X. Liu, Y. Hu, Y. Guo, Y. Wang, Contribution of different NbOx species in the hydrodeoxygenation of 2,5-dimethyltetrahydrofuran to hexane, ACS Sustain. Chem. Eng. 6 (2018) 13107−13113.

[107] Q.N. Xia, Q. Cuan, X.H. Liu, X.Q. Gong, G.Z. Lu, Y.Q. Wang, Pd/$NbOPO_4$ multifunctional catalyst for the direct production of liquid alkanes from aldol adducts of furans, Angew. Chemie Int. Ed. 53 (2014) 9755–9760.

[108] M. Chia, Y.J. Pagán-Torres, D. Hibbitts, Q. Tan, H.N. Pham, A.K. Datye, M. Neurock, R.J. Davis, J.A. Dumesic, Selective hydrogenolysis of polyols and cyclic ethers over bifunctional surface sites on rhodium–rhenium catalysts, J. Am. Chem. Soc. 133 (2011) 12675−12689.

[109] Q. Xia, Z. Chen, Y. Shao, X. Gong, H. Wang, X. Liu, S.F. Parker, X. Han, S. Yang, Y. Wang, Direct hydrodeoxygenation of raw woody biomass into liquid alkanes, Nat. Commun. 7 (2016) 1−10.

[110] J.G. Dickinson, J.T. Poberezny, P.E. Savage, Deoxygenation of benzofuran in supercritical water over a platinum catalyst, Appl. Catal. B Environ. 123 (2012) 357–366.

[111] M. Boudar, G. Djega-Mariadassou, Kinetic coupling in and between catalytic cycles, Catal. Lett.. 29 (1994) 7−13.

[112] X. Li, G. Li, W. Zang, L. Wang, X. Zhang, Catalytic activity of shaped platinum

nanoparticles for hydrogenation: a kinetic study, Catal. Sci. Technol. 9 (2014) 3290−3297.

[113] S. Sitthisa, T. Sooknoi, Y. Ma, P.B. Balbuena, D.E. Resasco, Kinetics and mechanism of hydrogenation of furfural on Cu/SiO_2 catalysts, J. Catal. 277 (2011) 1−13.

[114] C.L. Lee, D.F. Ollis, Catalytic hydrodeoxygenation of benzofuran and o-ethylphenol, J. Catal. 87 (1984) 325–331.

[115] P. Bui, A. Takagaki, R. Kikuchi, S.T. Oyama, Kinetic and infrared spectroscopy study of hydrodeoxygenation of 2-methyltetrahydrofuran on a nickel phosphide catalyst at atmospheric pressure, ACS Catal. 6 (2016) 7701–7709.

[116] M.C. Edelman, M.K. Maholland, R.M. Baldwin, S.W. Cowley, Vapor-phase catalytic hydrodeoxygenation of benzofuran, J. Catal. 111 (1988) 243–253.

[117] V. LaVopa, C.N. Satterfield, Catalytic hydrodeoxygenation of dibenzofuran, Energy & Fuels. 1 (1987) 323–331.

[118] L.A. Petrov, Y. Alhamed, A. Al-Zahrani, M. Daous, Role of chemical kinetics in the heterogeneous catalysis studies, Chinese J. Catal. 32 (2011) 1085–1112.

[119] E. Furimsky, F. E. Massoth, Deactivation of hydroprocessing catalysts, Catal. Today. 52 (1999) 381–495.

[120] V.N. Bui, D. Laurenti, P. Delichère, C. Geantet, Hydrodeoxygenation of guaiacol. Part II: Support effect for CoMoS catalysts on HDO activity and selectivity, Appl. Catal. B Environ. 101 (2011) 246–255.

[121] E. Laurent, B. Delmon, Study of the hydrodeoxygenation of carbonyl, carboxylic and guaiacyl groups over sulfided $CoMo/Al_2O_3$ and $NiMo/Al_2O_3$ catalyst: II. Influence of water, ammonia and hydrogen sulfide, Appl. Catal. A: Gen 109(1994) 97−115.

[122] J.R. Kitchin, J.K. Norskov, M.A. Barteau, J.G. Chen, Role of strain and ligand effects in the modification of the electronic and chemical properties of bimetallic surfaces, Phys. Rev. Lett. 93 (2004) 156801.

[123] E. Bus, J.A. Van Bokhoven, Electronic and geometric structures of supported platinum, gold and platinum−gold catalysts, J. Phys. Chem. C 111 (2007) 9761–9768.

[124] W. Yu, M.D. Porosoff, J.G. Chen, Review of Pt-based bimetallic catalysis: from model surfaces to supported catalysts, Chem. Rev. 112 (2012) 5780–5817.

[125] D.M. Alonso, S.G. Wettstein, J.A. Dumesic, Bimetallic catalysts for upgrading of biomass to fuels and chemicals, Chem. Soc. Rev. 41 (2012) 8075−8098.

[126] O.S. Alexeev, B.C. Gates, Supported bimetallic cluster catalysts, Ind. Eng. Chem. 42 (2003) 1571−1587.

[127] P.K. Babu, H.S. Kim, J.H. Chung, E. Oldfield, A. Wieckowski, Bonding and motional aspects of CO adsorbed on the surface of Pt nanoparticles decorated with Pd, J. Phys. Chem. B 108 (2004) 20228−20232.

[128] C. Liu, Z. Shao, Z. Xiao, C. Liang, Hydrodeoxygenation of benzofuran over activated carbon supported Pt, Pd and Pt–Pd catalysts, React. Kinet. Mech. Catal. 107 (2012) 393−404.

[129] G.L. Dimas-Rivera, J.R. De la Rosa, C.J. Lucio-Ortiz, D.X. Martínez-Vargas, L. Sandoval-Rangel, D.I.G. Gutiérrez, C.S. Maldonado, Bimetallic Pd-Fe supported on γ-Al_2O_3 catalyst used in the ring opening of 2-methylfuran to selective formation of alcohols, Appl. Catal. A 543 (2017) 133−140.

[130] T. Li, N. Ji, Z. Jia, X. Diao, Z. Wang, Q. Liu, C. Song, X. Lu, Effects of metal promoters in bimetallic catalysts in hydrogenolysis of lignin derivatives into value-added chemicals, ChemCatChem 12 (2020) 5288−5302.

[131] B. Saha, C.M. Bohn, M.M. Abu-Omar, Zinc-assisted hydrodeoxygenation of biomass–derived 5-hydroxymethylfurfural to 2,5-dimethylfuran, ChemSusChem 7 (2014) 3095–3101.

[132] L. McEwan, M. Julius, S. Roberts, J.C.Q. Fletcher, A review of the use of gold catalysts in selective hydrogenation reactions, Gold Bull. 43 (2010) 298–307.

[133] S. Nishimura, N. Ikeda, K. Ebitani, Selective hydrogenation of biomass-derived 5-hydroxymethylfurfural (HMF) to 2,5-dimethylfuran (DMF) under atmospheric hydrogen pressure over carbon supported PdAu bimetallic catalyst, Catal. Today. 232 (2014) 89–98.

[134] O. Poole, K. Alharbi, D. Belic, E.F. Kozhevnikova, I.V Kozhevnikov, Hydrodeoxygenation of 3-pentanone over bifunctional Pt-heteropoly acid catalyst in the gas phase: Enhancing effect of gold, Appl. Catal. B Environ. 202 (2017) 446–453.

[135] K. Sun, A.R. Wilson, S.T. Thompson, H.H. Lamb, Catalytic deoxygenation of octanoic acid over supported palladium: effects of particle size and alloying with gold, ACS Catal. 5 (2015) 1939−1948.

[136] T.J. Schwartz, S.D. Lyman, A.H. Motagamwala, M.A. Mellmer, J.A. Dumesic, Selective hydrogenation of unsaturated carbon–carbon bonds in aromatic-containing platform molecules, ACS Catal. 6 (2016) 2047−2054.

Chapter 2. Experimental Techniques

2

2.1. Chemicals and Catalysts

Chemicals and catalysts were purchased from different sources. 2,5-Dimethylfuran (99%) was purchased from Acros Organics. Tetrahydrofuran (99%), 2,5-dimethyltetrahydrofuran (*cis/trans* isomer mixture) (96%) and 2-hexanol (98%) were purchased from Sigma-Aldrich. 2-Hexanone (98%) was purchased from Alfa Aesar and n-hexane (98%) from Fisher Chemicals. 1%Pt/Al_2O_3 and carbon-supported noble metal catalysts 7.0%Pt/C, 9.6%Pt/C, 7.8%Pd/C, 3.0%Ru/C and 4.0%Rh/C were from Sigma-Aldrich; these were oven dried at 100 °C prior to use. The metal loading in these catalysts was determined after drying in-house by inductively coupled plasma optical emission spectroscopy (ICP-OES) analysis. 7.0%Pt/C and 9.6%Pt/C were different samples of the same commercial catalyst with different moisture content after oven drying. H_2PtCl_6 hydrate, $Pt(acac)_2$, $PdCl_2$ hydrate and $HAuCl_4$ were also purchased from Sigma-Aldrich. Heteropoly acid hydrate $H_3PW_{12}O_{40}$ (HPW, 99%) was purchased from Sigma-Aldrich. The amount of crystallization water in the heteropoly acid was determined by TGA. Zeolites NH_4^+-ZSM-5 (Si/Al = 12 and 47, specific surface area S_{BET} = 400 $m^2\ g^{-1}$) were from Zeolyst International. The zeolites were converted into the H^+ forms by air calcination at 500 °C for 6 h; these are hereinafter designated as HZSM-5-12 and HZSM-5-47. Commercial Aerosil 300 silica support ($S_{BET} \approx 300\ m^2g^{-1}$) was from Degussa. H_2 (>99%) was supplied by the British Oxygen Company.

2.2. Catalysts Preparation

2.2.1. Preparation of Cesium Salt of 12-Tungstophosphoric Acid (CsPW)

Cesium tungstophosphate $Cs_{2.5}H_{0.5}PW_{12}O_{40}$ (CsPW) was prepared according to the literature procedure [1, 2] by partial neutralization of the heteropoly acid with Cs^+ cation to form porous insoluble salts. CsPW was prepared by adding dropwise the required amount of aqueous solution of cesium carbonate Cs_2CO_3 (0.47 M) to an aqueous solution of heteropoly acid $H_3PW_{12}O_{40}$ (0.75 M) at 40 °C with continuous stirring. The precipitate obtained was aged in an aqueous slurry for 48 h at room temperature. The slurry was then slowly evaporated to dryness in a rotary evaporator at 45 °C to afford CsPW as a white precipitate, which was isolated, vacuum dried at 150 °C/10^{-3} kPa for 1.5 h and ground to 45–180 μm particle size.

2.2.2. Preparation of Silica-Supported Heteropoly Acid (HPW/SiO_2)

Silica-supported $H_3PW_{12}O_{40}$ catalyst (25%HPW/SiO_2) was prepared (6 g total catalyst weight) by wet impregnation of 4.5 g Aerosil 300 silica in 60−80 ml aqueous solution of HPW (1.75 g) [3]. The mixture was stirred for 4 h and left overnight at room temperature, followed by drying in a rotary evaporator. Finally, the catalyst was vacuum dried at 150 °C/10^{-3} kPa for 1.5 h. Silica-supported HPW catalyst was kindly provided by Mrs. Rawan Alfaze.

2.2.3. Preparation of Pt/CsPW

Two kinds of CsPW-supported bifunctional Pt-acid catalyst was prepared through the wet impregnation method using excess solvent. The support was mixed with a solution of Pt precursor and then dried and reduced by H_2 [4,5]. The first catalyst, 1.0%Pt/CsPW-w, was

obtained from aqueous solution of H_2PtCl_6. The second, 1.0%Pt/CsPW-b, was prepared water-free from benzene solution of platinum (II) acetylacetonate $Pt(acac)_2$.

1.0%Pt/CsPW-w (3 g total catalyst weight) was prepared by wet impregnation of CsPW powder with an aqueous solution of H_2PtCl_6 as described previously [6]. The water content in H_2PtCl_6 was determined by thermogravimetric analysis (TGA). CsPW (2.97 g) was added with stirring to 0.02 M aqueous solution of H_2PtCl_6 (0.1 g) at 40−50 °C. After stirring for 3 h, the obtained pale-yellow suspension was allowed to stand overnight at room temperature. The water was removed using a rotary evaporator to obtain a pale-yellow solid. Then the sample was reduced by a hydrogen flow at 250 °C for 2 h. A similar catalyst designated as 1.0%Pt/CsPW-b (3 g total catalyst weight) was prepared by adding a benzene solution of $Pt(acac)_2$ to CsPW. This was done by stirring CsPW powder (2.97 g) with 0.02 M solution of $Pt(acac)_2$ (0.06 g) in benzene at 40−50 °C for 2 h followed by rotary evaporation of benzene at room temperature and reduction by hydrogen as above. The Pt content in the catalyst was determined by ICP-OES elemental analysis.

2.2.4. Preparation of Au/CsPW

4.7%Au/CsPW (2 g total catalyst weight) was prepared via wet impregnation method by adding 0.02 M aqueous solution of $HAuCl_4$ (0.20 g) to CsPW (1.8 g) at 50 °C with stirring. The slurry was left for 2 h and then evaporated to dryness on a rotary evaporator. The resulting powder was reduced with a H_2 flow at 250 °C for 2 h.

2.2.5 Preparation of PtAu/CsPW

5.9%Pt/4.4%Au/CsPW (2 g total catalyst weight) was prepared via wet co-impregnation method by adding an aqueous solution of H_2PtCl_6 (0.02 g) and $HAuCl_4$ (0.03 g) to CsPW (1.95 g) at 50 °C with stirring then left for 2 hours. The resulting slurry was then rotary evaporated to dryness and reduced with a H_2 flow at 250 °C for 2 hours.

2.2.6. Preparation of Silica-Supported Metal Catalysts (Pt/SiO_2, Pd/SiO_2 and Au/SiO_2)

6.0%Pt/SiO_2, 6.0%Pd/SiO_2 and 6.0%Au/SiO_2 were prepared by wet impregnation method (4 g each catalyst weight) using Aerosil 300 silica support and H_2PtCl_6, $PdCl_2$ and $HAuCl_4$ as the metal precursors followed by rotary evaporation to dryness and reduction with H_2 flow at 250 ºC for 2 h.

2.2.7. Preparation of bimetallic catalysts ($PtPd/SiO_2$, $PtAu/SiO_2$ and $PdAu/SiO_2$)

All these catalysts were prepared by wet co-impregnation of metal precursors onto Aerosil 300 silica (surface area S_{BET} = 300 m^2g^{-1}) followed by reduction with H_2. 6.0%Pt/6.0%Au/SiO_2 catalyst was prepared by adding an aqueous solution (0.02 M) of H_2PtCl_6 (0.71 g) and $HAuCl_4$ (0.48 g) to Aerosil 300 silica (3.5 g) at 50 °C with stirring. The slurry was left overnight then rotary evaporated. The resulting powder was reduced with a H_2 flow at 250 °C for 2 h.

Similarly, the 6.0%Pt/6.0%Pd/SiO_2 and 6.0%Pd/6.0%Au/SiO_2 bimetallic catalysts (4 g catalyst weight) were prepared using 0.02 M aqueous solutions of H_2PtCl_6 (0.71 g), $PdCl_2$ (0.39 g) and $HAuCl_4$ (0.48 g) at 50 °C with stirring. The slurry was left overnight then rotary evaporated to dryness. Catalyst powders was reduced with a H_2 flow at 250 °C for 2 h. The loading expected from the preparation stoichiometry agreed with the loading resulted from ICP-OES analysis (e.g., 6.0%Pt/6.0%Au/SiO_2 from stoichiometry and 6.6%Pt/5.9%Au/SiO_2 from ICP-OES analysis).

2.3. Catalyst Characterisation Techniques

2.3.1. Surface Area and Porosity

Brunauer–Emmett–Teller (BET) and Barrett–Joyner–Halenda (BJH) models are the commonly used methods for the characterisation of the texture of porous solid catalysts. BET is employed to evaluate the specific surface area. The BJH method is employed to calculate pore size distribution and pore volume. Experimentally, physical adsorption of N_2 is measured at -196 ^oC, the N_2 boiling point. The nitrogen isotherm is obtained by plotting the volume of nitrogen adsorbed against its relative pressure P/P_o [7−16]. The BET adsorption is described by equation (2.1).

$$\frac{P}{V(P_0-P)} = \frac{1}{V_m C} + \frac{C-1}{V_m C} \times \frac{P}{P_0} \quad (2.1)$$

In this equation, V is the volume of adsorbed gas at the equilibrium pressure P, V_m is the volume of adsorbed gas to form a monolayer, P_o is the saturation pressure of adsorbate and C is a constant at standard temperature and pressure conditions (STP).

The plot of $\frac{P}{V(P_0-P)}$ against $\frac{P}{P_0}$ is linear in the range of relative pressures $\frac{P}{P_0}$ = 0.05−0.2, from which V_m and C are calculated. Then, the total surface area (SA_{total}) can be calculated by applying Eq. 2.2, where V_0 is the molar volume of nitrogen at standard conditions.

$$SA_{total} = (\frac{V_m}{V_0})\, N_a\, \sigma \quad (2.2)$$

It is assumed that every molecule of adsorbed N_2 occupies the cross-section surface area of a single adsorbed gas molecule (σ =16.2×10^{-22} m^2), N_a is Avogadro's number of molecules per mole (6.023×10^{23}), V_0 is the molar volume of one mole of gas at STP conditions (22414×10^{-6} m^3/mol) and M is the sample weight (g), The specific surface area, S_{BET}, is calculated as follows:

$$S_{BET}\left[\frac{m^2}{g}\right] = \frac{V_m\,(m^3)\times 6.023\ X\ 10^{23}\left(\frac{molecules}{mol}\right)\times 16.2\times 10^{-22}\,\left(\frac{m^2}{N^2\ molecular}\right)}{22414\times 10^{-6}\frac{m^3}{mol}\times M\,(g)} \quad (2.3)$$

Furthermore, the isotherms of mesoporous solids display hysteresis, that is adsorption and desorption do not follow the same path due to capillary condensation [12]. According to the IUPAC classification, there are four kinds of hysteresis loops experimentally observed in adsorption isotherms for mesoporous materials depending on the shape of pores [13].

In this work, the catalyst texture was characterised from nitrogen physisorption measured on a Micromeritics ASAP 2010 instrument at -196 °C (Fig. 2.1). Firstly, the catalyst (150−200 mg) was placed in a sample tube and degassed at a specific temperature depending on the catalyst nature, usually between 150−200 °C under vacuum for 2 hours. When the pressure reached 8 μmHg, the sample was cooled to room temperature. Next, the tube was removed from the degasser and catalyst weight was recorded then the tube was inserted onto the analyser. Finally, the analysis was programmed to start the absorption process using nitrogen as the absorbent (usually 55 doses) at -196 °C. The BET model was used to calculate the specific surface area from the adsorption data obtained (P/P_o = 0.05–0.25). The single point total pore volume at P/P_o=0.99 and the pore size distribution were calculated using the BJH method on the adsorption and desorption branch of the isotherm.

Nitrogen adsorption and desorption isotherms and pore size distribution plot for 9.6%Pt/C, $Cs_{2.5}H_{0.5}PW_{12}O_{40}$, 1.0%Pt/CsPW-w (prepared from water using H_2PtCl_6), 1.0%Pt/CsPW-b (prepared from benzene using $Pt(acac)_2$), 5.9%Pt/4.4%Au/CsPW, SiO_2 support, 6.4%Pt/SiO_2 and 6.6%Pt/5.9%Au/SiO_2 catalysts are shown in Fig. 2.2−2.9. All data were collected from Micromeritics ASAP 2010 instrument software and plotted by Excel.

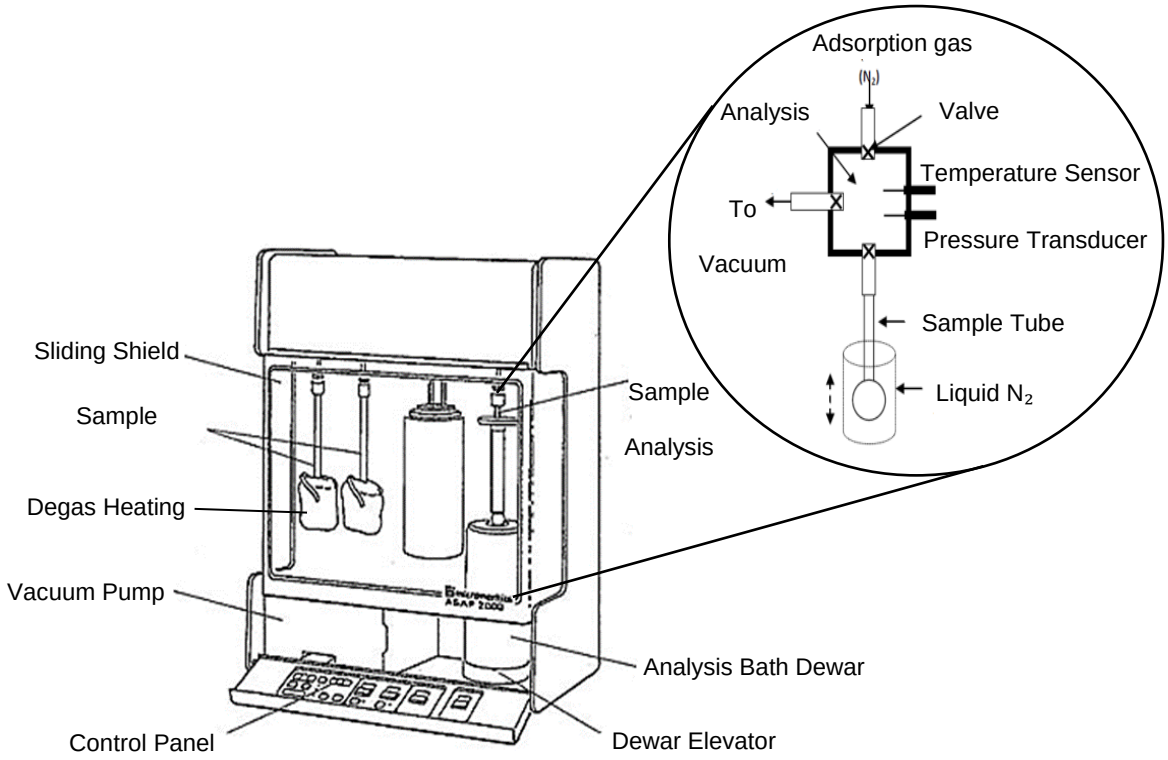

Fig. 2.1 Basic components of volumetric physical adsorption analyzer of Micromeritics ASAP 2010 instrument.

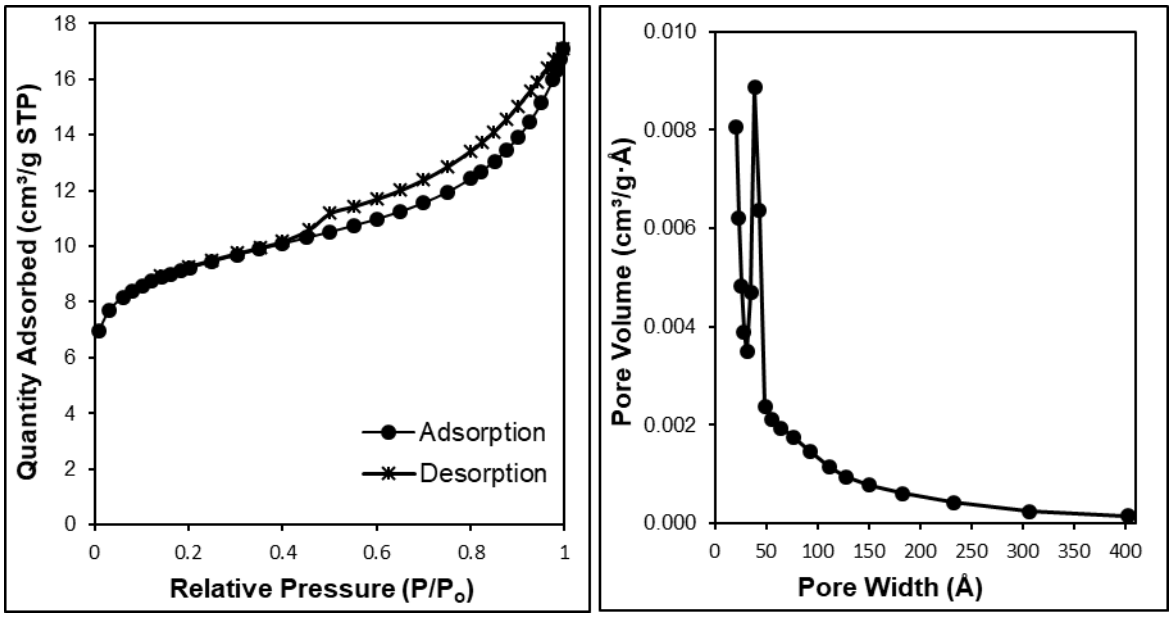

Fig. 2.2 N_2 adsorption-desorption isotherms (left) and pore size distribution (right) for 9.6% Pt/C catalyst.

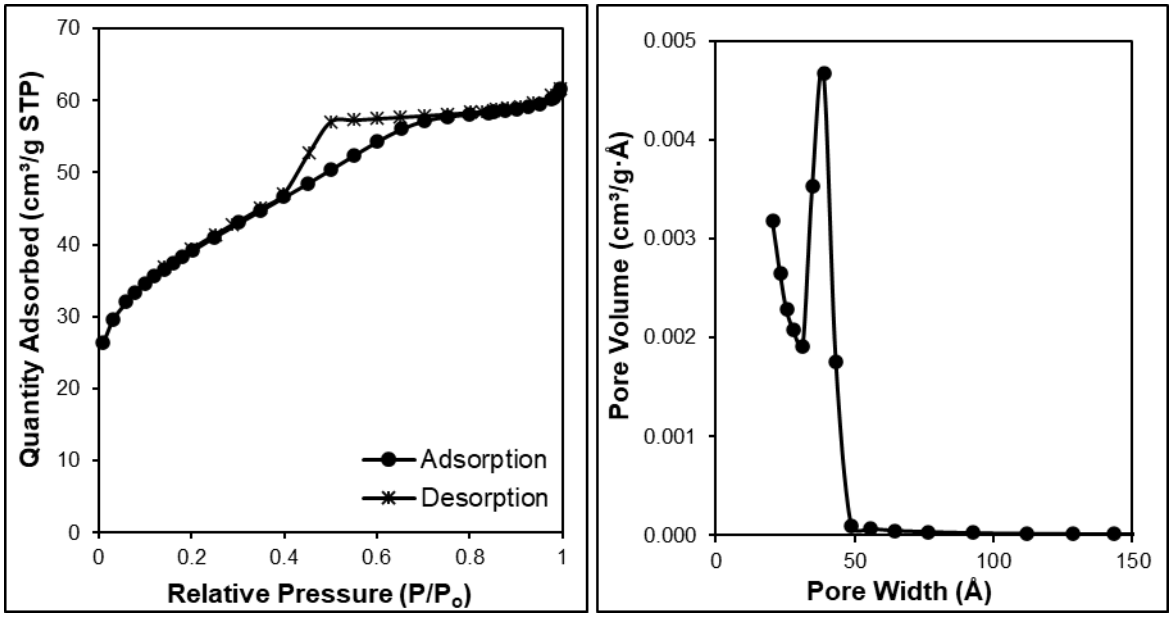

Fig. 2.3 N_2 adsorption-desorption isotherms (left) and pore size distribution (right) for $Cs_{2.5}H_{0.5}PW_{12}O_{40}$ (CsPW) catalyst.

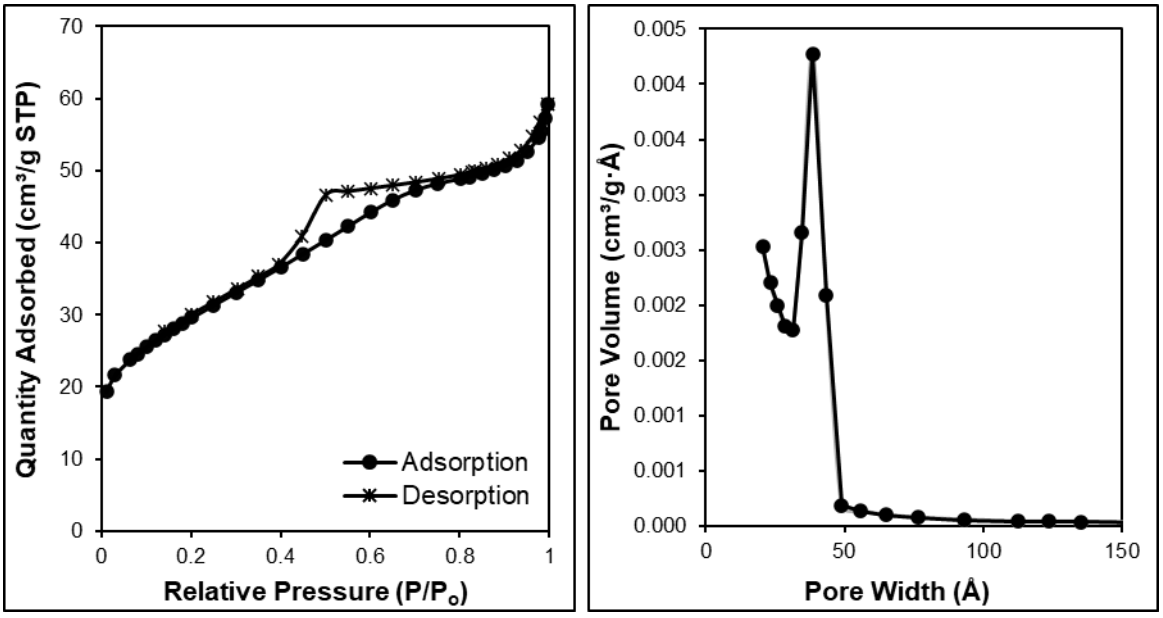

Fig. 2.4 N_2 adsorption-desorption isotherms (left) and pore size distribution (right) for 1.0%Pt/CsPW-b catalyst.

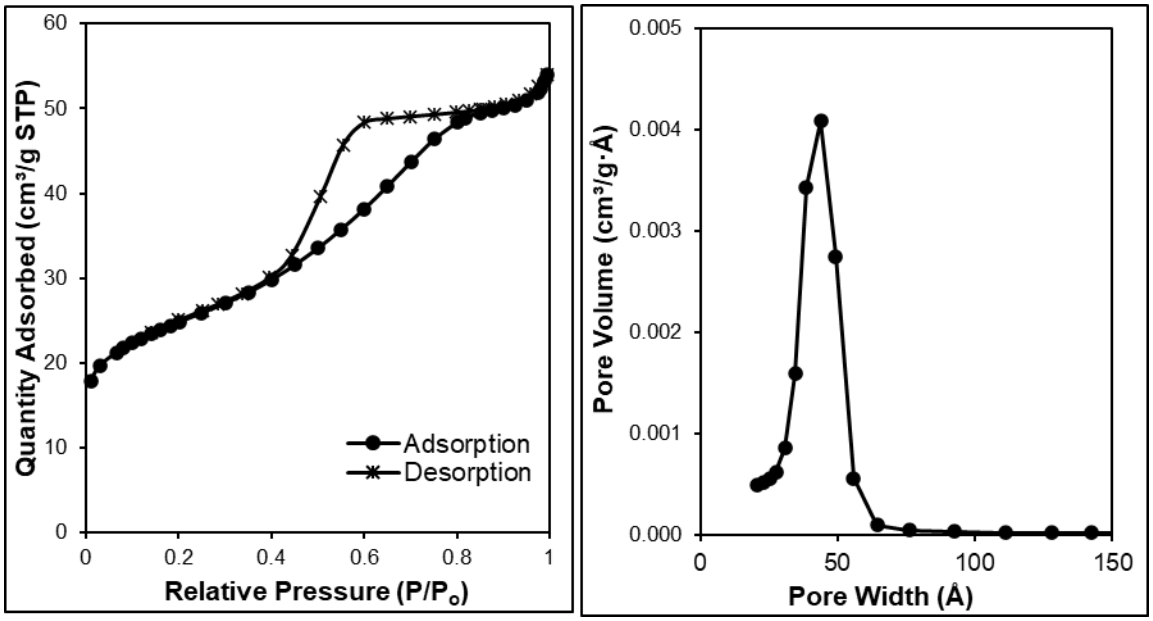

Fig. 2.5 N_2 adsorption-desorption isotherms (left) and pore size distribution (right) for 1.0%Pt/CsPW-w catalyst.

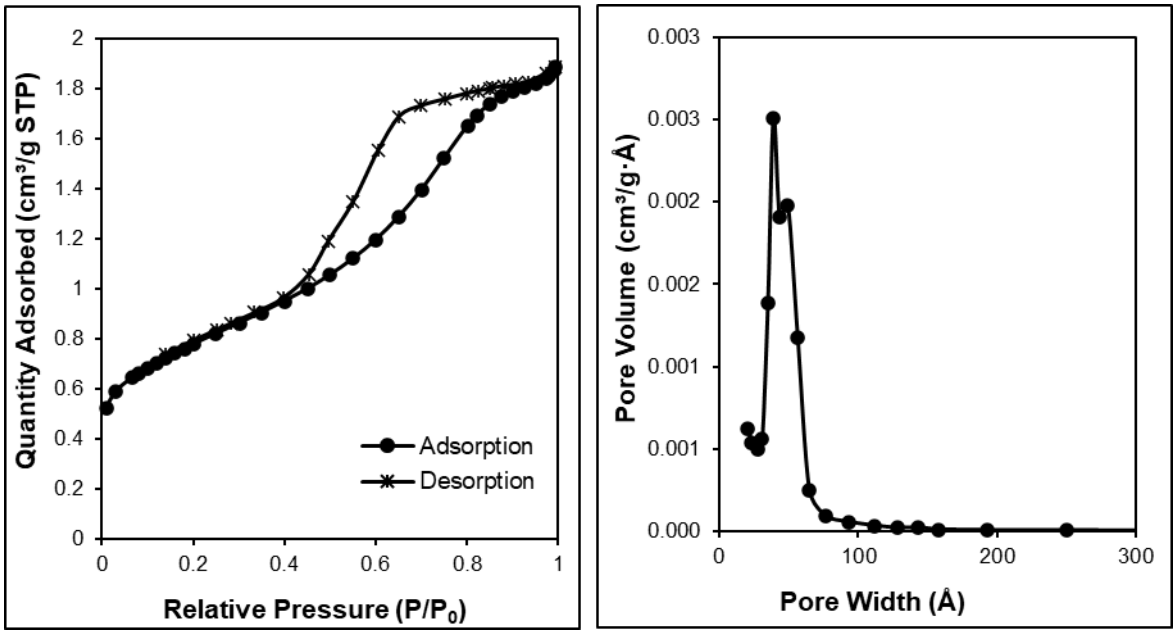

Fig. 2.6 N_2 adsorption-desorption isotherms (left) and pore size distribution (right) for 5.9%Pt/4.4%Au/CsPW catalyst.

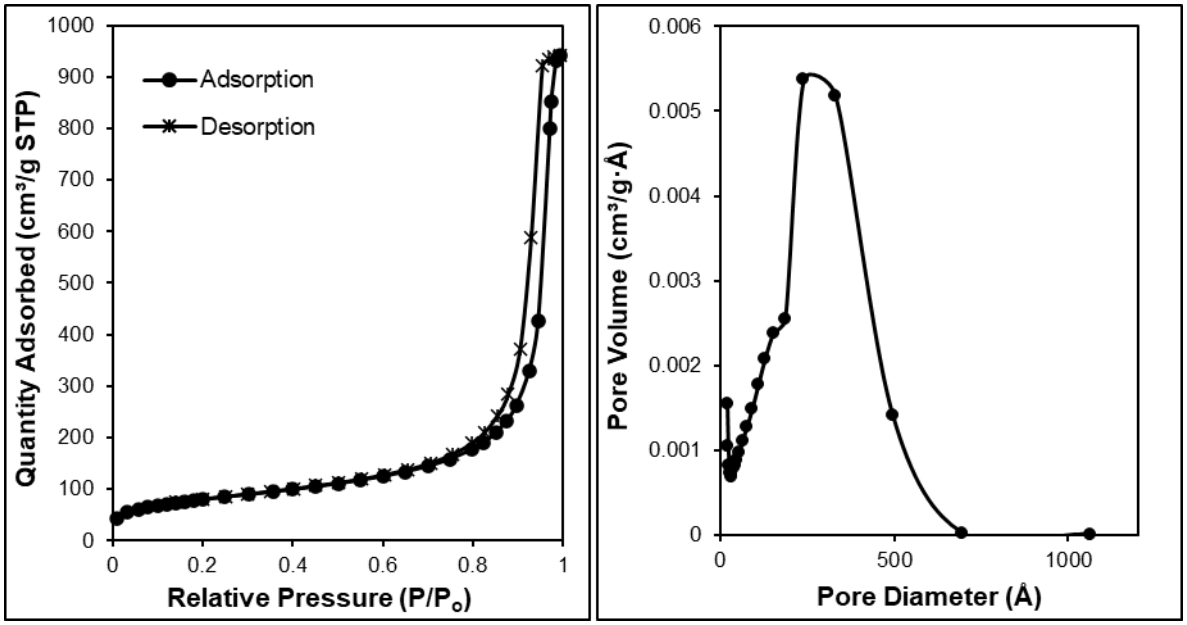

Fig. 2.7 N_2 adsorption-desorption isotherms (left) and pore size distribution (right) for SiO_2 support.

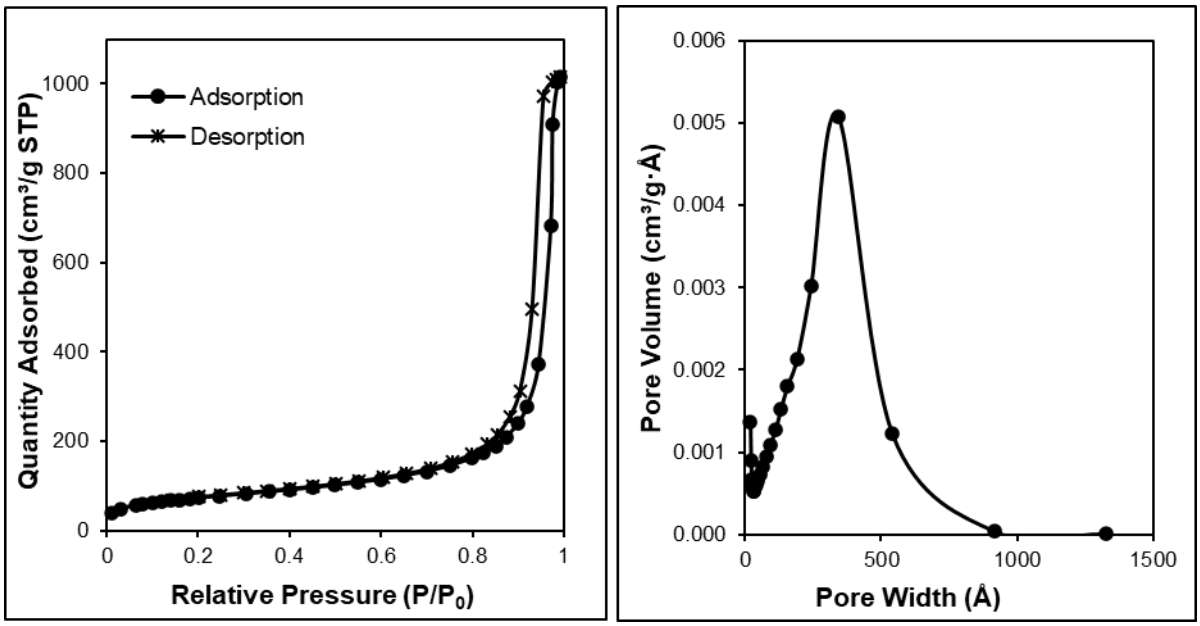

Fig. 2.8 N_2 adsorption-desorption isotherms (left) and pore size distribution (right) for 6.4%Pt/SiO_2 catalyst.

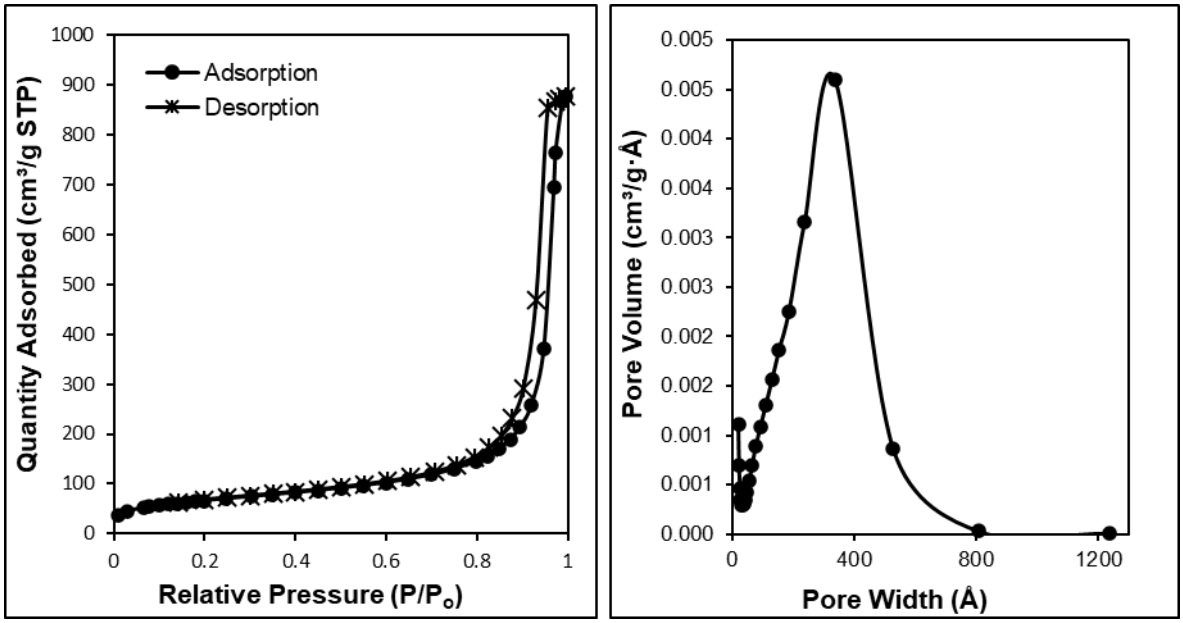

Fig. 2.9 N_2 adsorption-desorption isotherms (left) and pore size distribution (right) for 6.6%Pt/5.9%Au/SiO_2 catalyst.

2.3.2. Powder X-ray Diffraction (XRD)

Powder X-ray diffraction is one of the most important characterisation techniques used to identify bulk phases and estimate particle sizes of crystalline materials. This technique is also used to reveal the crystal structure and lattice parameters of materials in addition to the purity of the solid. In this method, an x-ray beam is focused on the powder of the material under study and its intensity is measured by a detector at an angle (2θ). The position, intensity, shape and width of the diffraction lines give information on the samples. The diffraction pattern is a graphical representation of the intensity vs diffraction angle (2θ) [17].

Using Bragg's law (Eq. 2.4), the inter-atomic spacing (d) can be computed if it is close to the wavelength of the beam being scattered by the crystal.

$$d = \frac{n\lambda}{2\sin\theta} \tag{2.4}$$

Here n is an integral value, λ is the incident wavelength of X-ray, d is the distance between the lattice planes and θ is the diffraction angle.

The average particle size of crystals can be computed applying the Scherrer equation (Eq. 2.5):

$$t = 0.9\lambda/B\cos\theta \tag{2.5}$$

In this equation, t is the particle size of crystals, λ is the incident wavelength of x-ray, B is the total width at half height of the diffraction peak and θ is the diffraction angle [17].

In this work, powder X-ray diffraction patterns were recorded over a range of 2θ 20−90° on a PANalytical Xpert diffractometer with CuKα radiation (λ = 1.542 Å) and attributed using the JCPDS database to deliver information on the crystalline nature of the catalysts. The catalyst was ground, placed in the sample holder and levelled for XRD analysis. The XRD

patterns for 9.6%Pt/C, $Cs_{2.5}H_{0.5}PW_{12}O_{40}$, 1.0%Pt/CsPW-w (prepared from water using H_2PtCl_6) and 1.0%Pt/CsPW-b (prepared from benzene using $Pt(acac)_2$) are shown in Fig. 2.10 and 2.11.

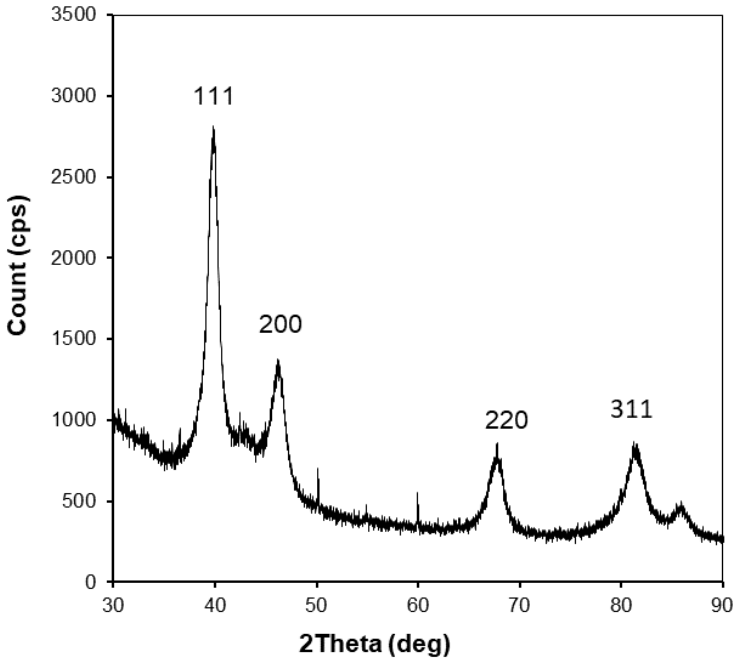

Fig. 2.10 XRD pattern for 9.6%Pt/C. Average Pt particle size is 7.2 nm calculated from the Scherrer equation using [111] diffraction peak.

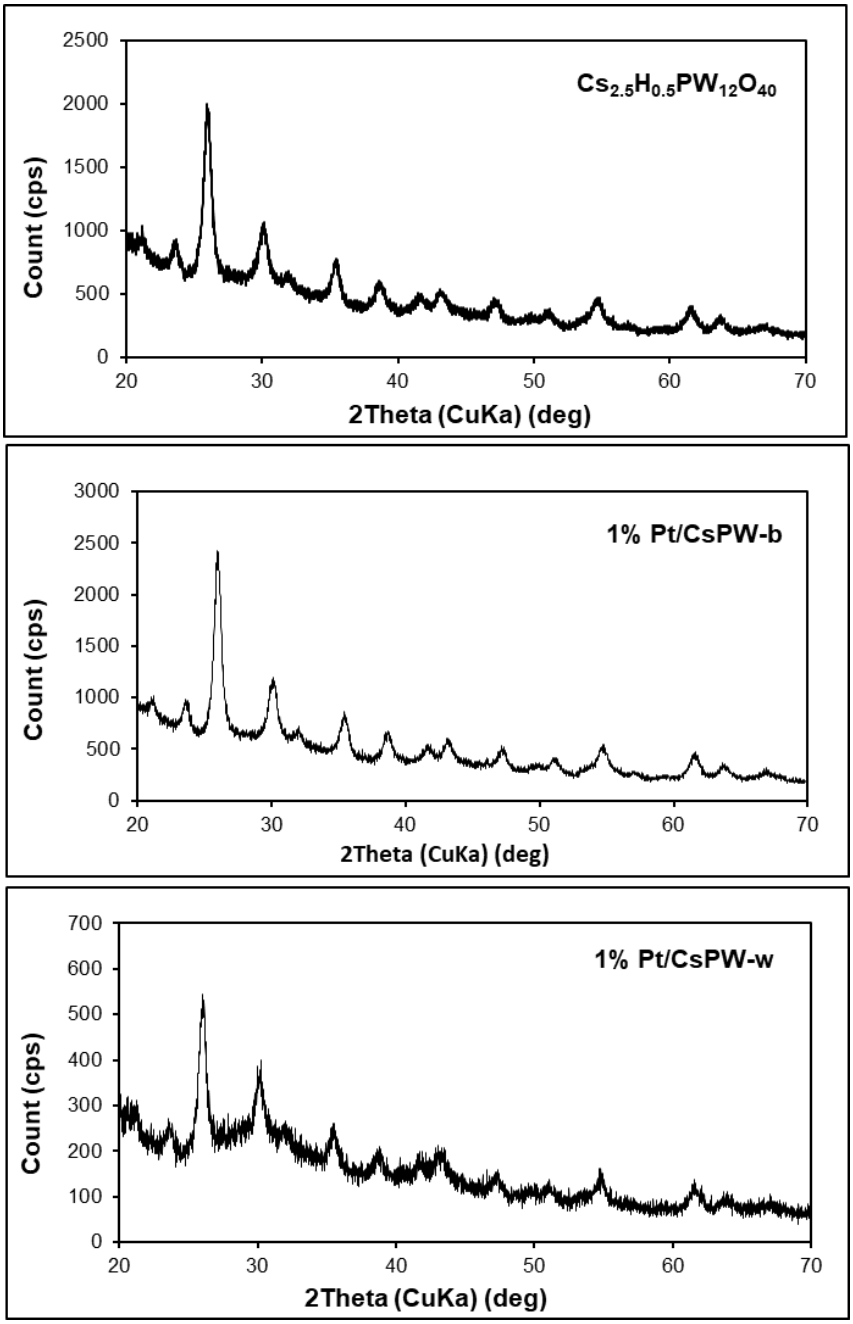

Fig. 2.11 XRD patterns for $Cs_{2.5}H_{0.5}PW_{12}O_{40,}$ 1.0%Pt/CsPW-w (prepared from water using H_2PtCl_6) and 1.0%Pt/CsPW-b (prepared from benzene using $Pt(acac)_2$).

2.3.3. Transmission Electron Microscopy (TEM)

Transmission electron microscopy is very powerful technique for determining particle size, morphology, shape and structure of supported metal catalysts [18−20]. In this work, the metal particle size (*d*) in carbon-supported noble metal catalysts was determined by TEM on a FEI Tecnai Spirit BioTWIN instrument at 120 kV operation using an Olympus-SIS MegaView III digital camera. The TEM images of the carbon-supported noble metal catalysts are shown in Fig. 2.12. This measurement was kindly performed by Dr. Casper Kunstmann-Olsen.

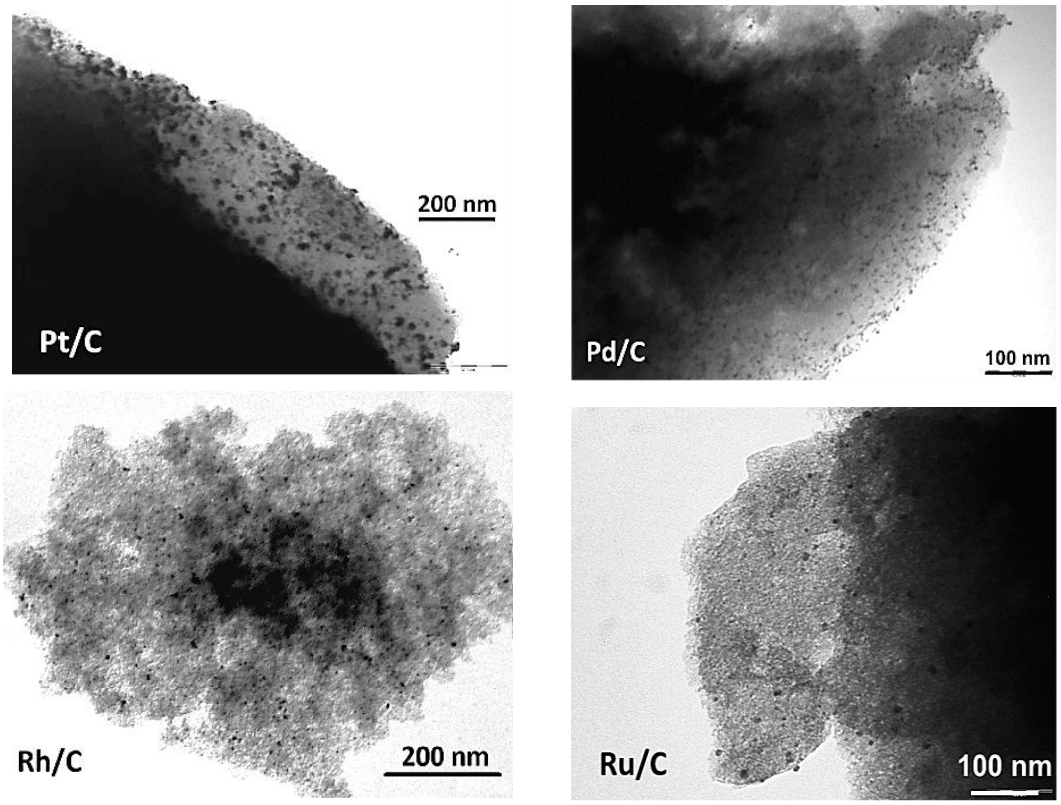

Fig. 2.12 TEM images for carbon-supported noble metal catalysts showing metal particles as dark spots. Average metal particle sizes (*d*): 9.6%Pt/C (11.7±3.0 nm), 7.8%Pd/C (4.2±1.3 nm), 4.0%Rh/C (3.3±0.7 nm) and 3.0%Ru/C (7.6±2.6 nm).

2.3.4. Scanning Transmission Electron Microscopy (STEM) with Energy Dispersive X-Ray Analysis (EDX)

STEM-EDX is an effective technique for the characterisation of bimetallic (alloy) catalysts [20,21]. In this study, it was used for the characterisation of supported bimetallic PtAu catalysts. The STEM–EDX work was performed in the Albert Crewe Centre for Electron Microscopy, a University of Liverpool Shared Research Facility (SRF). High-angle annular dark-field scanning transmission electron microscopy (HAADF-STEM) images were obtained on a spherical aberration-corrected JEOL 2100 F microscope at an accelerating voltage of 200 kV. Energy dispersive X-ray spectroscopy (EDX) mapping was performed using JEOL Silicon Drift Detector DrySD100GV with a solid angle of up to 0.98 steradians from a detection area of 100 mm^2.

2.3.5. Metal Dispersion

The knowledge of metal dispersion is important for understanding the activity of supported metal catalysts in terms of turnover reaction rate [22–28]. The metal dispersion (D) is defined as the ratio of the number of surface atoms (M_s) to the total number of atoms (M_t) in the sample given by Eq. 2.6 [22].

$$D = \frac{M_s}{M_t} \times 100 \tag{2.6}$$

In this work, the metal dispersion of supported metal catalysts was determined from adsorption of H_2 and CO. A schematic diagram of the dynamic pulse apparatus for adsorption measurement is shown in Fig. 2.13.

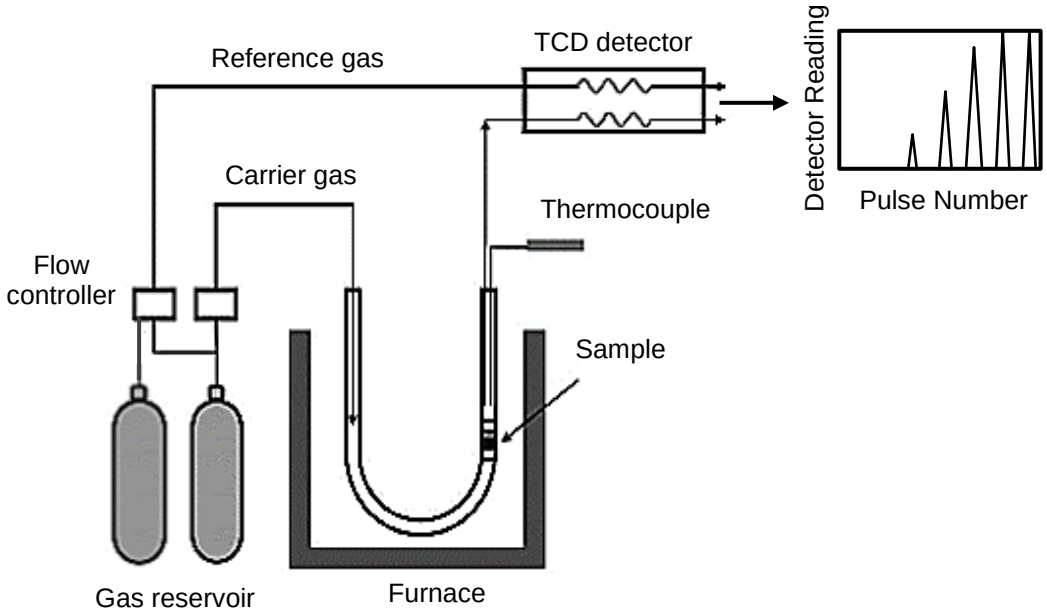

Fig. 2.13 Schematic diagram of dynamic pulse apparatus for adsorption measurements (adapted from [24]).

2.3.5.1. H_2 Chemisorption

In this work, metal dispersion was measured by H_2 chemisorption using the hydrogen-oxygen titration pulse method and calculated assuming the stoichiometry of H_2 adsorption $M_s/H_2 = 1.5$, as shown in Eq. 2.8 [26,27].

$$M_sO + 1.5\,H_2 \rightarrow M_sH + H_2O \quad (2.8)$$

Initially, the catalyst sample (10−50 mg) was exposed to air at room temperature for 24 hours to allow oxygen to adsorb on metal atoms on the catalyst surface. After that, the solid catalyst was placed in a quartz U-tube reactor connected to a Micromeritics TPD/TPR 2900 instrument equipped with a thermal conductivity detector (TCD). The catalyst sample was stabilised at room temperature in nitrogen flow. A series of (20−50 µl) pulses of pure H_2 (heated to 75 °C) was injected in the flow every 2 min until the catalyst was saturated with hydrogen. The signal was recorded by a computer and plotted versus time. The total volume of adsorbed hydrogen was calculated at 75 °C (348 K) using Eq. 2.9:

$$V_{348K} = \sum \{V - [(P_{ads}/P_{av})\} \times V] \quad (2.9)$$

where V_{348K} is the total volume of hydrogen absorbed at 75 °C (348 K), V is the hydrogen pulse volume, P_{ads} is the peak area of adsorbed hydrogen and P_{av} is the average peak area for about four to six injections at saturation with no further hydrogen adsorption.

The total adsorbed volume of H_2 at standard conditions (0 °C (273 K)) is given by Eq. 2.10:

$$V_{273K} = V_{348K} \times (273/348) \quad (2.10)$$

Equation 2.11 below shows how the total dispersion was calculated, where D is the metal dispersion, A_r is the relative atomic mass of metal, M_{cat} is the mass of the catalyst used in the experiment (g), 22414 ml mol^{-1} is the volume of one mole of H_2 under standard

conditions (273 K, 1 bar), C_M is the concentration of metal as a fraction of catalyst mass and S is the adsorption stoichiometry of the gas adsorbed on the metal surface (M_s/H_2 = 1.5).

$$D = \frac{V_{273}(ml) \times A_r(\frac{g}{mol})}{M_{cat}(g) \times 22414\left(\frac{ml}{mol}\right) \times C_M \times S} \times 100 \quad (2.11)$$

The average diameter of metal particles (d) was calculated from the empirical equation (Eq. 2.12), where c = 0.9−1.2 depending on particle shape [26,27]:

$$d\ (nm) = c/D \quad (2.12)$$

2.3.5.2. CO Chemisorption

In addition to H_2/O_2 titration described above, metal dispersion was also measured by pulse chemisorption of CO. This measurement was carried out in a helium flow at 50 °C using Micromeritics TPD/TPR 2900 instrument with a thermal conductivity detector (TCD). A catalyst sample (10−20 mg) was placed in the sample U-tube and pre-treated in H_2 flow at 200 °C for 1 h. Then (25−50 µl) pulses of pure CO were injected manually until the catalyst was saturated with CO. The stoichiometry of CO adsorption on the metal surface (M_s/CO) was assumed to be 1 for Pt, Rh, Ru and 2 for Pd [29−31]. The measurement of D for 9.6%Pt/C, 7.8%Pd/C, 3.0%Ru/C and 4.0%Rh/C is illustrated in Fig. 2.14.

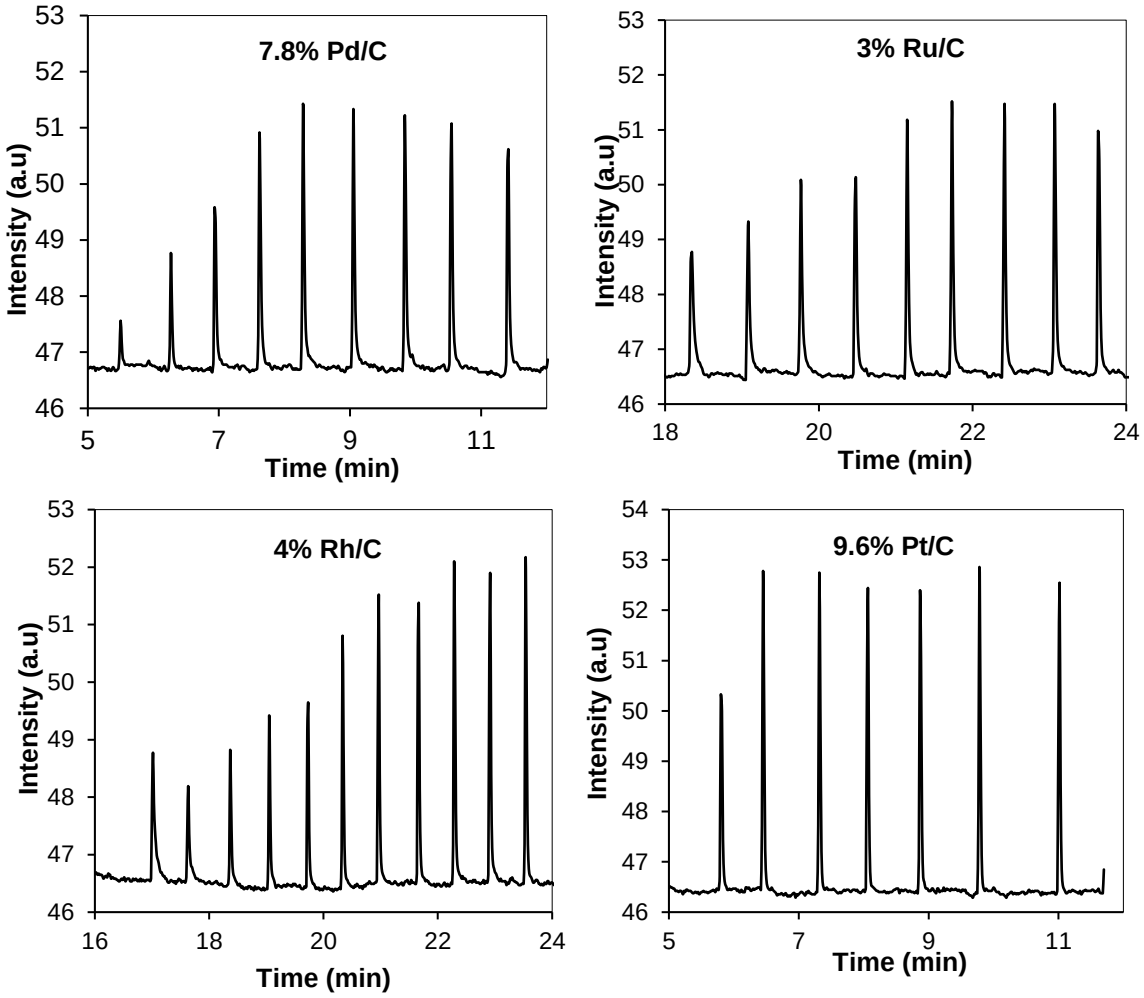

Fig. 2.14 Pulse chemisorption of CO on 7.8%Pd/C, 3.0%Ru/C, 4.0%Rh/C and 9.6% Pt/C, (10 mg) at 50 °C in He flow (30 mL min^{-1}) (catalyst pre-treatment at 200 °C/0.5 h in 30 mL min^{-1} H_2 flow, 25 µL pulses of pure CO.

2.3.6. Inductively Coupled Plasma-Optical Emission Spectroscopy (ICP-OES)

In this work, the ICP–OES technique [32−34] was used to determine the metal loading in supported metal catalysts. The catalyst sample (30−50 mg) was weighed into a volumetric flask (50 mL). A solution of HCl and HNO_3 mixture with a molar ratio of 3:1 was added to the flask in small portions and the mixture was boiled for 3 h. The mixture was cooled then made up to 50 mL with distilled water followed by shaking the flask and finally left overnight. The clear solution of the sample was then transferred to a sample vial and submitted to the Microanalysis Service at Chemistry Department of the University of Liverpool. The analysis was kindly performed by Mr. Stephen Moss using an Agilent 5110 ICP-OES spectrometer with SVDV detection equipped with the sample changer.

2.3.7. Thermal Gravimetric Analysis (TGA)

TGA is widely used to characterise the thermal stability of materials and the content of volatile components present in them by monitoring the weight change upon heating a sample at a constant rate [35].

In this study, a Perkin Elmer TGA 7 instrument was used to conduct TGA analysis in the temperature range 30–700 ^{o}C with a heating rate of 10 or 20 °C/ min, under continuous N_2 flow. The procedure required 0.01−0.015 g of catalyst. Dr. Elena F. Kozhevnikova kindly carried out the TGA analysis in this group.

2.4. Catalytic Activity Measurement and Product Analysis

2.4.1. Gas Chromatography (GC)

Gas chromatography is used for quantitative analysis and separation of volatile compounds. A simple schematic of a gas chromatograph with flame ionisation detector (FID) is shown in Fig. 2.15. The analysed sample is volatilised into gas state and mixed with a carrier gas (usually nitrogen or helium). It is transported through a packed or capillary column containing a solid or liquid stationary phase. The components of the sample are separated at different retention times depending on their boiling points and solubility and are analysed by a suitable detector, for example FID [36−39].

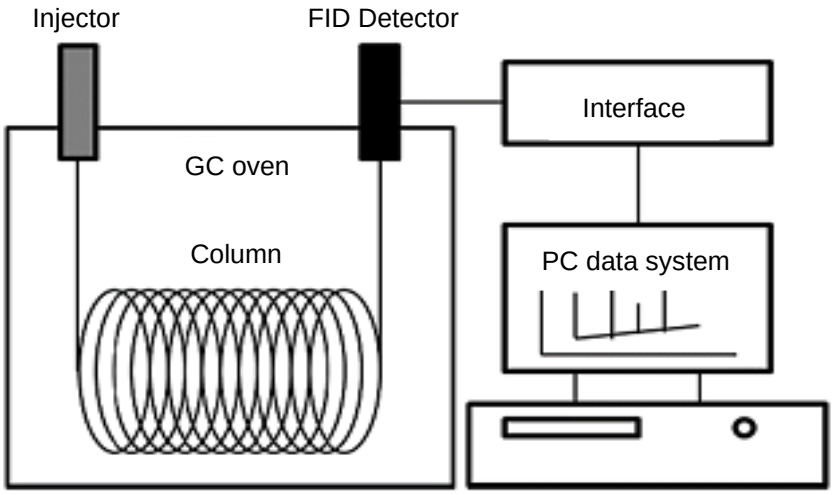

Fig. 2.15 Simplified schematic of the gas chromatography-FID system (adapted from [36−38]).

Packed columns are generally a glass coil or chromium steel tube, packed with a stationary phase. On the other hand, capillary columns are made of fused quartz, which is coated with a thin layer of stationary phase such as silicon grease. Generally, capillary columns offer a better separation than the packed ones. Factors that affect the GC separation include the boiling points and the polarity of the analysed compounds. At the entrance of the GC

column, a split/spitless injector is used to inject a controlled quantity of samples into the column (Fig. 2.16). The split ratio refers to the ratio of spilt flow rate to the column flow rate.

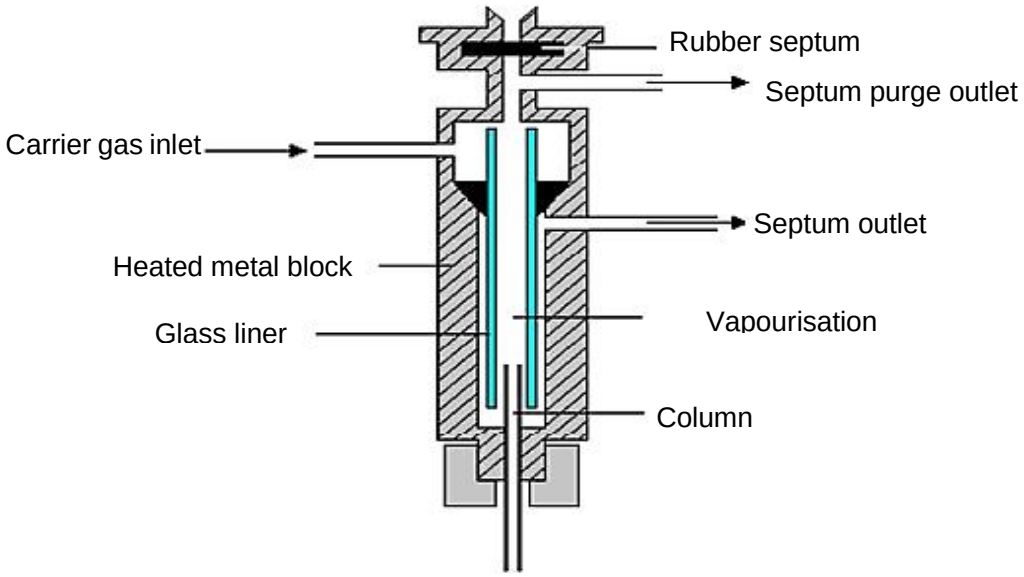

Fig. 2.16 GC split/spitless vaporising injector [36,38].

The flame ionisation detector is usually utilised in GC to analyse organic compounds (Fig. 2.17). Within the FID detector, the outflow from the column is subjected to intense heating with a high temperature flame created by mixing H_2 and air. This flame ionises organic molecules with lower ionisation potential to generate electric current proportional to the density of ions formed. The current is then amplified and a chromatogram is produced on an external computer. For FID, the molar response factors for molecules depend mainly on the number of carbon atoms in the molecule based on the effective carbon number (ECN) concept [40–42].

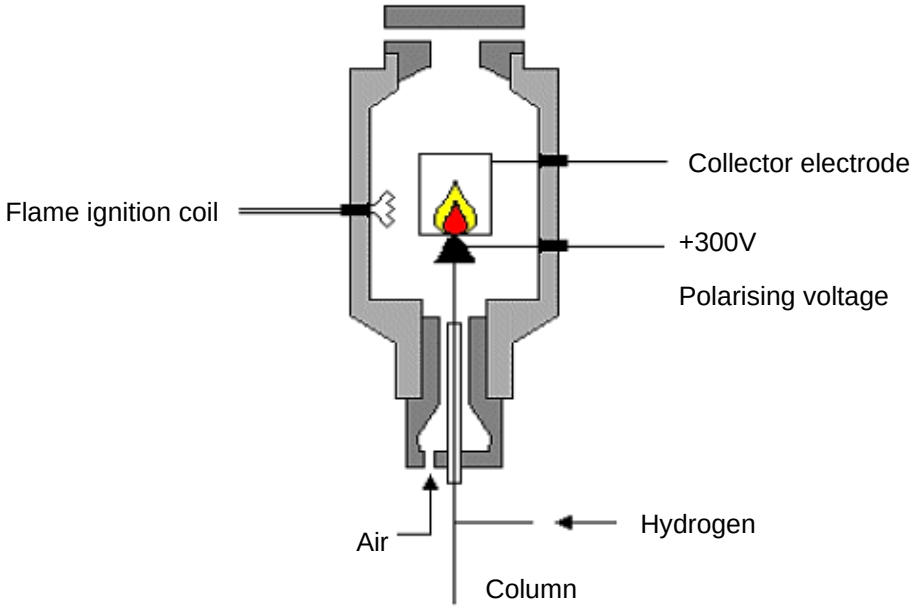

Fig. 2.17 Flame ionisation detector [36,38].

In this work, a Varian 3800 gas chromatograph with a 30 m×0.32 mm×0.5 μm Zebron ZB-WAX capillary column and a flame ionization detector was used for on-line and off-line product analysis. The off-line analysis of light hydrocarbons was also carried out using a Varian 3800 GC with 60 m x 0.32 mm GS-Gas Pro capillary column and FID detector, which allowed for complete separation of these hydrocarbons. In both GC instruments, the detector and injector temperatures were set at 300 °C.

The temperature and pressure programs for GC analysis of DMF hydrogenation on ZB-WAX capillary column are shown in Fig. 2.18 and Fig. 2.19, respectively. Fig. 2.20 shows a typical GC trace for DMF hydrogenation on Pt/C catalysts (ZB-WAX capillary column).

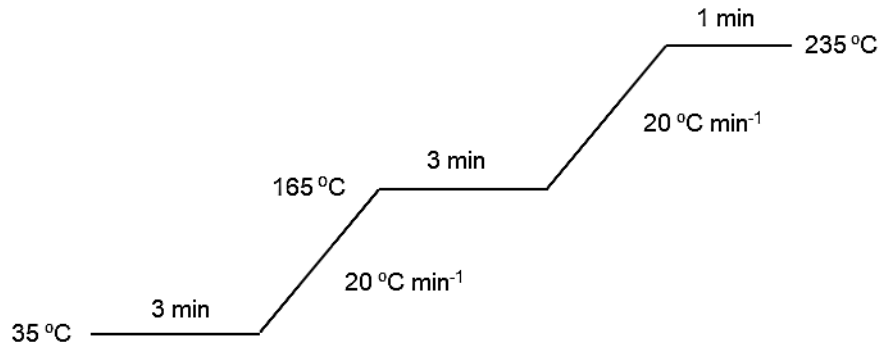

Fig. 2.18 ZB-WAX capillary column temperature program used in the DMF hydroconversion reaction (injector spilt ratio = 20, temperature = 300 °C and FID temperature = 300 °C).

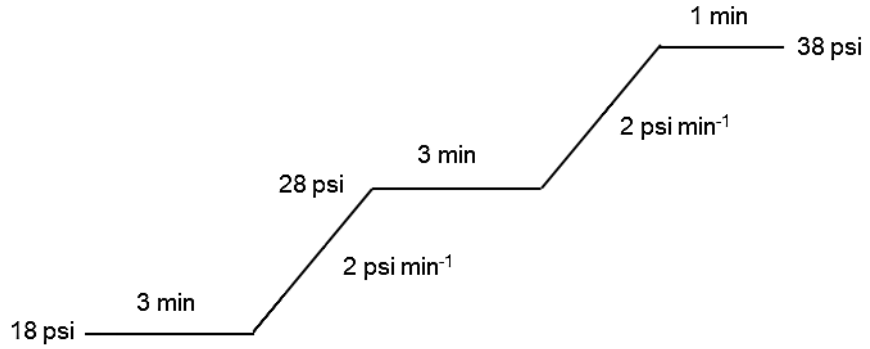

Fig. 2.19 ZB-WAX capillary column pressure program used in the DMF hydroconversion reaction (injector spilt ratio = 20, temperature = 300 °C and FID temperature = 300 °C).

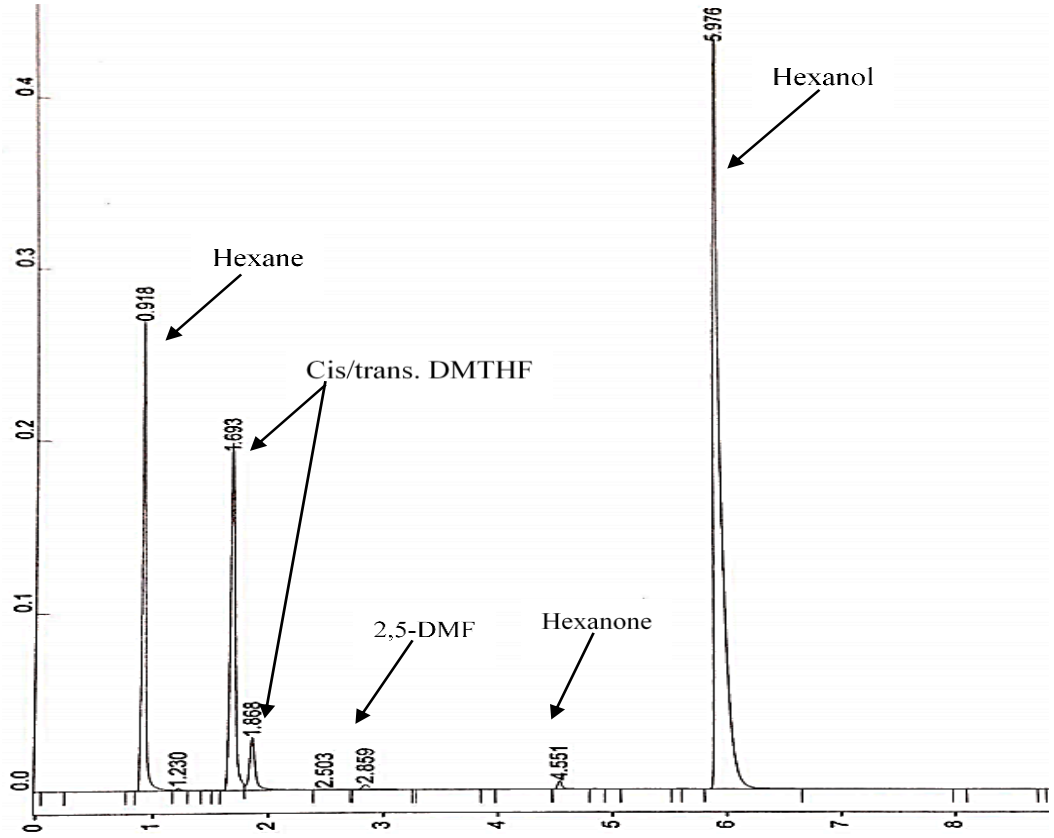

Fig. 2.20 GC trace for DMF hydrogenation over 9.6%Pt/C at 70 °C.

2.4.2. Gas Chromatography Calibration

Chromatographic peak areas for different compounds depend on the response characteristics of the detector. The peak area may also be affected by the type of detector, column temperature and the carrier gas flow rate. To eliminate the effect of these factors, calibration methods employing the internal or external standard can be used.

In this study, all components in the reaction mixture were quantified using the internal standard method. The calibrations were carried out using n-decane as a GC standard and acetone as a solvent. Calibration factors (Table 2.1, Fig. 2.21) were determined by preparing a series of solutions with a different concentration of analyte and a constant concentration of the standard dissolved in acetone. The molar ratio of the analyte (M) to the internal standard (M_o) was plotted against the peak area ratio of the two components (S/S_o) (Eq.

2.13). The gradient of the straight line obtained is the calibration factor *K*. The reactants and products were identified by comparing their retention times with those of commercial standards.

$$M/M_0 = K \times S/S_0 \quad (2.13)$$

Table 2.1 Molecular weights (MW), boiling points, retention times and calibration factors (*K*) for all components involved in the gas phase hydrogenation of DMF.[a]

Compound	MW (g mol^{-1})	Boiling point (°C)	Retention time (min)	$K_{(exp)}$ [b] experimental	$K_{(calcd)c}$ calculated
n-hexane	86.18	68	0.92	0.98±0.02	0.83
cis-DMTHF	100.16	90	1.69	1.00±0.01	0.96
trans-DMTHF	100.16	90	1.87	1.00±0.01	0.96
2-hexanone	100.16	127	4.55	0.94±0.15	0.96
2-hexanol	102.17	140	5.98	0.84±0.04	0.91

[a] ZB-WAX capillary column (30 m×0.32 mm×0.5μm).
[b] Calibration factors relative to n-decan standard.
[c] Calibration factors estimated using the effective carbon number relative to DMF [40−42].

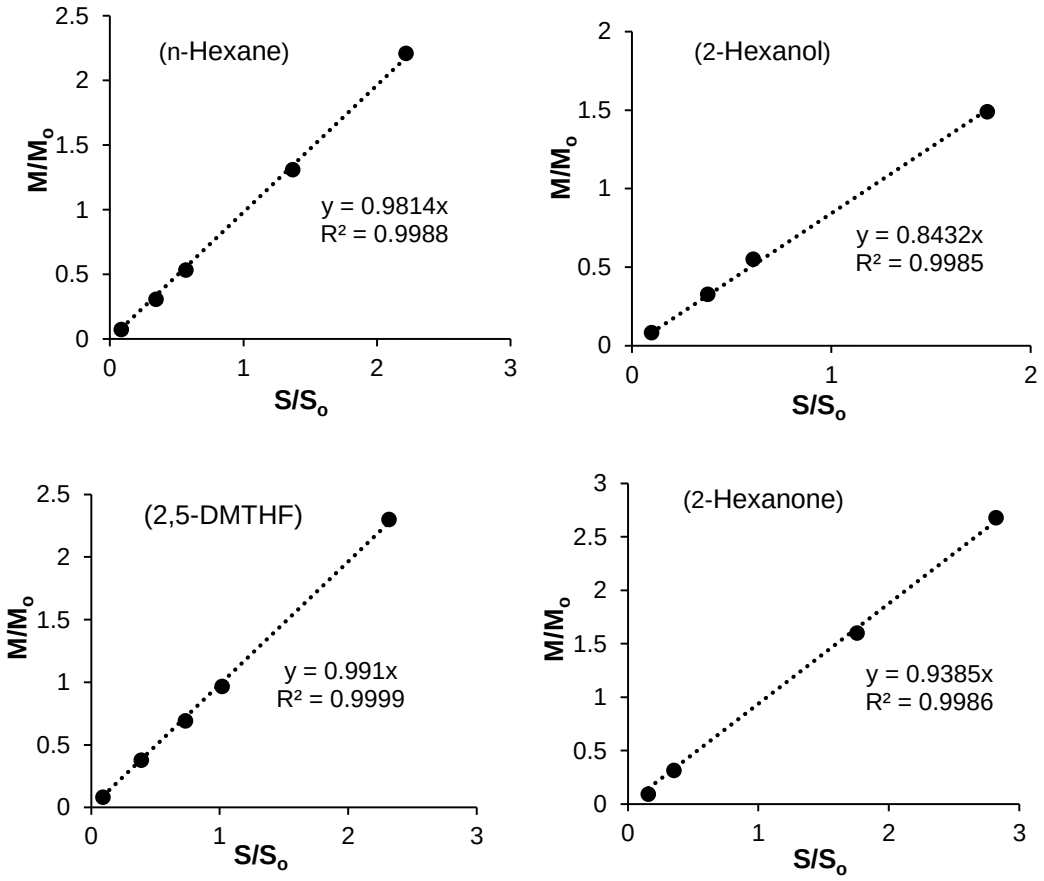

Fig. 2.21 GC calibration factors of n-hexane, 2,5-DMTHF, 2-hexanol and 2-hexanone versus n-decane as internal standard.

2.5. Catalyst Testing Procedure

The hydrogenation, hydrogenolysis and hydrodeoxygenation reactions of furanic compounds (DMF, DMTHF and THF) were carried out at the gas-solid interface in flowing H_2 at 1 bar pressure in the temperature range 60–100 °C using a Pyrex fixed-bed down-flow microreactor (9 mm internal diameter) fitted with an on-line gas chromatograph (Varian 3800 instrument with a 30 m×0.32 mm×0.5 μm Zebron ZB–WAX capillary column and a flame ionisation detector) (Fig. 2.22 and 2.23). The reactor was packed with 0.20 g catalyst powder of <100 μm particle size. The catalyst bed for the hydrogenation and hydrogenolysis reactions (chapter 3) was a homogeneous physical mixture of a carbon-supported metal catalyst (M/C) and silica (M/C:SiO_2 = 1:2–1:1000 w/w, 1:3–1:1300 v/v, 0.20 g total weight).

The catalyst bed for the HDO reaction (chapter 4 and 5) contained a uniform physical mixture (0.20 g total weight, <100 μm particle size) of powdered catalyst components (supported metal catalyst and acid co-catalyst or SiO_2). Silica was added to minimize the effect of reaction heat and to keep the size of the catalyst bed constant upon varying the amount of metal catalyst.

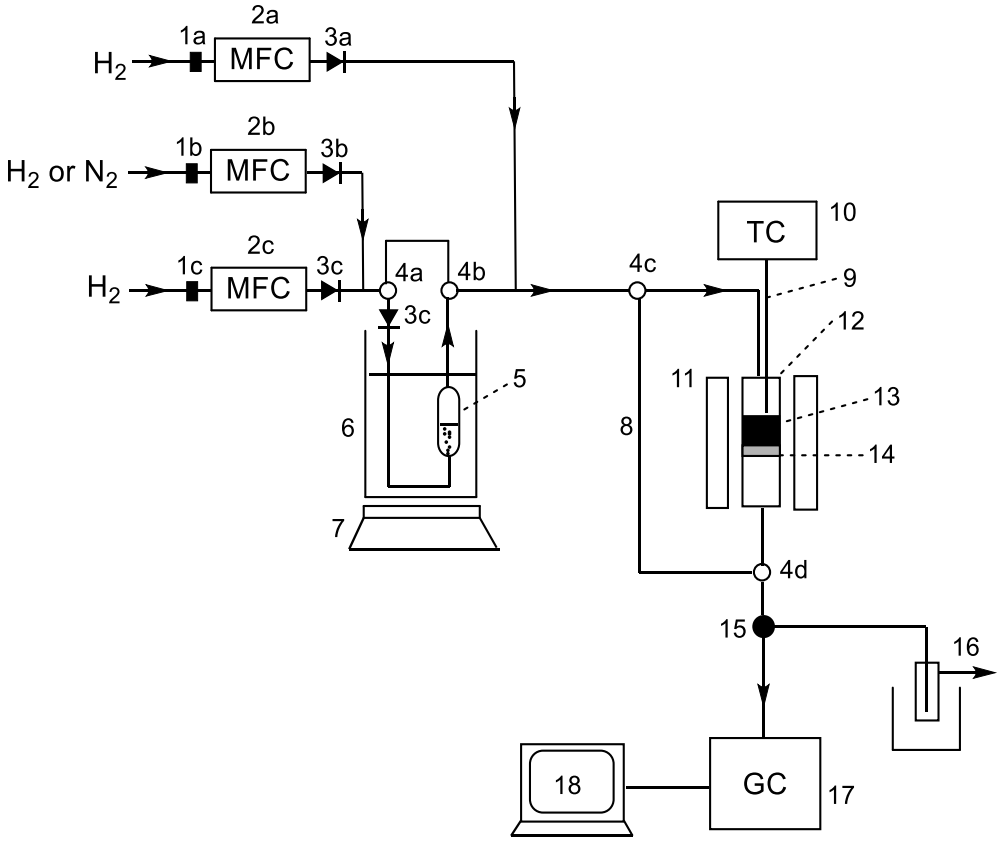

Fig. 2.22 Schematic of gas phase fixed-bed flow reactor system coupled with on-line GC analysis.

Key: (1) particulate filter, (2) Brooks mass flow controller [MFC 2a-c allow to vary substrate pressure at constant H_2 flow rate and to vary gas composition (H_2 + N_2) at constant substrate pressure], (3) check valve (non-return valve), (4) 3-way valve, (5) saturator containing liquid substrate, (6) temperature-controlled water bath, (7) stirring hotplate, (8) bypass, (9) thermocouple, (10) Eurotherm temperature controller, (11) furnace, (12) Pyrex or quartz tubular reactor, (13) catalyst bed, (14) glass wool support, (15) Valco multiposition sampling valve with air actuator, (16) product trap, (17) gas chromatography, (18) computer.

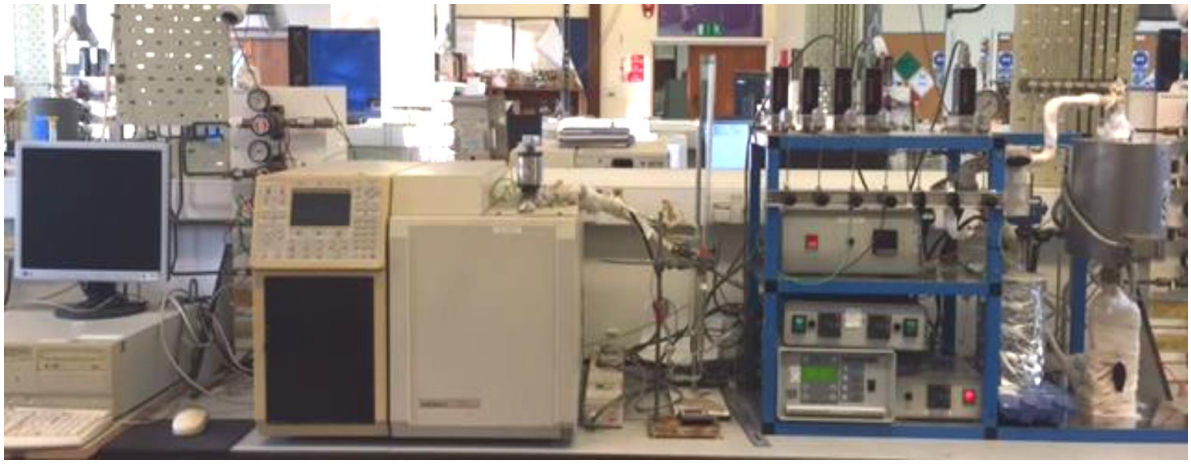

Fig. 2.23 Continuous flow fixed-bed reactor with on-line GC analysis.

The temperature in the reactor was controlled by a Eurotherm controller (±0.5 °C) using a thermocouple placed at the top of the catalyst bed. The furanic substrate was fed by passing H_2 flow controlled by a Brooks mass flow controller through a stainless-steel saturator with 10:1–62:1 H_2/DMF ratio range, which held the liquid substrate at an appropriate temperature to maintain the chosen reactant partial pressure. The downstream gas lines and valves were heated to 150 °C to prevent substrate and product condensation. The gas feed entered the reactor from the top at a flow rate of 20 mL min^{-1} unless stated otherwise. Prior to reaction, the catalysts were pre-treated in situ for 1 h at the reaction temperature in H_2 flow. The reactions were carried out for 3–20 h time on stream (TOS) at a space time W/F = 0.13–125 g h mol^{-1}, where W is the catalyst weight (gram) and F is the inlet molar flow rate of the furanic substrate (mol h^{-1}). Once the reaction started, the downstream gas flow was analysed by the on-line GC to obtain reactant conversion and product composition. The selectivity was determined as moles of product formed per one mole of substrate converted and quoted in % mol. The carbon balance was maintained within 95%. Each catalyst test was repeated at least twice. The mean absolute percentage error in conversion and product selectivity was usually ≤5%.

Regeneration of Pt/C catalyst was carried out in-situ and included the following steps: (i) purging the reactor with N_2, (ii) treating the catalyst with air (20 mL min^{-1}) at 200 °C for 1 h, (iii) purging the reactor again with N_2 and finally (iv) reducing the catalyst with H_2 (20 mL min^{-1}) at 200 °C for 1 h.

The hydrodeoxygenation of DMF in the liquid phase was carried out in a 120 mL stainless steel autoclave with a magnetic stirrer. In a typical run, the reactor was charged with 9.6%Pt/C + CsPW (1:9 w/w) catalyst (0.20 g, 1% Pt loading per total catalyst weight), DMF (5.2 mmol), dodecane (GC standard, 5.0 mmol), decane (solvent, 3.0 mL), 20 bar H_2 pressure (at room temperature) and placed in an oil bath heated to 90–140 °C. The reaction was carried out at 600 rpm stirring speed for 2 h time. At the end of the reaction, the reactor was allowed to cool down to room temperature and the liquid sample was collected. All samples were filtered with a 0.2 μm pore size filter and analysed using a high-performance GC equipped with a 30 m × 0.32 mm × 0.5 μm Zebron ZB–WAX capillary column and a flame ionisation detector. At such conditions, the reaction did not depend on the stirring speed (300-800 rpm), hence was not affected by external diffusion limitations.

2.6. Calculation of Catalyst Testing Results

2.6.1. Gas Phase

The conversion (X) of substrate, yield (Y_p) and selectivity (S) of products were calculated using the equations below:

$$Yp = \frac{Sp \times Kg \times A}{Sr + (\sum Sp \times Kg \times A)} \times 100 \quad (2.14)$$

$$X = \sum Y_p \quad (2.15)$$

$$S = \frac{Yp}{X} \times 100 \quad (2.16)$$

In equations (2.14 – 2.16), S_p is the product peak area, K_g is the calibration factor of product relative to the substrate, A is the product stoichiometry factor relative to the substrate, S_r is the area count of unreacted substrate and ($\Sigma S_P \times K_g \times A$) is the summation for all products in a reaction**.**

Antoine equation (Eq. 2.17) was used to estimate vapor pressure of the pure reactants [43].

$$Log_{10}(P) = A - \frac{B}{(T+C)} \tag{2.17}$$

In this equation, P is vapour pressure of the substances (kPa). T is the temperature (K). A, B and C are the constants characteristic of the substance in the given temperature range (from the Handbook of Chemistry & Physics, 80th Ed. [44]).

2.6.2. Liquid Phase

In the liquid phase processes, the percentage yield of products (Y_p) was calculated using Eq. 2.18.

$$Y_p = \frac{A \times K_p \times S_p \times M_s}{M_r \times S_s} \times 100 \tag{2.18}$$

In Eq. 2.18, A is the stoichiometry factor of the product relative to the substrate, K_p is the calibration factor of the product relative to the internal standard, S_p is the relative area of the product peak(s), M_s is the amount of standard added to the reaction mixture (mol), M_r is the amount of the substrate in the reaction mixture (mol) and S_s is the relative area of the standard peak.

The total conversion (X) and the individual product selectivity (S) was calculated using equations (2.19) and (2.20), respectively.

$$Conversion\ (mol\%) = \frac{moles\ of\ substrate\ reacted}{moles\ of\ substrate\ loaded} \times 100 \tag{2.19}$$

$$Selectivity\ (mol\%) = \frac{moles\ of\ desirable\ product}{\sum moles\ of\ all\ products} \times 100 \quad (2.20)$$

2.6.3. Kinetic Studies

Kinetic studies were carried out using the fixed-bed reactor, whenever possible at low substrate conversions (≤ 20%), which was achieved by choosing short contact times, decreasing catalyst amount in the reactor or increasing feed flow rate [45−48]. Under these conditions, the rate of reaction, *R*, is given as (in mol g^{-1} h^{-1}):

$$R = \frac{XF}{W} \quad (2.21)$$

where *X* is the substrate conversion, *W* is the catalyst weight and *F* is the inlet molar flow rate of substrate. A schematic representation of a fixed-bed reactor illustrating the flow through a differential cross section of catalyst bed is shown in Fig. 2.24.

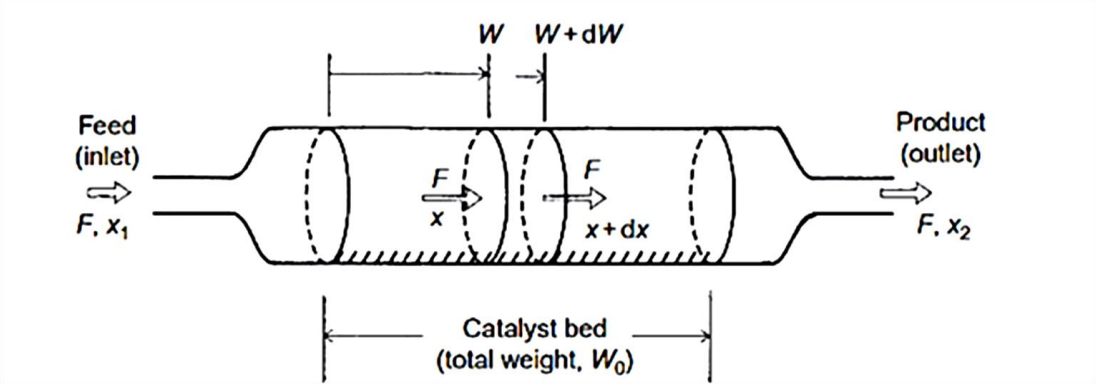

Fig. 2.24 Schematic representation of continuous flow fixed-bed reactor [48].

The turnover frequency (TOF) was calculated as the number of moles of substrate converted per unit time per mole of accessible metal sites using Eq. 2.22. The number of accessible metal sites was determined from the metal dispersion of catalysts measured by chemisorption of CO or H_2/O_2 titration.

$$TOF = \frac{change\ of\ molecules\ of\ reactant}{active\ site \times time} \quad (2.22)$$

The activation energy, E, of reactions was determined by measuring the reaction rate at different temperatures and calculated using the Arrhenius equation (Eq. 2.23):

$$k = A \times exp\,(-E / RT) \tag{2.23}$$

Here k is the rate constant, A is the pre-exponential factor (collision frequency), E is the activation energy of the reaction (kJ mol^{-1}), R is the gas constant (R = 8.31 kJ mol^{-1}) and T is the absolute temperature. Values of A and E can be determined by plotting ln k against 1/T from Eq. 2.24.

$$ln\,k = \frac{-E}{R}\left(\frac{1}{T}\right) + ln\,A \tag{2.24}$$

References

[1] S. Tatematsu, T. Hibi, T. Okuhara, M. Misono, Preparation process and catalytic activity of $C_{sx}H_{3-x}PW_{12}O_{40}$, Chem. Lett. 13 (1984) 865−868.

[2] Y. Izumi, M. Ono, M. Kitagawa, M. Yoshida, K. Urabe, Silica-included heteropoly compounds as solid acid catalysts, Microporous Mater. 5 (1995) 255−262.

[3] R. Al-Faze, A. Finch, E.F. Kozhevnikova, I.V. Kozhevnikov, Dehydration of methanol and ethanol over silica-supported heteropoly acids in the gas phase: surface-type versus bulk-type catalysis mechanism, Appl. Catal. A Gen. 597 (2020) 117549.

[4] S. Itagaki, N. Matsuhashi, K. Taniguchi, K. Yamaguchi, N. Mizuno, Efficient hydrodeoxygenation of ketones, phenols and ethers promoted by platinum–heteropolyacid bifunctional catalysts, Chem. Lett. 43 (2014) 1086−1088.

[5] F. Pinna, Supported metal catalysts preparation, Catal. Today, 41 (1998) 129−137.

[6] O. Poole, K. Alharbi, D. Belic, E.F. Kozhevnikova, I.V. Kozhevnikov, Hydrodeoxygenation of 3-pentanone over bifunctional Pt-heteropoly acid catalyst in the gas phase: Enhancing effect of gold, Appl. Catal. B 202 (2017) 446−453.

[7] K. Sing, The use of nitrogen adsorption for the characterization of porous materials, Colloids and Surfaces A: Physicochem. Eng. Aspects, 187 (2001) 187−188.

[8] J.B. Condon, Surface area and porosity determinations by physisorption: measurement, classical theories and quantum theory, 2nd ed., E Amsterdam, Netherlands: Elsevier, 2006.

[9] K. S. Sing, F. Rouquerol, J. Rouquerol, K. Sing, P. Llewellyn, G. Maurin, Adsorption by powders and porous solids, 2nd ed., Academic Press, Oxford, 2014 pp. 237−298.

[10] F. Rouquerol, J. Rouquerol, K. Sing, Adsorption by powders & porous solids, Academic Press, London, 1999, pp. 79−83.

[11] S. Lowell, J.E. Shields, M.A. Thomas, M. Thommes, Characterization of porous solids and powders: surface area, pore size and density, Springer Science & Business Media, 2006.

[12] R. Bardestani, G.S. Patience, S. Kaliaguine, Experimental methods in chemical engineering: specific surface area and pore size distribution measurements—BET, BJH and DFT. Can. J. Chem. Eng. 97 (2019) 2781−2791.

[13] K.S.W. Sing, D.H. Everett, R.A.W. Haul, L. Moscou, R.A. Pierotti, J. Rouquerol, T. Siemieniewska, Reporting physisorption data for gas/solid systems with special reference to the determination of surface area and porosity (Provisional), Pure Appl. Chem. 57 (1985) 603−619.

[14] E.P. Barrett, L.G. Joyner, P.P. Halenda, The determination of pore volume and area distributions in porous substances. J. Am. Chem. Soc. 73 (1951) 373−380.

[15] Z. Chen, T. Bai, Z. Pan, Coal reservoir characterization. Coal production and processing technology. CRC Press, Taylor & Francis Group, Boca Raton, United States, 2015.

[16] S.J. Gregg, K.S.W. Sing, Adsorption, Surface area and porosity, Academic Press, London, 1982.

[17] Q. Pan, P. Guo, J. Duan, Q. Cheng, H. Li. Comparative crystal structure determination of griseofulvin: powder X-ray diffraction versus single-crystal X-ray diffraction, Chin. Sci. Bull. 57 (2012) 3867−71.

[18] B. Fultz, J.M. Howe, The TEM and its optics. In: Transmission electron microscopy and diffractometry of materials, New York: Springer, 2012, pp. 59−66.

[19] J.M. Zuo, J.C.H. Spence, Advanced transmission electron microscopy, Springer Science, Business Media, New York, 2017.

[20] J. Zheng, K. Nagashima, D. Parmiter, J. de la Cruz, A. K. Patri, SEM X-ray microanalysis of nanoparticles present in tissue or cultured cell thin sections. In: Characterization of nanoparticles intended for drug delivery, Humana Press, Springer, 697 (2011) 93−99.

[21] D.E. Newbury, N.W.M. Ritchie, Is scanning electron microscopy/energy dispersive X-ray spectrometry (SEM/EDS) quantitative, Wiley Online Library, 9 (2012) 141−168.

[22] M. Boudart, Turnover rates in heterogeneous catalysis, Chem. Rev. 95 (1995) 661−666.

[23] G.C. Bond, Chemisorption and reactions of hydrogen. In: Metal-Catalysed Reactions of Hydrocarbons. Fundamental and applied catalysis, Boston, MA, Springer, 2005, pp. 93−152.

[24] D. Cox, K. Reichmann, D. Trevor, A. Kaldor, CO chemisorption on free gas phase metal clusters, J. Chem. Phys. 88 (1988) 111−119

[25] X. Shen, L.J. Garces, Y. Ding, K. Laubernds, R.P. Zerger, M. Aindow, E.J. Neth, S.L Suib, Behavior of H_2 chemisorption on Ru/TiO_2 surface and its application in evaluation of Ru particle sizes compared with TEM and XRD analyses. Appl. Catal. 335 (2008) 187−195.

[26] J.E. Benson, M. Boudart, Hydrogen-oxygen titration method for the measurement of supported platinum surface areas, J. Catal. 4 (1965) 704−710.

[27] J.E. Benson, H.S. Hwang, M. Boudart, Hydrogen-oxygen titration and carbon monoxide chemisorption for the measurement of supported palladium surface areas, J. Catal. 30 (1973) 146−153.

[28] F. Menegazzo, M. Manzoli, A. Chiorino, F. Boccuzzi, T. Tabakova, M. Signoretto, F. Pinna, N. Pernicone, Quantitative determination of gold active sites by chemisorption and by infrared measurements of adsorbed CO, J. Catal. 237 (2006) 431−434.

[29] K. Shin'inchi, Y. Yzawa, A. Satsuma, T. Hattori, Determination of metal dispersion of Pt/CeO_2 catalyst by CO-pulse method, J. Jpn. Pet. Inst. 48 (2005) 173−177.

[30] G. Leofanti, G. Tozzola, M. Padovan, G. Petrini, S. Bordiga, A. Zecchina, Catalyst characterization: characterization techniques. Catal. Today 34 (1997) 307−327.

[31] P.Canton, G. Fagherazzi, M. Battagliarin, F. Menegazzo, F. Pinna, N. Pernicone, Pd/CO average chemisorption stoichiometry in highly dispersed supported Pd/γ-Al2O3 catalysts, Langmuir 18 (2002) 6530−6535.

[32] F.W. Fifield, D. Kealy, Principles and practice of analytical chemistry, fifth ed., Hoboken, Blackwell Science Ltd, 2000.

[33] B. Charles, J. Kenneth, Concepts, Instrumentation and techniques in inductively coupled plasma optical emission spectrometry, Third ed., Perkin Elmer, 3 (1997) 36−71.

[34] S. Ghosh, V. Prasanna, B. Sowjanya, P. Srivani, M. Alagaraja, D. Banji, Inductively coupled plasma–optical emission spectroscopy: a review, Asian J. Pharm. Anal. 3 (2013) 24−33.

[35] F. Najafi, M. Rajabi, Thermal gravity analysis for the study of stability of graphene oxide–glycine nanocomposites. Int. Nano Lett. 5 (2015) 187−190.

[36] F. Rouessac, A. Rouessac, Gas Chromatography in: Chemical analysis. Modern instrumentation methods and techniques, 2nd ed., John Wiley & Sons, 2013.

[37] K.D. Bartle, P. Myers, History of gas chromatography. Trends Analyt. Chem. 21(2002) 547−557.

[38] E. Lundanes, L. Reubsaet, T. Greibrokk, Chromatography: basic principles, sample preparations and related methods, Wiley-VCH, Weinheim, 2013.

[39] L.O. Fagundes, R. M. Lago, F. C. C. Moura, F. G. Pinto, E. N Santos, Experiments on heterogeneous catalysis using a simple gas chromatograph, J. Chem. Educ. 83 (2006) 417.

[40] J.T. Scanlon, D. E. Willis, Calculation of flame ionization detector relative response factors using the effective carbon number concept, J. Chromatogr. Sci. 23 (1985) 333–340.

[41] M. Kállai, Z. Veres, J. Balla, Response of flame ionization detectors to different homologous series, Chromatographia 54 (2001) 511−517.

[42] J.E. Szulejko, Y.H. Kim, K.H. Kim, Method to predict gas chromatographic response factors for the trace-level analysis of volatile organic compounds based on the effective carbon number concept, J. Sep. Sci. 36 (2013) 3356−3365.

[43] T. Boublik, V. Fried, E. Hala, The Vapour Pressures of Pure Substances; Elsevier: Amsterdam, 1973.

[44] D.R. Lide, Handbook of Chemistry and Physics, 84th ed., CRC press, 2004.

[45] C. Perego, S. Peratello, Experimental methods in catalytic kinetics, Catal. Today 52 (1999) 133−145.

[46] J.A. Dumesic, G.W. Hube, M. Boudart, Principles of heterogeneous catalysis. In: Handbook of heterogeneous catalysis, Wiley Online Library, 2008, pp.1−15.

[47] P.B. Weisz, C.D. Prater, Interpretation of measurements in experimental catalysis, Adv. Catal. 6 (1954) 143−196.

[48] M. Misono, Basis of Heterogeneous catalysis in: Heterogeneous catalysis of mixed oxides, Elsevier, 176 (2013) 1−23.

Chapter 3. Turnover Rate of Metal-Catalysed Hydroconversion of 2,5-Dimethylfuran: Gas-Phase Versus Liquid-Phase

3

3.1. Introduction

Furanic compounds derived from biomass attract considerable interest as a renewable feedstock, which can be converted to transportation fuels, lubricants and a wide range of value-added chemicals such as aldehydes, ketones and alcohols via catalytic hydrogenation, hydrogenolysis and hydrodeoxygenation, hereinafter referred to as hydroconversion ([1–14] and references therein). These reactions can be carried out over supported metal catalysts in the gas or liquid phase. It has been reported that in the hydrogenation of furanic compounds, such as 2-methylfuran, 2,5-dimethylfuran (DMF) and furfural, Pt exhibits a higher selectivity to ring-opened products (ketones and alcohols), whereas Pd, Rh and Ru have high selectivity to ring-saturated tetrahydrofuran derivatives ([6,8,13] and references therein). The difference in selectivity of Pt from Pd, Rh and Ru has been explained by the different bonding of furanic compounds to these metals [6,15]. According to a density functional theory (DFT) study [15], the furan ring binds parallel to the noble metal surface either via a single π C=C bond or via two σ bonds with two C atoms of the C=C bond. The σ-bonding is preferred for Pt, whereas the π-bonded mode is favourable for Pd, Rh and Ru. It is suggested that σ-bonding, distorting the aromaticity of the furan ring, favours ring hydrogenolysis, whereas π-bonding favours ring hydrogenation [6,15]. Nevertheless, the initial π-bonding of DMF to a Pt site may play an important role in this reaction (see Section 3.2.4 below).

Platinum, due to its high activity in the hydrogenolysis of furan rings, is one of the most efficient catalysts for hydroconversion of furanic compounds to ring-opened products. It has been demonstrated that in hydroconversion of DMF on Pt, 2-hexanone, the primary ring-opened product and 2,5-dimethyltetrahydrofuran (DMTHF), the primary ring-saturated product, are formed directly from DMF in parallel pathways [6,13]. Ring cleavage of DMF has been reported to be 14 times faster than ring saturation on 5%Pt/C in the liquid phase batch reaction (in nonane, 80 °C, 5.5 bar H_2) [6] and 9 times faster in the gas phase reaction in a fixed-bed flow reactor on 1% Pt/h-BN (hexagonal boron nitride support, 200 °C, 1 bar H_2) [13].

The gas phase hydroconversion process can be expected to be more efficient and environmentally benign than the liquid phase process due to low hydrogen pressure, continuous operation and easy product separation. In this connection, it is interesting to compare catalyst turnover rates for the gas phase and liquid phase hydroconversion of furanic compounds. Turnover rate or turnover frequency (TOF) is the rate of reaction referred to the number of catalytic sites. It provides information about the rate at which catalytic cycles turn over, which is useful both for the theory and practice of catalysis. According to Boudart, in a mechanistic sense, the comparison of TOF values is more insightful than that based on a specific rate. However, obtaining accurate TOF values is a rather difficult task. The difficulty in measuring TOF is two-fold: (i) determining correct reaction rate unaffected by diffusion limitations and catalyst deactivation and (ii) counting catalytic active sites that may not be uniform [16].

Recently, Louie et al. [6] have reported a detailed kinetic study of liquid phase DMF hydroconversion in a batch reactor over commercial carbon-supported Pt, Pd, Rh and Ru catalysts (5–10% nominal metal loading) and provided the TOF values for all the catalysts

at identical conditions (80 °C, 5.5 bar H_2, nonane as a solvent), with the number of surface metal sites determined from CO chemisorption.

In this work, we investigate the gas phase hydroconversion of 2,5-dimethylfuran (DMF), chosen as a model for biomass-derived furanic compounds, in a fixed-bed flow reactor at the gas solid interface over the same commercial carbon-supported noble metal catalysts (3–10 wt% nominal metal loading) at similar conditions (70–90 °C), except at ambient pressure. The metal dispersion is measured using CO chemisorption as in [6]. Kinetics of DMF hydroconversion over Pt/C was studied at DMF conversion ≤ 20%. The reaction rate (R) was determined as $R = XF/W$, where X is the fractional conversion of DMF, F is the inlet molar flow rate of DMF and W is the catalyst weight. The TOF values of metal sites are determined from zero-order kinetics in the absence of diffusion limitations and compared with those reported for the liquid phase reaction [6]. It is demonstrated that the gas phase hydroconversion of DMF over the carbon-supported noble metal catalysts is much more efficient than the corresponding liquid phase reaction, with the TOF values one order of magnitude greater than those in the liquid phase. In addition, hydrogenolysis of ring-saturated furanic compounds, tetrahydrofuran (THF) and 2,5-dimethyltetrahydrofuran (DMTHF) are studied for comparison with DMF. Experimental techniques and procedures are described in detail in Chapter 2.

3.2. Results and Discussion

3.2.1. Catalyst Characterisation

Table 3.1 presents information about the catalysts studied including catalyst texture (surface area, pore volume and pore size), metal dispersion (determined from CO adsorption) and metal particle size (determined by TEM). The TEM images of carbon-supported metal catalysts are shown in Fig. 2.12 in Chapter 2. For 9.6%Pt/C, the metal particle size also determined by XRD using the Scherrer equation, which agrees with TEM (Table 3.1).

Table 3.1 Characterisation of carbon-supported noble metal catalysts.[a]

Catalyst	Surface area[a] (m^2g^{-1})	Pore volume[b] (cm^3g^{-1})	Pore diameter[c] (Å)	D[d]	d[e] (nm)
7.8%Pd/C	820	0.561	27	0.326±0.034	4.2±1.3
3.0%Ru/C	1108	0.935	34	0.232±0.010	7.6±2.6
4.0%Rh/C	830	0.703	34	0.513±0.032	3.3±0.7
9.6%Pt/C[f]	713	0.558	31	0.039±0.007	11.7±3.0[g]
7.0%Pt/C[f]	746	0.581	31	0.039±0.010	9.3[h]

[a]BET surface area. [b]Single point total pore volume. [c]Average BET pore diameter. [d]Metal dispersion from CO adsorption (average of three measurements). [e]Metal particle size from TEM. [f]7.0%Pt/C and 9.6%Pt/C are two samples of the same commercial catalyst with different moisture content. [g] For 9.6%Pt/C, d = 7.2 nm from XRD. [h]From XRD.

3.2.2. Gas-Phase Hydroconversion of DMF over Carbon-Supported Noble Metal Catalysts

Table 3.2 shows the performance of Pt, Pd, Rh and Ru carbon-supported catalysts in the gas phase hydroconversion of DMF at 70–90 °C and relatively long contact times *W/F* = 25–125 g h mol^{-1}. At such conditions, all these catalysts gave ~100% DMF conversion. As expected, Pt gave mainly ring-cleavage products (2-hexanone, 2-hexanol and hexane) in 85% total selectivity together with a small amount of the ring-hydrogenation product 2,5-dimethyltetrahydrofuran (DMTHF, *cis* and *trans* isomers, 7–13% selectivity). Reaction time course with Pt/C at 90 °C for 20 h time on stream (TOS) is shown in Fig. 3.1, with an average 2-hexanol yield of 74%. In contrast, Pd, Rh and Ru were active in ring hydrogenation, yielding almost exclusively DMTHF, with the selectivity increasing in the order Ru < Rh ≤ Pd. *cis*-DMTHF, having a lower boiling point and shorter GC retention time [17], was the predominant isomer (*cis/trans* = 6–10).

Table 3.2 Hydroconversion of 2,5-dimethylfuran over noble metal catalysts.[a]

Catalyst	Conv.[b]	Product selectivity [b] (mol %)				
	(%)	Hexane	DMTHF	2-Hexanone	2-Hexanol	Other
9.6%Pt/C+SiO_2 (1:9 w/w)	>99	11.6	13.1	0.9	72.5	1.9
9.6%Pt/C+SiO_2 (1:9 w/w)[c]	>99	8.8	10.7	2.1	74.2	4.2
7.0%Pt/C+SiO_2 (1:1 w/w)[c,d]	>99	19.8	7.3	4.6	61.4	6.9
7.8%Pd/C+SiO_2(1:7 w/w)	>99	0.0	99.8	0.0	0.0	0.2
3.0%Ru/C+SiO_2(1:2 w/w)	>99	0.0	94.6	0.0	4.7	0.6
4.0%Rh/C+SiO_2 (1:4 w/w)	>99	0.0	99.6	0.0	0.3	0.1

[a]70 °C, 0.20 g catalyst (1% metal loading per total catalyst weight), 1.6 kPa DMF partial pressure, 20 mL min^{-1} H_2 flow rate, 4 h TOS, *W/F* = 25–125 g h mol^{-1}. [b]Average conversion and product selectivity over 4 h TOS. [c] At 90 °C. [d] 3.5% Pt loading, in H_2 + N_2 (1:3 v/v) gas flow (0.25 bar H_2 partial pressure).

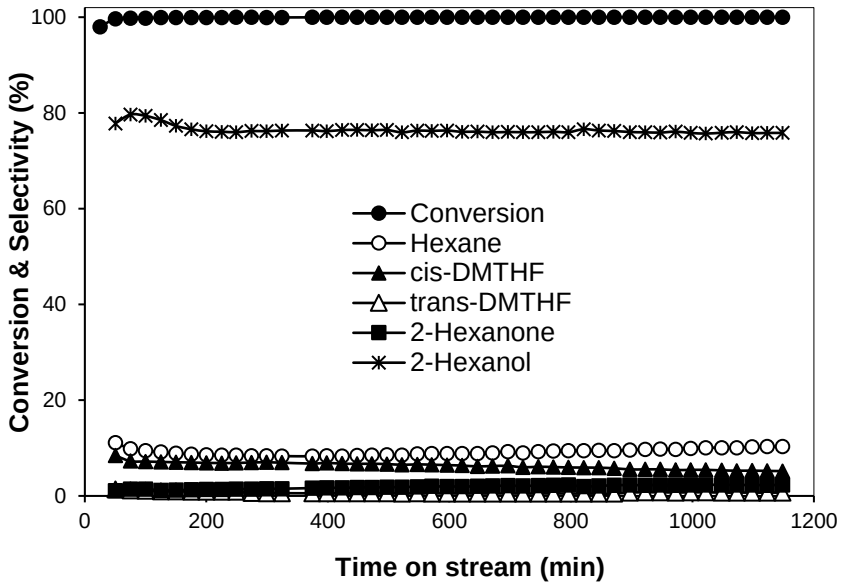

Fig. 3.1 Catalyst performance in hydrogenation and hydrogenolysis of DMF during 20 h TOS (1.6 kPa partial pressure) over 7.0%Pt/C + SiO_2 catalyst (0.20 g total weight, 30 mg Pt/C), 90 °C, 20 mL min^{-1} H_2 flow rate, W/F = 37.6 g h mol^{-1}.

The M/C catalysts, except Pd/C, exhibited some deactivation, which can be seen at shorter contact times. Thus, for Pt/C, the conversion of DMF at 70 °C and W/F = 2.5 g h mol^{-1} declined from 100 to 77% in 5 h TOS, while the product selectivity remained unchanged (Fig. 3.2). At such conditions, 2-hexanone rather than 2-hexanol was the main reaction product (57% selectivity). Catalyst deactivation was not unexpected since metal catalysts usually experience deactivation in the hydrogenation of C=C bonds, which is thought to be caused by carbonaceous deposits blocking active metal sites [18]. Surprisingly, Pd/C exhibited stable activity at least for 3 h TOS as can be seen from Fig. 3.3 at 61% DMF conversion level. The deactivation obeyed first-order rate equation $\ln(X_t/X_o) = -k_d t$ with the deactivation rate constant $k_d = 8.0 \cdot 10^{-4}$ min^{-1} (Fig. 3.4), where X_o and X_t are the initial conversion and the conversion at any time t. Here, conversion X is used instead of the reaction rate because the reaction was zero-order in DMF (see Section 3.2.3); for a zero-order reaction the rate is directly proportional to the conversion. The fact that the selectivity

did not change while the activity decayed suggests that deactivation reduced the number of active metal sites without affecting the state of the remaining sites.

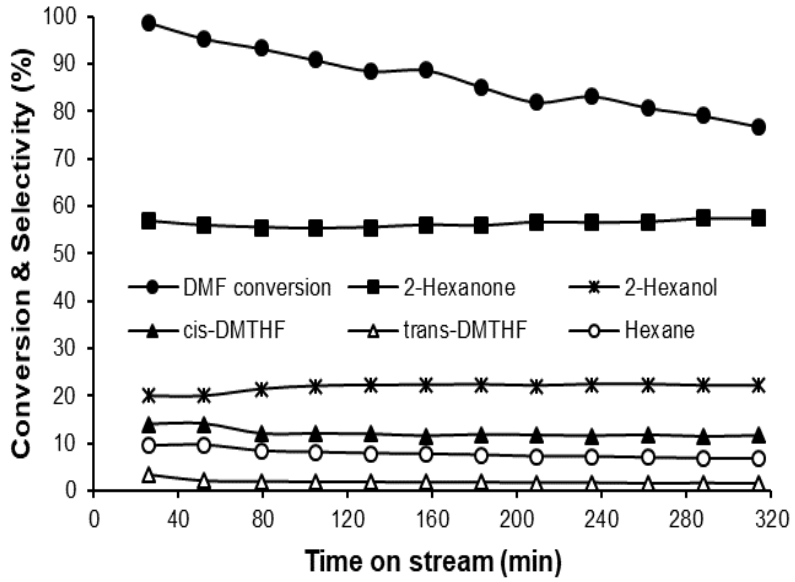

Fig. 3.2 Time course for DMF hydroconversion over 7.0%Pt/C + SiO_2 catalyst (0.20 g total weight, 2.0 mg Pt/C) at 1.6 kPa DMF partial pressure, 70 °C, 20 ml min^{-1} H_2 flow rate, W/F = 2.5 g h mol^{-1}).

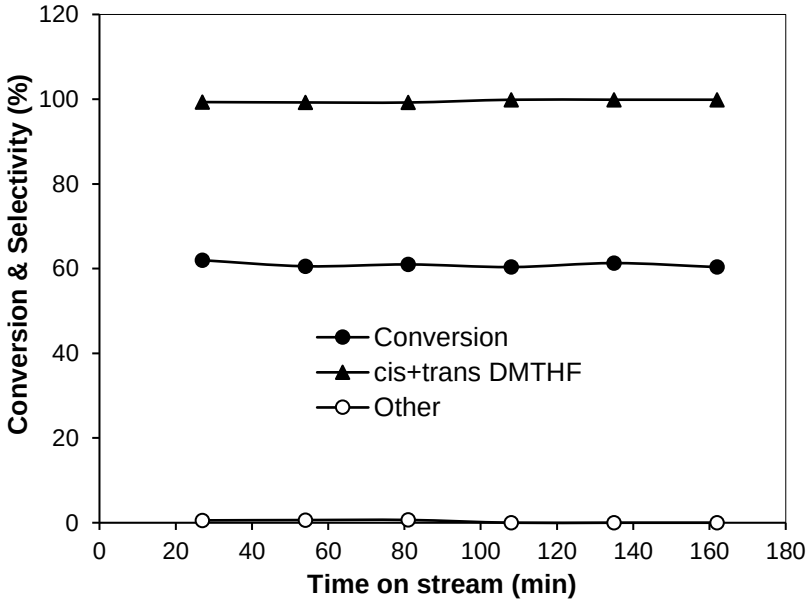

Fig. 3.3 Time course for DMF hydrogenation over 7.8%Pd/C + SiO_2 catalyst (0.20 g total weight, 0.6 mg Pd/C) at 1.6 kPa DMF partial pressure, 70 °C, 40 ml min^{-1} H_2 flow rate, W/F = 0.38 g h mol^{-1}.

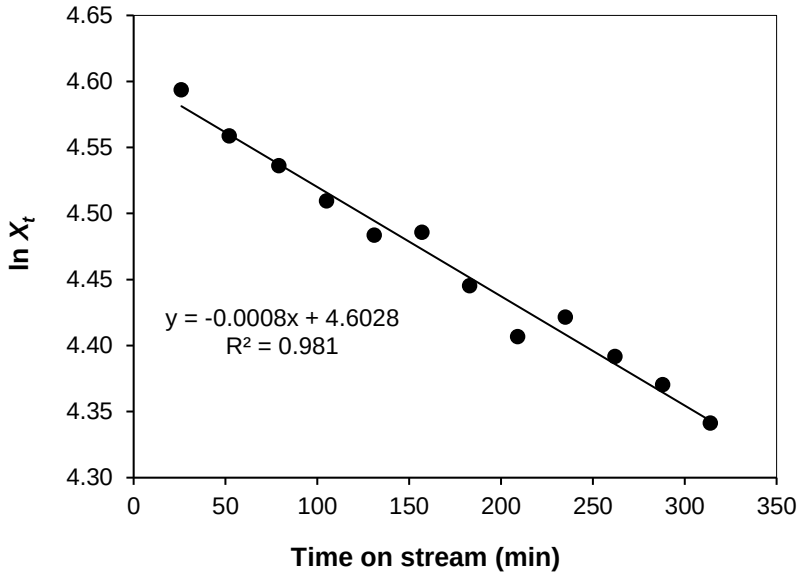

Fig. 3.4 Deactivation plot ln (X_t/X_o) = -$k_d t$ for DMF hydrogenation over 7.0%Pt/C + SiO_2 catalyst (0.20 g total weight, 2.0 mg Pt/C) at 1.6 kPa DMF partial pressure, 70 °C, 20 ml min^{-1} H_2 flow rate, W/F = 2.5 g h mol^{-1}, catalyst pre-treatment at 200 °C/1h/H_2. The first order deactivation rate constant $k_d = 8.0 \cdot 10^{-4}$ min^{-1}.

An attempt was made to regenerate the Pt catalyst by treating it with hydrogen and air. In-situ treatment of spent Pt/C catalyst with hydrogen alone (20 ml min^{-1} flow) at 200 °C and 1 bar pressure for 1 h was not successful to regain catalyst activity. However, in-situ catalyst treatment with air flow (20 ml min^{-1}, 1 bar pressure) at 200 °C/1 h followed by reduction with H_2 at the same conditions fully restored catalyst activity. This is demonstrated in Fig. 3.5, which shows two catalyst regenerations in succession. Effective catalyst regeneration using successive air and H_2 treatment and failed regeneration using H_2 alone indicate that the deactivation was caused by carbonaceous deposits on metal particles, which often occur in hydrogenation on metal catalysts [18].

The process of carbon deposition is suggested to start with the removal from the chemisorbed hydrocarbon of more hydrogen atoms than are necessary to achieve the desired product [18]. Carbon formation can then proceed in various ways. The di-carbon species may break down to mono-carbon species then polymerize, or polymerization may occur without this. Crabon deposition can include free radical coking mechanism or acidity in the

catalyst. At the gas/coke interface, the polyaromatics are not completely dehydrogenated. At this surface, hydrogen abstraction reactions by free radicals from the gas phase can occur. Hydrogen, methyl, and ethyl radicals are the most active species. Carbon deposition can affect catalyst activity in different ways. It may either dissolve in and diffuse through the metal, forming some kind of carbide. It may also cover some or all of the metal surface, or migrate to the support and block the pores of a microporous catalyst [18].

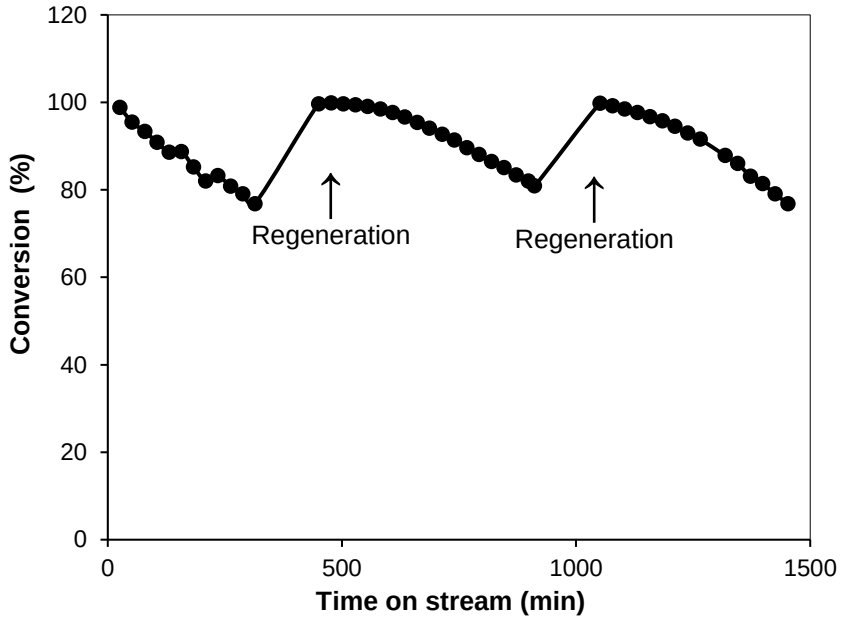

Fig. 3.5 Time course of DMF hydrogenation over Pt/C with catalyst regeneration over 7.0%Pt/C + SiO_2 catalyst (1:99 w/w, 0.20 g total weight, 2.0 mg Pt/C, 0.07% Pt loading), 1.6 kPa DMF partial pressure, 70 °C, 20 mL min^{-1} H_2 flow rate, *W/F* = 2.5 g h mol^{-1}, catalyst pre-treatment at 200 °C/1h/H_2, catalyst regeneration at 200 °C/1h/air followed by reduction at 200 °C/1h/H_2).

The results shown in Table 3.2 demonstrate that the selectivity pattern in the gas phase DMF hydroconversion in a flow system is similar to that reported previously for the liquid phase batch reaction in the presence of similar carbon-supported noble metal catalysts [6]. Importantly, the gas phase reaction occurred more efficiently and under milder conditions than the liquid phase one. Thus, in the gas phase, Pt/C gives ~100% DMF conversion at 70 °C and ambient pressure (Table 3.2), whereas in the liquid phase 80% conversion in 0.5 h at 80 °C and 5.5 bar H_2 pressure [6]. The liquid phase reaction requires elevated H_2 pressure

to overcome low H_2 solubility [19]. The gas phase reaction with Pt/C occurs with full DMF conversion even at a H_2 partial pressure as low as 0.25 bar (Table 3.2). Consequently, the gas phase hydroconversion of DMF occurs deeper than the liquid phase one. In the liquid phase reaction over Pt/C, 2-hexanone has been reported to be the main product [6], whereas in the gas phase 2-hexanone underwent further hydrogenation to give 2-hexanol (74% yield at 90 °C, Table 3.2, Fig. 3.6).

Therefore, the gas phase process offers significant economic and environmental benefits over the liquid phase counterpart due to the milder reaction conditions, absence of solvent, continuous rather than batch operation and easy product separation. It should be noted, however, that the efficiency of DMF hydroconversion in the gas phase may depend significantly on the support. Thus, the reaction on Pt/BN (h-BN boron nitride) and Pt/SiO_2 has been reported to proceed at higher temperatures (150–350 °C) with a low DMF conversion (<10% at 150 °C), albeit with the selectivity pattern similar to that on Pt/C [13].

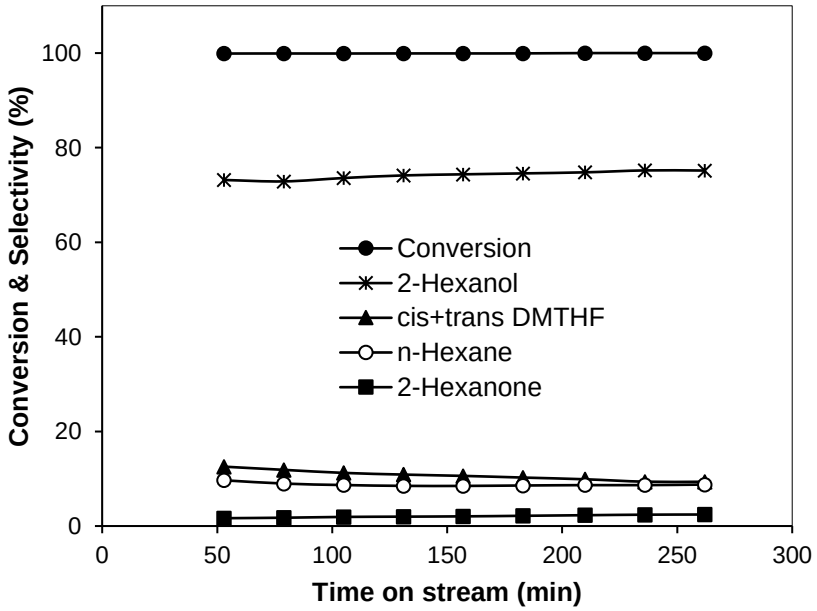

Fig. 3.6 Time course for hydrogenation and hydrogenolysis of DMF (1.6 kPa partial pressure) over 9.6%Pt/C + SiO_2 catalyst (1:9 w/w, 0.20 g total weight, 20 mg Pt, 1% Pt loading), 90 °C, 20 mL min^{-1} H_2 flow rate, W/F = 25 g h mol^{-1}, 4 h TOS.

The proposed reaction network for the metal catalysed DMF hydroconversion in the gas phase is shown in Scheme 3.1. It reflects upon the different reaction selectivity of Pt, on one hand and Pd, Rh and Ru, on the other. The parallel pathways of ring saturation (1) and ring cleavage (2) on Pt occur with a cleavage/saturation molar ratio of 6–12 (Table 3.2) in agreement with previous reports [6,13]. It has been suggested that the ring-cleavage pathway on Pt may proceed via initial enol formation, followed by keto-enol tautomerization [6]. Further consecutive hydrogenations lead to the formation of 2-hexanone, 2-hexanol and hexane. In liquid phase DMF hydroconversion on Pt/C, 2-hexanol has been reported to be partly formed in parallel to 2-hexanone by direct hydrogenation of enol [6]. In our system, no such pathway was observed; our results indicate that 2-hexanol is formed by hydrogenation of 2-hexanone as shown in Scheme 3.1. This is supported by the plot of reaction selectivity versus the contact time *W/F* (Fig. 3.7), which clearly shows that 2-hexanol is produced by hydrogenation of 2-hexanone. Therefore, the ring-cleavage pathway (2) in the gas phase is different from that in the liquid phase.

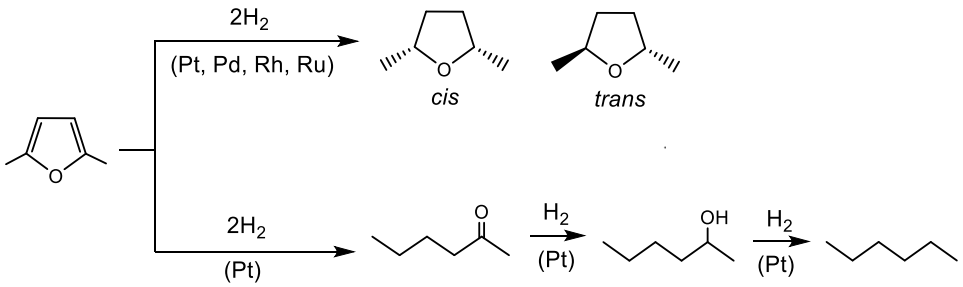

Scheme 3.1 Reaction network for hydroconversion of DMF catalysed by noble metals.

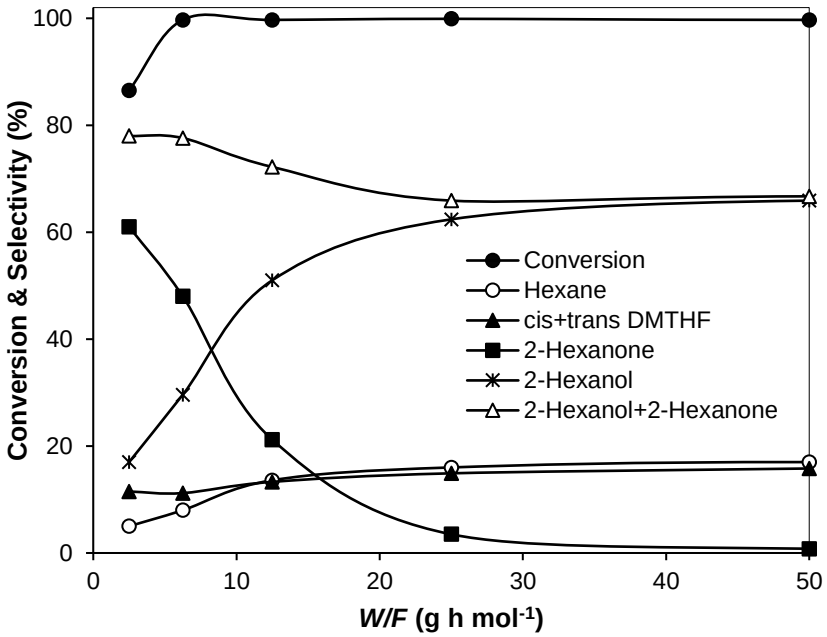

Fig. 3.7 Plot of DMF conversion and product selectivity versus contact time *W/F* for hydroconversion of DMF over 7.0%Pt/C + SiO_2 catalyst (0.20 g total weight), 1.6 kPa DMF partial pressure, 70 °C, 20 mL min^{-1} H_2 flow rate, 1 h TOS; the *W/F* was varied by varying the amount of 7.0%Pt/C in the Pt/C + SiO_2 mixture).

Less clear is the source of hexane since it could form from 2-hexanol and/or directly from 2-hexanone. This is supported by increasing hexane selectivity at the expense of the total 2-hexanone + 2-hexanol selectivity as the contact time increased (Fig. 3.7). Due to the low hexane selectivity, it is hardly possible to identify its source from this graph. More useful are the results in Table 3.2 showing that an increase in Pt loading from 1 to 3.5% caused a 2-fold increase in hexane selectivity from 8.8 to 19.8% at 90 °C, which was mainly at the expense of 2-hexanol. This, therefore, supports the formation of hexane through 2-hexanol hydrogenation, although more work is required to strengthen this conclusion.

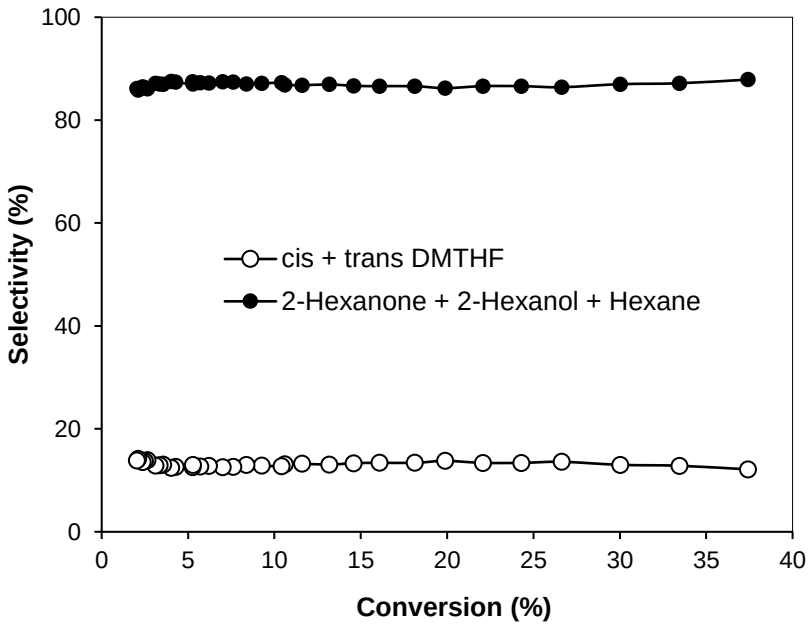

Fig. 3.8 Parallel furan ring hydrogenation and ring cleavage in hydroconversion of DMF over 7.0%Pt/C + SiO_2 catalyst (1:99 w/w, 0.05 g total catalyst weight, 0.07% Pt loading), 1.6 kPa DMF partial pressure, 70 °C, 40 mL min^{-1} H_2 flow rate, 20 h TOS, W/F = 0.31 g h mol^{-1}).

The parallel formation of DMTHF and 2-hexanone (together with 2-hexanol and hexane) on Pt is further supported by the data presented in Fig. 3.8, which shows the product selectivity as a function of DMF conversion at a short contact time W/F = 0.31 g h mol^{-1}. It is evident that both the total 2-hexanone + 2-hexanol + hexane selectivity and *cis* + *trans*-DMTHF selectivity do not depend on DMF conversion, which shows that the ring hydrogenation pathway (yielding DMTHF) and the ring cleavage pathway (yielding 2-hexanone, 2-hexanol and hexane) occur in parallel, similar to the reaction in the liquid phase [6]. This is also in agreement with [13] suggesting the same parallel pathways for gas phase DMF hydroconversion on Pt/h-BN and Pt/SiO_2, whereas a consecutive route with ring hydrogenation preceding ring hydrogenolysis has been suggested elsewhere [7−10]. From Fig. 3.8, the rate of ring hydrogenolysis is 9 times greater than the rate of ring hydrogenation on Pt/C. The same result has been reported for Pt/h-BN at 200 °C [13]. For the liquid phase reaction over Pt/C, DMF ring hydrogenolysis has been reported to occur 14 times faster than ring hydrogenation (in nonane, 80 °C, 5.5 bar H_2 pressure) [6]. It should be noted that the

hydrogenolysis of DMTHF to 2-hexanol occurs three orders of magnitude slower than the hydrogenolysis of DMF (see below), hence does not affect this conclusion.

3.2.3. Turnover rate: Gas-Phase versus Liquid-Phase

Kinetics of the gas phase hydroconversion of DMF over M/C catalysts was examined at DMF conversion ≤ 20% in the temperature range 70–90 °C, focusing mainly on Pt/C as the most active catalyst. The reaction rates were determined at short contact times W/F = 0.13–1.9 g·h·mol^{-1} and 1 h TOS. At such conditions, catalyst deactivation was small (see Section 3.2.2 for details).

The rate of DMF hydroconversion on Pt/C was found to be zero order in DMF partial pressure (Fig. 3.9), which indicates that the catalyst was saturated with DMF molecules. The order in hydrogen partial pressure was found to be 0.40 (Fig. 3.10). Zero order in DMF was also found for Pd/C, Rh/C and Ru/C. It should be noted that a zero-order reaction rate does not depend on DMF conversion and is equal to the rate constant.

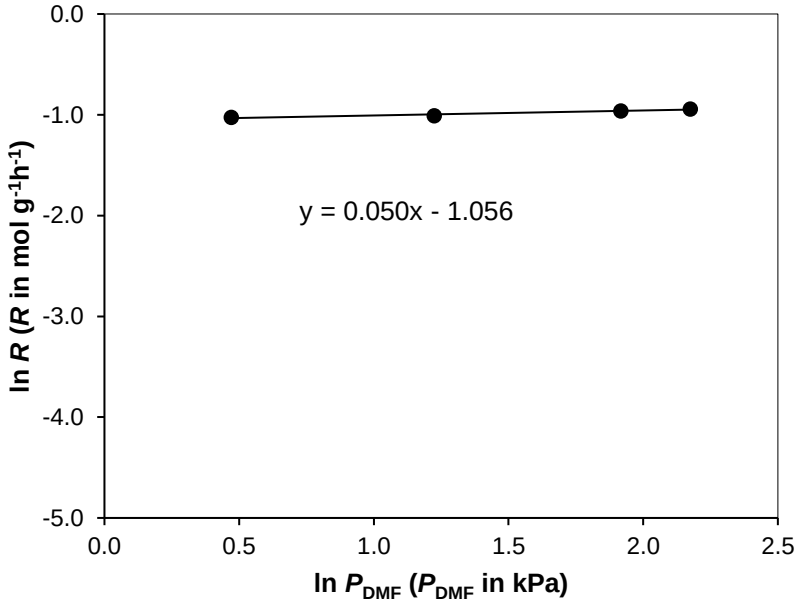

Fig. 3.9 Effect of DMF partial pressure on the rate of DMF hydroconversion over Pt/C (9.6%Pt/C + SiO_2 (1:78 w/w, 0.20 g total weight, 0.1% Pt loading), 70 °C, 40 mL min^{-1} H_2 flow rate), 1 h TOS.

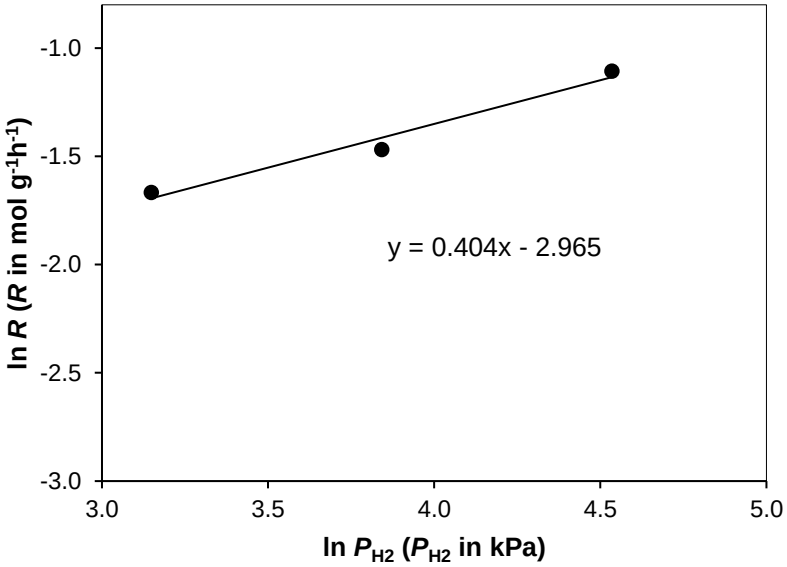

Fig. 3.10 Effect of hydrogen partial pressure on the rate of DMF hydroconversion over Pt/C, 6.8 kPa DMF partial pressure, 9.6%Pt/C + SiO_2 catalyst (1:78 w/w, 0.20 g total weight, 0.1% Pt loading), 70 °C, 40 mL min^{-1} H_2 + N_2 flow rate, varied H_2/N_2 ratio), 1 h TOS.

The reaction over Pt/C had an activation energy E = 59.2 kJ·mol^{-1} (see the Arrhenius plot in Fig. 3.11). Given zero reaction order, this is a true value of E. The high E value and zero order in DMF indicate that the reaction is not diffusion limited and occurs under kinetic control. This conclusion was further strengthened via Weisz-Prater analysis [20].

The Weisz-Prater criterion, C_{WP} (Eq. 3.1), uses measured values of reaction rate to determine if internal diffusion is limiting the reaction [20]. If $C_{WP} << 1$, there are no diffusion limitations; when $C_{WP} >> 1$, internal diffusion strongly limits the reaction.

$$C_{WP} = \frac{r\rho l^2}{DC_b} \tag{3.1}$$

In this equation, r is the observed reaction rate per unit catalyst weight (mol $g^{-1}s^{-1}$), ρ is the bulk density of catalyst (g cm^{-3}), l is the radius of catalyst particle (cm), D is the effective diffusion coefficient (cm^2s^{-1}) and C_b is the bulk concentration of substrate in the feed (mol cm^{-3}).

For DMF hydrogenation over 9.6%Pt/C at 70 ºC, DMF conversion was 24.2% at W/F = 0.63 g h mol^{-1} (Table 3.3, first entry). This gives the rate: $r = XF/W$ = 0.386 mol g^{-1}h^{-1} = 1.07·10^{-4} mol g^{-1}s^{-1}. Other parameters are as follows: ρ = 0.33 g cm^{-3}, l = 0.25·10^{-2} cm (average particle radius for commercial 9.6%Pt/C with 20 – 80 μm diameter of catalyst particles) and C_b = 5.7·10^{-7} mol cm^{-3} at 70 ºC. The catalyst had a pore diameter of 3.1 nm in mesoporous range (Table 3.1). The Knudsen diffusion coefficient D for transport of DMF molecule into the pore was calculated by Eq. 3.2 [21]:

$$D = \left(\frac{d}{3}\right)\left(\frac{8RT}{\pi M}\right)^{1/2} \tag{3.2}$$

where R is the gas constant (8.314 J K^{-1}mol^{-1}), M is the molecular mass of DMF (0.0961 kg mol^{-1}), d is the mean pore diameter (3.1×10^{-9} m). From this equation, D = 2.9 ×10^{-7} m^{2}s^{-1} = 2.9 ×10^{-3} cm^{2}s^{-1}.

Overall, from Eq. 3.1, this gives C_{WP} = 0.14 < 1, which indicates no internal diffusion limitations. This agrees with [13], which reported no internal diffusion limitations for DMF hydroconversion over Pt/h-BN and Pt/SiO_2 at 150–250 °C (C_{WP} = 0.02 at 150 °C).

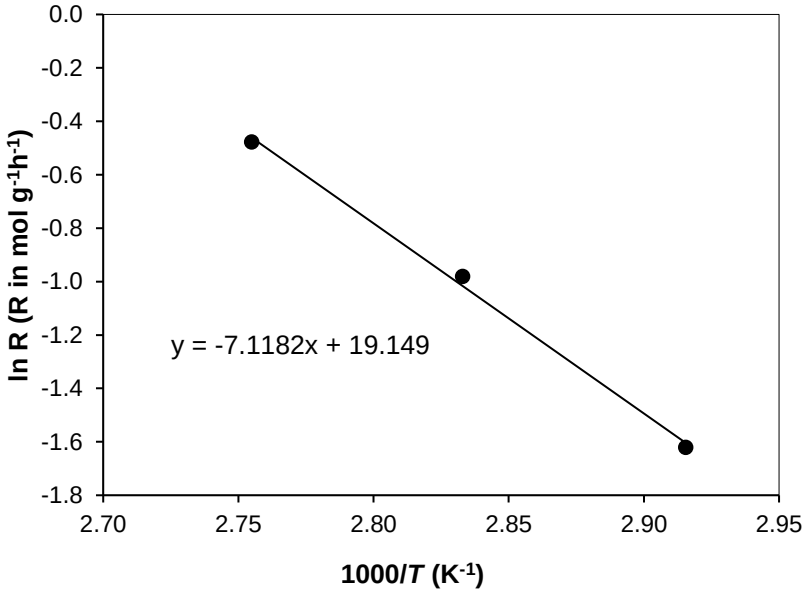

Fig. 3.11 Arrhenius plot for DMF hydroconversion over Pt/C (6.8 kPa DMF partial pressure, 9.6%Pt/C + SiO_2 catalyst (1:78 w/w, 0.20 g total weight, 0.1% Pt loading), 70–90 °C, 40 mL min^{-1} flow (E = 59.2 kJ mol^{-1}), 1 h TOS.

The kinetic parameters found for Pt/C are similar to those reported for the liquid phase reaction over Pt/C in nonane as a solvent: E = 45.3 kJ·mol^{-1} (70–100 °C), zero order in DMF and 0.6 order in H_2 [6]. For the liquid phase DMF hydroconversion on Pt/C, a mechanism involving non-competitive adsorption of DMF and H_2 on Pt sites has been suggested [6]. A similar mechanism may be expected to operate in the gas phase hydroconversion of DMF over Pt/C as follows from the similar reaction kinetics in both cases.

Table 3.3 presents the total turnover frequency of metal sites and product selectivity of DMF hydroconversion over M/C catalysts in the gas phase at 70 °C, 1 bar H_2 pressure and DMF conversion range X = 24–61%. The TOF values were calculated from zero-order reaction rates using metal dispersion given in Table 3.1. Selectivity patterns (Table 3.3) at lower DMF conversion X = 24–61% (short contact times W/F = 0.13–1.88 g h mol^{-1}) were similar to that at X = ~100% (W/F = 25–125 g·h·mol^{-1}) (Table 3.2), except for Pt/C, which gave 2-hexanone as the main product rather than 2-hexanol, as expected at shorter contact times.

Table 3.3 Turnover frequencies of noble metals in DMF hydroconversion.[a]

Catalyst	W/F (g h mol^{-1})	Conv.[b] (%)	TOF (s^{-1})	Product selectivity (mol %)[b]				
				Hexane	DMTHF[c]	2-Hexanone	2-Hexanol	Other
9.6%Pt/C	0.63	24.2	5.6	3.3	12.9	61.3	20.8	1.7
9.6%Pt/C[d]	0.44	42.8	14	5.2	10.5	60.0	23.3	1.0
4.0%Rh/C	0.13	48.8	5.4	0.0	83.6	1.4	0.0	15.0
7.8%Pd/C	0.38	60.7	3.8	0.0	99.2	0.2	0.0	0.6
3.0%Ru/C	1.88	12.1	0.26	0.0	84.2	6.6	1.2	8.0

[a]70 °C, 0.20 g total catalyst weight (M/C + SiO_2), 1.6 kPa DMF partial pressure, 40 mL min^{-1} H_2 flow rate. [b]DMF conversion and product selectivity at 1 h TOS. [c]A mixture of cis and trans isomers (cis/trans = 6–10). [d]At 80 °C, 9.6%Pt/C (0.7 mg) + SiO_2 (0.10 g total catalyst weight).

As seen from Table 3.3, the TOF values (s^{-1}) decrease in the order: Pt (5.6) > Rh (5.4) > Pd (3.8) >> Ru (0.26) at 70 °C. The TOF value for Pt increased to 14 s^{-1} at 80 °C. Our TOF values can now be compared with those reported by Louie et al. [6] for the liquid phase hydroconversion of DMF in nonane at 80 °C and 5.5 bar H_2 pressure. These TOF values (s^{-1}) are as follows: 5%Pt/C (1.77) > 5%Rh/C (0.62) > 10%Pd/C (0.25) >> 5%Ru/C (0.0) (given nominal metal loadings) [6]. 5%Ru/C was not active in the liquid phase at 80 °C; it showed a moderate activity at 160 °C (TOF = 0.27 s^{-1}) [6]. The two sets of total TOF values are reliable and fully comparable. In both cases, the rates are unaffected by diffusion limitations. The carbon-supported catalysts are practically the same commercial samples with 3–10% metal loading from Sigma-Aldrich, with metal dispersion measured by CO adsorption using a pulse method and the same stoichiometric coefficients. Given the very close reaction temperature range (70–80 °C), the active sites in both cases are most likely the same if not uniform.

Two facts emerge from these results. First, the TOF values for the gas phase and liquid phase reactions follow a similar order: Pt > Rh > Pd >> Ru; albeit the liquid phase set of TOF shows a greater diversity than the gas phase set. For the gas phase reaction, the TOF values for the most active metals Pt, Rh and Pd differ by only a factor of 3, whereas for the liquid phase reaction they differ by almost 1 order of magnitude, let alone Ru which is far less active. Second and more important, the TOF values for the gas phase reaction are about 1 order of magnitude greater than those for the liquid phase reaction (note the temperature difference between gas phase (70 °C) and liquid phase (80 °C) results). Hence, the gas phase process is potentially more efficient than the liquid phase process.

Clarification of the reasons for the higher efficiency of the gas phase process will require more detailed kinetic studies with systematic variation of reaction parameters. The difference in H_2 concentration in the two systems is not large and should have a relatively

small effect on reaction rate [20]. In the liquid phase system (nonane), [H_2] = ~0.02 M at 5.5 bar H_2 and 80 °C [6], whereas in our gas phase system, [H_2] = ~0.04 M in flowing hydrogen at 1 bar H_2 and 70 °C. Given the reaction order in H_2 pressure of ~0.5, this would account for only a factor of 1.4 increase in the rate in the gas phase compared to the liquid phase. The gas phase system with a low DMF concentration ([DMF] = $5.7 \cdot 10^{-4}$ M) can be viewed as an ideal gas with negligible intermolecular interactions, whereas the condensed liquid phase system ([DMF = 1.0 M) [6] is a much more complicated one, involving strong intermolecular forces that may significantly affect the reactivity. In the gas phase, at full DMF conversion, the concentration of reaction products such as 2-hexanone, 2-hexanol and water that could adsorb on the catalysts is less than 10^{-3} M, whereas in the liquid phase, even at 10% DMF conversion, it will be 0.1 M, i.e., two orders of magnitude greater. Hence, in the batch liquid phase system, competitive adsorption of reaction products could both impede the rate and differentiate the activity of metal sites to a greater extent than in the flow gas system.

3.2.4. Hydrogenolysis of Tetrahydrofuran and 2,5-Dimethyltetrahydrofuran

Next, we looked at the gas phase hydrogenolysis of ring-saturated furan derivatives, THF and DMTHF, over Pt/C and Pd/C catalysts for comparison with the hydroconversion of DMF. These reactions were carried out at 90–100 °C and 1 bar H_2 pressure. Table 3.4 shows the representative results for THF and Table 3.5 for DMTHF.

Table 3.4 Hydrogenolysis of tetrahydrofuran.[a]

Catalyst	*W/F* (h g mol^{-1})	Conversion [b] (%)	Product Selectivity [b] (%)	
			Butane	1-Butanol
9.6%Pt/C + SiO_2 (20)	7.0	0.6	6.5	93.5
7.8%Pd/C + SiO_2 (25)	8.8	0.0		

[a] 100 °C, M/C + SiO_2 catalyst bed (0.20 g total weight, in brackets the amount of M/C in mg), 5.7 kPa THF partial pressure, 20 mL min^{-1} H_2 flow, 4 h TOS. [b]Average conversion and product selectivity over 4 h TOS.

Table 3.5 Hydrogenolysis of DMTHF.[a]

Catalyst	*W/F* (h g mol^{-1})	T (°C)	Conv.[b] (%)	Product Selectivity [b] (%)			
				Hexane	2-Hexanone	2-Hexanol	Other
9.6%Pt/C + SiO_2 (20)	17.3	90	1.6	8.1	1.4	87.6	2.9
9.6%Pt/C + SiO_2 (20)	17.3	100	2.9	7.4	2.7	88.3	1.7
7.8%Pd/C + SiO_2 (25)	21.8	100	0.1	67.0	0.0	0.0	33.0

[a] M/C + SiO_2 catalyst bed (0.20 g total weight, in brackets the amount of M/C in mg), 2.3 kPa DMTHF partial pressure, 20 mL min^{-1} H_2 flow, 4 h TOS. [b] Average conversion and product selectivity over 4 h TOS.

As seen from Table 3.4, THF had negligible reactivity compared to DMF. Pt/C showed a tiny ring cleavage activity across the C−O bond (0.6% THF conversion), yielding 1-butanol in 94% selectivity at 100 °C. With Pd/C, no reaction was observed at all. DMTHF was more reactive than THF due to the presence of two electron-donating methyl groups (Table 3.5), yet far less reactive than the aromatic DMF. Again, Pt/C exhibited the ring hydrogenolysis activity, giving 88% of 2-hexanol at 1.6 and 2.9% DMTHF conversion at 90 and 100 °C, respectively. As expected, Pd/C showed almost no hydrogenolysis activity (0.1% DMTHF conversion at 100 °C).

The kinetics of the gas phase hydroconversion of THF and DMTHF over Pt/C was examined at 80 °C and substrate conversion ≤ 10%. In contrast to DMF, no catalyst deactivation was observed in THF and DMTHF hydroconversion. The reaction rates were determined using average conversion values for 3 h TOS. The hydroconversion of both THF and DMTHF was found to be zero order in the furanic substrate within the range of substrate partial pressure of 0.5–6 kPa.

Table 3.6 shows TOF values for the hydroconversion of DMF, DMTHF and THF catalysed by Pt/C at 80 °C calculated from initial substrate conversion at 1 h time on stream. The reactivity of furanic compounds towards ring hydrogenolysis across the C-O bond over Pt decreases in the order DMF (14) >> DMTHF (0.0058) > THF (0.0023), where in round brackets are the TOF values (s^{-1}) from Table 3.6. This order is in line with decreasing the electron density on the ring in this series. It is noteworthy that the aromatic DMF molecule is 2400 times more reactive than its saturated derivative DMTHF. Previously, DMT has been reported to exhibit a factor of 30 greater reactivity than DMTHF in the gas phase hydroconversion over Pt/h-BN at 200 °C [13]. The difference between [13] and our results may be explained by the difference in reaction temperature.

Table 3.6 TOF values for Pt-catalysed hydroconversion of furanic compounds.[a]

	DMF[b]	DMTHF[c]	THF[d]
W/F (g h mol^{-1})	0.44	70	42
Conversion (%)	42.8	2.8	0.67
TOF (s^{-1})[e]	14	0.0058	0.0023

[a] 80 °C, 9.6%Pt/C + SiO_2 catalyst (0.10 g total weight), 1 h TOS. [b] 9.6%Pt/C (0.0007 g), 1.6 kPa DMF partial pressure, 40 mL min^{-1} H_2 flow rate). [c] 9.6%Pt/C (0.040 g), 2.3 kPa DMTHF partial pressure, 10 mL min^{-1} H_2 flow rate). [d] 9.6%Pt/C (0.060 g), 5.7 kPa THF partial pressure, 10 mL min^{-1} H_2 flow rate. [e] TOF values calculated from reaction rate $R = XF/W$ using Pt dispersion $D = 0.039$ (Table 3.1).

Much greater reactivity of DMF compared to DMTHF suggests an important role of π-bonding between the aromatic DMF molecule and Pt site. As discussed in the Introduction, DFT analysis [15] indicates the key role of σ-bonding between the furan ring and Pt site for the high activity of Pt in the ring cleavage of furanic compounds. From the large difference in reactivity of DMF from DMTHF, initial interaction between DMF and Pt can be suggested to occur via π-bonding followed by rearrangement of π-bonded to σ-bonded DMF, leading to hydrogenolysis of the DMF ring. A much lower reactivity of DMTHF in comparison to DMF gives additional support to the reaction network shown in Scheme 3.1, thus confirming the formation of DMTHF and 2-hexanone directly from DMF via independent parallel pathways. On the other hand, the reactivity of DMTHF and THF in hydrogenolysis on Pt sites is quite close, with DMTHF being only two-fold more reactive than THF. This points to an enhancement of reactivity by σ-donor methyl groups in DMTHF probably due to strengthening its σ-bonding to the Pt site.

2.3. Conclusion

In the past two decades, considerable research activity into the metal-catalysed hydroconversion of furanic has been reported ([1−14] and references therein). However, not much kinetics has been documented, especially for the most active carbon-supported noble metal catalysts in the gas phase. This is not an easy task due to very high catalyst activities complicated by catalyst deactivation and possible diffusion limitations. In this work, the gas phase hydroconversion of DMF, chosen as a model furanic compound, has been investigated over carbon-supported Pt, Pd, Rh and Ru catalysts in a fixed-bed reactor at 70–90 °C and ambient pressure. The total turnover frequency (TOF) of metal sites in the gas phase DMF hydroconversion, including ring-opening and ring-saturation pathways, has been determined from zero-order kinetics in the absence of diffusion limitations and catalyst deactivation. The TOF values decrease in the sequence: Pt > Rh > Pd >> Ru. Comparison of the two sets

of TOF leads to the following conclusions. First, the TOF values for the gas phase and liquid phase reactions follow the same order, albeit the liquid phase set of TOF shows a greater diversity. Second and more important, the TOF values for the gas phase reaction are about 1 order of magnitude greater than those for the liquid phase reaction. The gas phase process, therefore, is potentially more efficient than the liquid phase process. A possible explanation for these facts can be given considering the concentration of hydrogen, the effect of competitive adsorption of reaction products and the accessibility of metal sites in the two systems. Ring-saturated furan derivatives, THF and DMTHF, are much less reactive than the aromatic DMF in the gas phase hydroconversion on Pt/C, with the TOF values decreasing in the order: DMF >> DMTHF > THF. Much greater reactivity of DMF compared to DMTHF suggests the importance of π-bonding between DMF and Pt site and gives additional support to the formation of DMTHF and 2-hexanone directly from DMF via independent parallel pathways.

References

[1] A. Corma, S. Iborra, A. Velty, Chemical routes for the transformation of biomass into chemicals, Chem. Rev. 107 (2007) 2411−2502.

[2] Y. Román-Leshkov, J.N. Chheda, J.A. Dumesic, Phase modifiers promote efficient production of hydroxymethylfurfural from fructose, Science 312 (2006) 1933−1937.

[3] R.M. West, Z.Y. Liu, M. Peter, J.A. Dumesic, Liquid alkanes with targeted molecular weights from biomass-derived carbohydrates, ChemSusChem 1 (2008) 417−424.

[4] G.W. Huber, J.N. Chheda, C.J. Barrett, J.A. Dumesic, Production of liquid alkanes by aqueous-phase processing of biomass-derived carbohydrates, Science 308 (2005) 1446−1450.

[5] Z.J. Brentzel, K.J. Barnett, K. Huang, C.T. Maravelias, J.A. Dumesic, G.W. Huber, Chemicals from biomass: combining ring-opening tautomerization and hydrogenation reactions to produce 1,5-pentanediol from furfural, ChemSusChem 10 (2017) 1351−1355.

[6] Y.L. Louie, J. Tang, A.M.L. Hell, A.T. Bell, Kinetics of hydrogenation and hydrogenolysis of 2,5-dimethylfuran over noble metals catalysts under mild conditions, Appl. Catal. B 202 (2017) 557−568.

[7] J. Kliewer, C. Aliaga, M. Bieri, W. Huang, C.-K. Tsung, J.B. Wood, K. Komvopoulos, G. A. Somorjai, Furan hydrogenation over Pt (111) and Pt (100) single-crystal surfaces and Pt nanoparticles from 1 to 7 nm: a kinetic and sum frequency generation vibrational spectroscopy study, J. Am. Chem. Soc. 132 (2010) 13088−13095.

[8] J. Kang, A. Vonderheide, V.V. Guliants, Deuterium-labeling study of the hydrogenation of 2 methylfuran and 2,5-dimethylfuran over carbon-supported noble metal catalysts, ChemSusChem 8 (2015) 3044−3047.

[9] R.C. Runnebaum, T. Nimmanwudipong, J. Doan, D.E. Block, B.C. Gates, Catalytic conversion of furan to gasoline-range aliphatic hydrocarbons via ring opening and decarbonylation reactions catalyzed by Pt/γ-Al_2O_3, Catal. Lett. 142 (2012) 664-666.

[10] J. Kang, X. Liang, V.V. Guliants, Selective hydrogenation of 2-methylfuran and 2,5-dimethylfuran over atomic layer deposited platinum catalysts on multiwalled carbon nanotube and alumina supports, ChemCatChem 9 (2017) 282−286.

[11] A. Corma, O. de la Torre, M. Renz, N. Villandier, Production of high-quality diesel from biomass waste products, Angew. Chem. Int. Ed. 50 (2011) 2375−2378.

[12] J. Yang, S. Li, L. Zhang, X. Liu, J. Wang, X. Pan, N. Li, A. Wang, Y. Cong, X. Wang, T. Zhang, Hydrodeoxygenation of furans over Pd-FeOx/SiO_2 catalyst under atmospheric pressure, Appl. Catal. B 201 (2017) 266−277.

[13] H. Goto, A. Takagaki, R. Kikuchi, S. T. Oyama, Hydrogenation of 2,5-dimethylfuran on hexagonal-boron nitride- and silica-supported platinum catalysts, Appl. Catal. A 548 (2017) 122–127.

[14] T. Tong, Q. Xia, X. Liu, Y. Wang, Direct hydrogenolysis of biomass-derived furans over Pt/CeO_2 catalyst with high activity and stability, Catal. Commun. 101 (2017) 129–133.

[15] V. Vorotnikov, D.G. Vlachos, Group additivity and modified linear scaling relations for estimating surface thermochemistry on transition metal surfaces: Application to furanics, J. Phys. Chem. C 119 (2015) 10417−10426.

[16] M. Boudart, Turnover rates in heterogeneous catalysis, Chem. Rev. 95 (1995) 661-666.

[17] M.L. Mihailovic, R.I. Mamuzic, L. Zigic-Mamuzic, J. Bosnjak, Z. Cekovic, Assignment of cis-trans configuration to constitutionally symmetrical 2,5-dialkyltetrahydrofurans, Tetrahedron 23 (1967) 215−226.

[18] G.C. Bond, Metal-catalysed reactions of hydrocarbons, Springer, New York, 2005.

[19] T.K.H. Trinh, J.C.de Hemptinne, R. Lugo, N. Ferrando, J.P. Passarello, Hydrogen solubility in hydrocarbon and oxygenated organic compounds, J. Chem. Eng. Data 61 (2016) 19−34.

[20] P.B. Weisz, C.D. Prater, Interpretation of measurements in experimental catalysis, Adv. Catal. 6 (1954) 143−196.

[21] M.B. King, J.M. Winterbottom, Reactor design for chemical engineers, J.M Winterbottom, M.B. King, eds., Stanley Thorns, Padstow, 1999, p.154.

Chapter 4. Facile Gas Phase Hydrodeoxygenation of 2,5-Dimethylfuran over Bifunctional Metal-Acid Catalyst Pt-$Cs_{2.5}H_{0.5}PW_{12}O_{40}$

4

4.1. Introduction

Biomass-derived furanic compounds are a low-cost renewable feedstock, which can be converted to green fuels and a wide range of value-added chemicals by catalytic hydroconversion ([1−10] and references therein). Hydrodeoxygenation (HDO) of biomass-derived furanic compounds is an effective strategy to produce green fuels. Much current research is focussed on the deoxygenation using heterogeneous catalysis ([10−15] and references therein). Complete oxygen removal from furanic compounds over noble metals to produce hydrocarbons requires harsh conditions (200−400 °C, 7–20 MPa H_2 pressure) [11,12,14]. Bifunctional metal-acid catalysis has been found more efficient than monofunctional metal catalysis for the HDO of oxygenates such as ketones, alcohols, phenols, ethers and esters [17-21]. Previously, this group has reported that bifunctional catalysts comprising platinum on acidic supports such as zeolite HZSM-5 [17] and Keggin-type heteropoly acids [18,19] are highly active for HDO of a wide range of aliphatic and aromatic ketones in the gas phase under mild conditions to produce the corresponding alkanes in one step on a single catalyst bed [17-19]. This approach may be applicable to the HDO of furanic compounds. In hydroconversion of furanic compounds, Pt is selective to ring-opened products (ketones, alcohols and alkanes), whereas Pd, Rh and Ru have high

selectivity to ring-saturated tetrahydrofuran derivatives [6,13,15]. This has been explained by a different bonding of furanic compounds to these metals [6,7].

Here, the HDO of 2,5-dimethylfuran (DMF), chosen as a model for biomass-derived furanic compounds, is investigated in the presence of bifunctional metal-acid catalysts comprising carbon-supported Pt, Pd, Ru and Rh together with acidic Cs salt of Keggin-type tungstophosphoric heteropoly acid $Cs_{2.5}H_{0.5}PW_{12}O_{40}$ (CsPW). Attention is focussed on the Pt–CsPW catalyst because among the noble metals, Pt is the most active one for furan ring hydrogenolysis [6,15]. CsPW is well documented as a solid Brønsted acid catalyst [22−25]. It has important advantages over the parent heteropoly acid $H_3PW_{12}O_{40}$ (HPW) in much larger surface area, higher thermal stability (~500 °C decomposition temperature) and high tolerance to water, with proton sites almost as strong as those in HPW [22−25]. The previous H_2-TPR, XRD and FTIR studies have shown that CsPW in Pt/CsPW and Pd/CsPW catalysts is resistant toward reduction by H_2 below 600 °C and the Keggin structure of CsPW is retained in CsPW-supported Pt and Pd catalysts after H_2 treatment at 400 °C [17]. Therefore, these catalysts should be stable at rather mild reaction conditions applied in this work.

The HDO reaction is studied both in the gas and liquid phase, with the main emphasis on the gas phase process. The gas phase HDO is expected to be more efficient and environmentally benign compared to the liquid phase process due to the absence of solvent, continuous rather than batch operation and easy product separation. It is demonstrated that the gas phase HDO of DMF over Pt-CsPW is indeed a facile reaction, yielding 100% of n-hexane under mild conditions.

The gas phase HDO of DMF was carried out in flowing H_2 at ambient pressure and 70–100 °C using a Pyrex fixed-bed down-flow microreactor with online GC analysis. The liquid phase reaction was carried out in a 120 mL stainless steel autoclave with 9.6%Pt/C + CsPW

(1:9 w/w) catalyst (0.20 g, 1% Pt loading per total catalyst weight); other conditions were as follows: DMF (5.2 mmol), dodecane (GC standard, 5.0 mmol), decane (solvent, 3.0 mL), 20 bar H_2 pressure at room temperature (RT), 600 rpm stirring speed and 2 h reaction time. At such conditions, the reaction did not depend on the stirring speed, hence, was not limited by external diffusion. Experimental details including the chemicals used, catalyst preparation procedures, catalyst characterisation techniques and the description of the reactor setup for catalyst testing are given in Chapter 2.

4.2. Results and Discussion

4.2.1. Catalyst Characterisation

Information about the catalysts studied is summarised in Table 4.1; it includes catalyst texture (surface area, pore volume and pore diameter) and metal dispersion. Nitrogen adsorption and desorption isotherms and pore size distribution for Pt/C, $Cs_{2.5}H_{0.5}PW_{12}O_{40}$, 1.0%Pt/CsPW-w (prepared from water using H_2PtCl_6) and 1.0%Pt/CsPW-b (prepared from benzene using $Pt(acac)_2$) are shown in Fig. 2.4−2.6 in Chapter 2. The XRD analysis revealed that Pt/CsPW catalysts used in this study were crystalline and did not show any Pt metal phase on CsPW indicating that the metal was finely dispersed (Fig. 2.11, Chapter 2). Catalyst loading was confirmed by ICP-OES and was in good agreement with the loading expected from the preparation stoichiometry.

CsPW showed a type IV adsorption isotherm according to the IUPAC classification, with H2 hysteresis loop (Fig. 2.3, Chapter 2). This indicates that CsPW is a mostly mesoporous material (2 nm < pore diameter < 50 nm), with a non-uniform pore shape and size in agreement with the literature [22−25]. The surface areas of Pt/CsPW catalysts were lower than the surface area of bulk CsPW, particularly with 1.0%Pt/CsPW-w, which shows a

solvent effect on catalyst preparation. Moreover, Pt dispersion was lower in 1%Pt/CsPW-w compared to 1%Pt/CsPW-b.

Table 4.1 Characterisation of bifunctional metal-acid catalysts.[a]

Catalyst	Surface area[a] (m^2g^{-1})	Pore volume[b] (cm^3g^{-1})	Pore diameter[c] (Å)	D [d]
7.8%Pd/C	820	0.56	27	0.326±0.034
3.0%Ru/C	1108	0.94	34	0.232±0.010
4.0%Rh/C	830	0.70	34	0.513±0.032
9.6%Pt/C	713	0.56	31	0.039±0.007
1%Pt/Al_2O_3	163	0.49	121	0.63±0.042
6.4%Pt/SiO_2	266	1.06	159	0.28±0.041[f]
1.0%Pt/CsPW-w[e]	98	0.08	34	0.094±0.010[f]
1.0%Pt/CsPW-b[g]	106	0.09	32	0.13±0.01[f]
$Cs_{2.5}H_{0.5}PW_{12}O_{40}$	139	0.09	27	
25%HPW/SiO_2	188	0.80	178	
HZSM-5 (Si/Al = 12)	378	0.22	24	
HZSM-5 (Si/Al = 47)	411	0.26	26	

[a] BET surface area. [b] Single point total pore volume. [c] Average BET pore diameter. [d] Metal dispersion from CO adsorption (average of three measurements). [e] Prepared by impregnating H_2PtCl_6 from aqueous solution. [f] Pt dispersion determined by H_2/O_2 titration (average from three measurements). [g] Prepared by impregnating $Pt(acac)_2$ from benzene solution.

4.2.2. Gas Phase HDO of DMF over Bifunctional Metal-CsPW Catalysts

The aim of hydrodeoxygenation (HDO) of furanic compounds is to produce alkanes, which can be used as a green fuel [11,12,14,16]. The HDO of furanic compounds over noble metals requires harsh conditions (200−400 °C, 7–20 MPa H_2 pressure) to achieve complete oxygen removal resulting in hydrocarbon products [11,12,14]. Bifunctional metal-acid catalysis is expected to be more efficient for this.

Table 4.2 shows representative results on the gas phase HDO of DMF over bifunctional metal–CsPW catalysts (1% metal loading per total catalyst weight) at 70–100 °C and 1 bar H_2 pressure. CsPW alone was not active at such conditions. Physical mixtures of all carbon-supported metals with CsPW exhibited high catalytic activity, giving >99% DMF conversion. However, only Pt/C + CsPW gave ~100% selectivity to n-hexane at full DMF conversion at 90–100 °C (entry 3, 4) showing stable product selectivity for more than 5 h TOS (Fig. 4.1). Without CsPW present, Pt/C + SiO_2 at the same Pt loading also gave >99% DMF conversion but yielded 2-hexanol as the main product (74% selectivity at 90 °C, entry 5) rather than hexane. Hence, for efficient hydrodeoxygenation, the presence of both Pt and proton sites in the catalyst is essential. In contrast to Pt, other noble metals (Pd, Rh and Ru) that are inactive in opening furan ring exhibited poor activity in the HDO reaction under the conditions applied (entries 10−19).

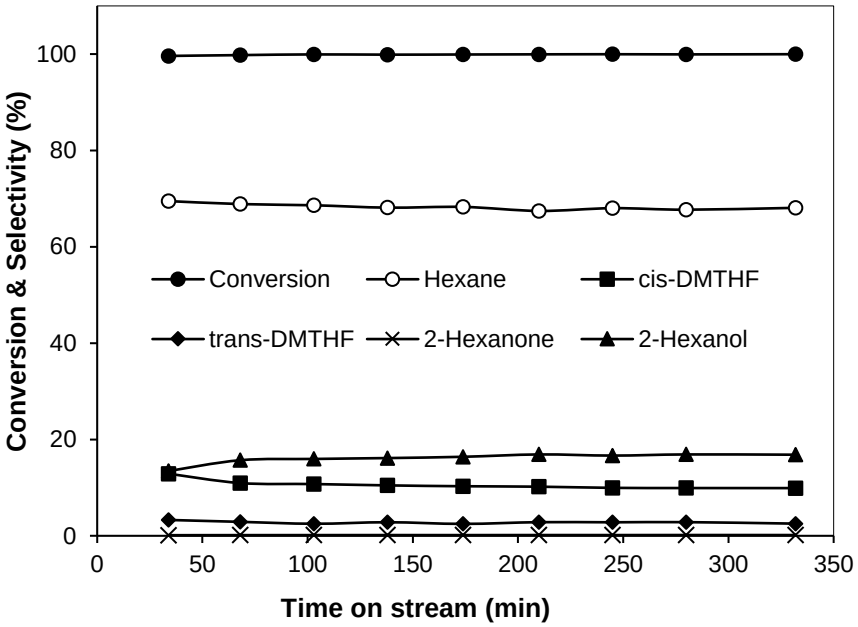

Fig. 4.1 Time course for HDO of DMF: 0.20 g total catalyst weight, 9.6%Pt/C+CsPW (1:9 w/w, 20 mg Pt/C, 1% Pt loading), 70 °C, 1.6 kPa DMF, 20 mL min^{-1} H_2 flow rate, 5 h TOS.

Table 4.2 Gas-phase HDO of DMF in the presence of bifunctional metal-acid catalysts [a]

Entry	Catalyst	T	Conv.[b]	Product selectivity[b] (% mol)				
		(°C)	(%)	n-Hexane	DMTHF	2-Hexanone	2-Hexanol	Other
1	CsPW	70	0					
2	Pt/C+CsPW[c]	70	>99	68.1	13.0	0.1	16.4	2.3
3	Pt/C+CsPW[c]	90	>99	99.6	0.3	0.0	0.1	0.0
4	Pt/C+CsPW[c]	100	>99	99.9	0.1	0.0	0.0	0.0
5	Pt/C+SiO_2[d]	90	>99	8.8	10.7	2.1	74.2	4.2
6	1%Pt/CsPW-w[e]	70	>99	61.2	30.7	0.3	6.5	1.1
7	1%Pt/CsPW-w[e]	90	>99	98.4	1.2	0.0	0.1	0.3
8	1%Pt/CsPW-b[f]	70	>99	59.1	37.2	0.0	3.1	0.5
9	1%Pt/CsPW-b[f]	90	>99	99.6	0.1	0.0	0.0	0.3
10	Pd/C+CsPW[g]	70	>99	0.2	98.8	0.1	0.0	0.9
11	Pd/C+CsPW[g]	90	>99	1.5	97.4	0.3	0.0	0.8
12	Pd/C+CsPW[g]	100	>99	2.8	93.5	0.9	0.1	2.7
13	Pd/C+SiO_2[h]	70	>99	0.0	99.8	0.0	0.0	0.2
14	Ru/C+CsPW[i]	70	98	7.2	89.8	0.4	2.1	0.6
15	Ru/C+CsPW[i]	90	>99	13.9	84.7	0.1	0.3	0.6
16	Ru/C+CsPW[i]	100	98	16.1	78.7	0.8	0.6	3.8
17	Rh/C+CsPW[j]	70	>99	1.4	97.5	0.9	0.1	0.2
18	Rh/C+CsPW[j]	90	>99	8.7	91.1	0.0	0.1	0.1
19	Rh/C+CsPW[j]	100	>99	17.4	82.3	0.03	0.02	0.2

[a]1.6 kPa DMF, 20 mL min^{-1} H_2 flow rate, 4 h TOS, 0.20 g catalyst. [b]Average conversion and product selectivity over 4 h TOS. [c]9.6%Pt/C+CsPW (1:9 w/w, 20 mg Pt/C, 1% Pt loading per total catalyst weight). [d]9.6%Pt/C+SiO_2 (1:9 w/w, 20 mg Pt/C, 1% Pt loading). [e]Catalyst prepared by impregnating H_2PtCl_6 from aqueous solution. [f]Catalyst prepared by impregnating $Pt(acac)_2$ from benzene solution. [g]7.8%Pd/C+CsPW (1:7 w/w, 25 mg Pd/C, 1% Pd loading). [h] 7.8%Pd/C+SiO_2 (1:7 w/w, 25 mg Pd/C, 1% Pd loading). [i]3.0%Ru/C+CsPW (1:2 w/w, 67 mg Ru/C, 1% Ru loading). [j]4.0%Rh/C+CsPW (1:3 w/w, 50 mg Rh/C, 1% Rh loading).

Pd, Rh and Ru exhibited high selectivity towards ring hydrogenation to form 2,5-dimethyltetrahydrofuran (DMTHF) (a mixture of *cis* and *trans* isomers, *cis/trans* = 6–10), with or without CsPW present (cf. Pd/C + SiO_2, entry 13). Therefore, the ability of Pt to break furan ring is the key to the deoxygenation of DMF. The bifunctional Pt–CsPW catalyst operated under very mild conditions (90–100 °C, 1 bar H_2) giving n-hexane in 100% yield. Importantly, no n-hexane isomerisation was observed at such conditions, thus allowing the complete transformation of DMF to alkane without carbon backbone alteration. The isomerisation of n-hexane on Pt-CsPW has been reported to proceed at higher temperatures, >150 °C [29]. These results show that the bifunctional catalyst Pt-CsPW is much more efficient than the monofunctional Pt catalysts reported previously [11,12,14]. Fig. 4.2 shows the long-term catalyst testing for 24 h at 90 °C. As seen, the DMF conversion remains 100% but there is a small decline in hexane selectivity from 100% to 90%, which can be explained by cocking of proton sites in the catalyst. This deactivation is reversible and the initial activity of the catalyst can be fully restored upon calcination in air at 200 °C.

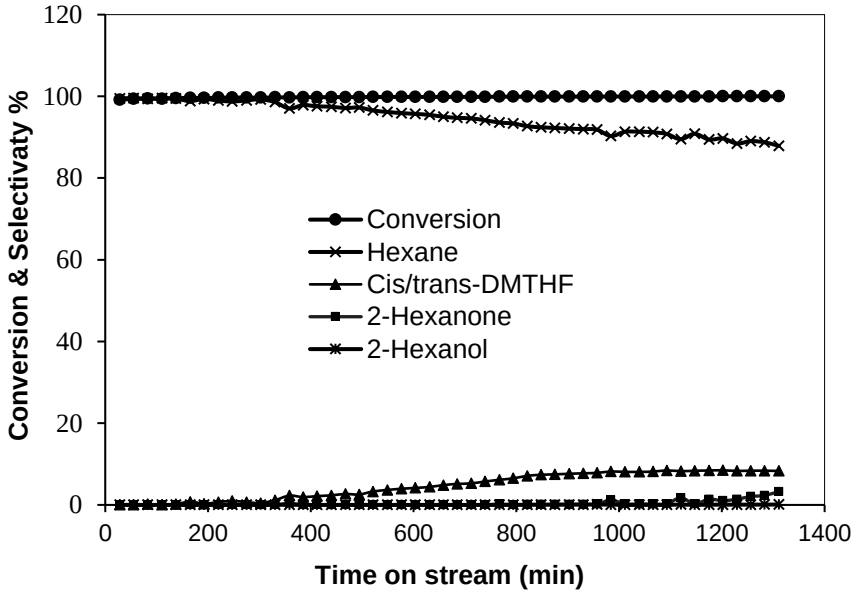

Fig. 4.2 Catalyst performance during 20 h TOS in HDO of DMF over 9.6%Pt/C+CsPW (0.2 g total catalyst weight, 1:9 w/w, 20 mg Pt/C, 1% Pt loading), 90°C, 1.6 kPa DMF, 20 mL/min H_2, pretreatment 90 °C/1h/H_2.

Reaction kinetics was examined at 80 °C and short contact times (at high flow rates and small amounts of Pt/C catalyst), which allowed reducing DMF conversion to 15–70%. Accurate measurement of reaction rates of the gas phase HDO of DMF over Pt/C + CsPW was difficult due to very high catalyst activity. At such conditions, the rates were reproducible with 10–15% accuracy. The rates (R) based on Pt/C were determined as $R = XF/W$, where X is the DMF conversion (average conversion for 1 h TOS), F is the inlet molar flow rate of DMF and W is the weight of Pt/C catalyst. The HDO reaction was found zero order in DMF at 1.6–6.8 kPa DMF partial pressure (Fig. 4.3), which indicates that catalyst active sites were saturated with DMF molecules. For a zero-order reaction, the rate does not depend on substrate conversion and is equal to the rate constant, which simplifies kinetic studies.

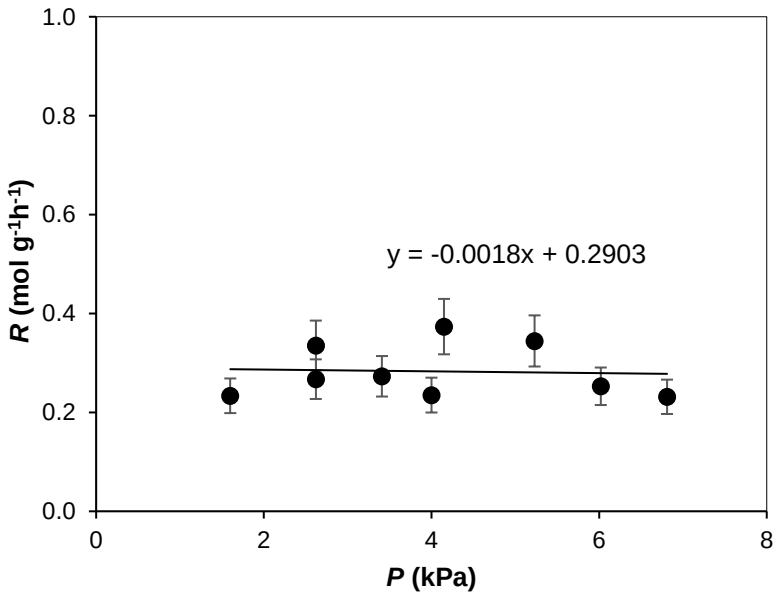

Fig. 4.3 Effect of DMF partial pressure on reaction rate (based on Pt/C): 9.6%Pt/C (5.0 mg), CsPW (0.20 g), 80 °C, 40 mL min^{-1} H_2 flow rate.

The reaction was first order in Pt/C catalyst as can be seen from the linear plot of DMF conversion versus the amount of Pt/C (Fig. 4.4). The same reaction orders have been reported for the gas and liquid phase hydroconversion of DMF in the presence of

monofunctional catalyst Pt/C [6,15]. The activation energy was estimated to be E = 65 kJ mol^{-1} in the temperature range of 70 – 90 °C, which is also close to the value 59 kJ mol^{-1} for the gas phase reaction in the presence of Pt/C [15]. This suggests that both reactions occur through the same rete-limiting step. The high E value and zero reaction order in DMF indicate no diffusion limitations in the HDO reaction over Pt-CsPW under the conditions studied.

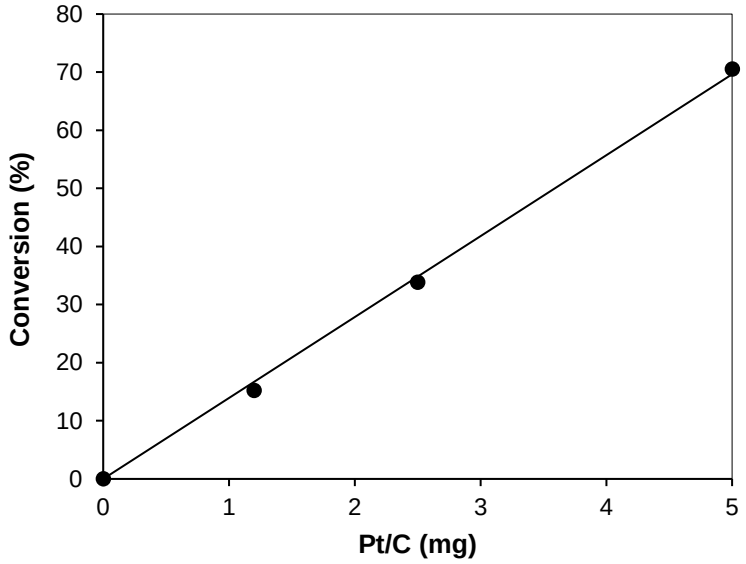

Fig. 4.4 Effect of catalyst amount on DMF conversion: 9.6%Pt/C (1.2 – 5.0 mg), CsPW (0.20 g), 80 °C, 1.6 kPa DMF partial pressure, 40 mL min^{-1} H_2 flow rate.

Supported bifunctional catalysts Pt/CsPW-w and Pt/CsPW-b prepared by impregnating CsPW with H_2PtCl_6 from water and with $Pt(acac)_2$ from benzene, respectively, showed practically the same performance in DMF deoxygenation as the Pt/C + CsPW physical mixture (Table 4.2, entries 6-9). This indicates that the reaction is not limited by the migration of reaction intermediates between metal and acid sites in bifunctional catalysts since the Pt and H^+ active sites in the mixed Pt/C + CsPW catalysts are much more distant from each other than in the supported Pt/CsPW catalysts (Weisz intimacy criterion [30]).

Table 4.3 shows the effect of Pt support (carbon, SiO_2 and γ-Al_2O_3) on the activity of Pt–CsPW catalysts in HDO of DMF at 70 °C under kinetic control (DMF conversion < 100%). From these results, the total turnover frequencies (TOF) per Pt site were calculated using the number of surface Pt sites in the catalysts from Pt dispersion (Table 4.1). The turnover activity of Pt sites decreases in the order of supports: C (9.3) > SiO_2 (2.3) > γ-Al_2O_3 (0.42), where in round brackets are the TOF values (s^{-1}) at 70 °C.

Table 4.3 Effect of support on Pt dispersion in HDO of DMF over Pt-CsPW.[a]

Catalyst [b]	Conv.	TOF	Product selectivity (% mol)				
	(%)	(s^{-1})	Hexane	DMTHF	2-Hexanone	2-Hexanol	Other
9.6%Pt/C+CsPW (0.038)	79.4	9.3	46.5	16.0	35.8	1.0	0.7
6.4%Pt/SiO_2+CsPW (0.18)	92.5	2.3	52.9	20.4	23.4	2.6	0.7
1%Pt/Al_2O_3+CsPW (0.065)	6.2	0.42	16.8	10.9	64.5	3.4	4.4

[a] Pt/support (2.0 mg) + CsPW (0.19 g), 70 °C, 1.6 kPa DMF partial pressure, 40 mL min^{-1} H_2 flow rate, 1 h TOS, W/F= 1.3 g h mol^{-1}. [b] In round brackets the number of surface Pt sites in catalysts (μmol) calculated from Pt dispersion (Table 4.1).

Although Pt plays a key role, the properties of acid co-catalyst (the strength and the number of acid sites) can also have a significant effect on the performance of a bifunctional metal-acid catalyst. Therefore, several Brønsted solid acids were tested for comparison with CsPW. These include silica-supported heteropoly acid HPW and zeolites HZSM-5 with different Si/Al atomic ratios listed in Table 4.1, namely, 25%HPW/SiO_2, HZSM-5-12 and HZSM-5-47. Their acid strength (initial enthalpy of ammonia adsorption, ΔH) and proton site density are given in Table 4.4. The proton site density was calculated as follows: for zeolites from their Si/Al ratio, for 25%HPW/SiO_2 assuming that all HPW protons were accessible [31,32] and for CsPW assuming the Keggin unit cross section of 144 $Å^2$ [24,31] and using the CsPW surface area of 139 m^2g^{-1} (Table 4.1).

Table 4.4 Acid properties of acid co-catalysts.

Catalyst	CsPW	25%HPW/SiO_2	HZSM-5-12	HZSM-5-47
H^+ density, mmol g^{-1}	0.080	0.26	1.28	0.35
-Δ*H*, kJ mol^{-1} (at 150 °C)	164 [31]	167 [32]	~129 [31]	~130 [31]

Table 4.5 shows the effect of acid co-catalysts on the HDO of DMF at 100 °C. As seen, with all co-catalysts studied, full conversion of DMF was achieved, but the selectivity to hexane significantly depended on the acid strength. The strongest acids, CsPW and HPW/SiO_2, gave >99% selectivity to hexane, whereas the weaker acids, HZSM-5 zeolites, 69–85% selectivity at 100 °C. HZSM-5-12 was notably more selective to hexane than HZSM-5-47, which can be explained by almost 4-fold higher H^+ density in HZSM-5-12 (Table 4.4). The deoxygenation activity of Pt–zeolite catalysts increased with increasing reaction temperature reaching ~100% hexane yield at 120 °C. These results show that the HDO activity of the bifunctional catalysts correlates with the strength and the number of their acid sites.

Table 4.5 Effect of acid co-catalyst on HDO of DMF in the gas phase.[a]

Catalyst	Temp.	Product selectivity [b] (mol %)				
	(°C)	n-Hexane	DMTHF	2-Hexanone	2-Hexanol	Other
Pt/C+CsPW	100	99.9	0.1	0.0	0.0	0.0
Pt/C+25%HPW/SiO_2	100	99.3	0.0	0.1	0.4	0.2
Pt/C+HZMS-5-47	100	68.5	8.0	0.7	20.3	1.6
Pt/C+HZMS-5-47	120	99.6	0.0	0.1	0.1	0.2
Pt/C+HZMS-5-12	100	84.8	5.4	0.2	7.1	1.9
Pt/C+HZMS-5-12	120	99.2	0.0	0.1	0.3	0.4

[a]1.6 kPa DMF, 20 mL min^{-1} H_2 flow rate, 4 h TOS, 0.20 g total catalyst weight of 9.6%Pt/C + solid acid (1:9 w/w, 20 mg Pt/C, 1% Pt loading). [b]Average product selectivity over 4 h TOS at conversion >99%.

It is interesting to compare the HDO reaction in the gas phase system with that in the liquid phase. The results for the liquid phase HDO of DMF over Pt/C + CsPW catalyst are given in Table 4.6. The reaction was carried out in a stainless-steel autoclave at 90–140 °C and 20 bar H_2 pressure at RT using decane as a solvent. Full DMF conversion was achieved in 2 h reaction time, yielding mainly 2-hexanone and DMTHF. The selectivity to hexane was much lower than in the gas phase reaction (Table 4.2). It increased from 5 to 48% with increasing the temperature from 90 to 140 °C.

Table 4.6 Liquid-phase HDO of DMF in the presence of bifunctional Pt-CsPW catalyst.[a]

Temp.	Conv.	Product selectivity (% mol)				
(°C)	(%)	n-Hexane	DMTHF	2-Hexanone	2-Hexanol	Other
90	98	5.0	20.0	45.0	20.0	10.0
100	>99	12.9	19.3	49.2	12.5	6.1
120	>99	40.2	13.3	42.7	0.1	3.7
140	>99	48.4	11.0	32.0	0.0	8.6

[a]In 120 mL stainless steel autoclave, 9.6%Pt/C+CsPW (1:9 w/w) catalyst (0.20 g total catalyst, 20 mg Pt/C, 1% Pt loading per total catalyst weight), DMF (5.2 mmol, 0.56 mL), dodecane (GC standard, 5.0 mmol, 1.14 mL), decane (solvent, 3.0 mL), 20 bar H_2 pressure (at room temperature), 600 rpm stirring speed, 2 h reaction time.

Therefore, the liquid phase HDO in a batch reactor is much less efficient and occurs under harsher conditions than the gas phase process in a flow reactor. The reasons for the higher efficiency of the gas phase process could be clarified via a more detailed kinetic study. This can be explained considering the concentration of H_2, the effect of competitive adsorption of reaction products and the accessibility of Pt sites in the two systems [15]. From the solubility data [33], the [H_2] was estimated to be 0.12 M in decane at 100 °C and 26 bar H_2 (20 bar H_2 pressure at RT increased to 26 bar at 100 °C), whereas in the gas phase it was almost four times lower (0.033 M in flowing hydrogen at 1 bar H_2 and 100 °C). Therefore,

from the H_2 concentration, the liquid phase reaction would be expected to be more efficient than the gas phase reaction. Another factor to be considered is the DMF concentration. In the batch liquid phase system, [DMF] = 1.1 M and it was much greater than in the gas phase system ($5.3 \cdot 10^{-4}$ M). Hence in the liquid phase, competitive adsorption of reaction products (2-hexanone, 2-hexanol and water) on Pt sites could decrease the rate to a greater extent than in the gas phase system. Finally, the accessibility of metal sites in Pt/C should be better in the gas phase than in the liquid phase. The pore structure of carbon support is dominated by microporosity. In the liquid phase, the access of reactant molecules to the metal sites located in micropores filled with solvent is difficult. It is likely that only the metal sites placed on the external surface and pore mouth are accessible in the liquid phase [15].

4.2.3. Reaction Network for Hydrodeoxygenation of DMF

From the above data, the hydrodeoxygenation of DMF over Pt-CsPW can be represented by Scheme 4.1. This reaction network includes two parallel pathways (1) and (2) starting from the interaction of DMF with Pt sites, which leads to DMF ring hydrogenolysis (pathway (1)) and ring hydrogenation (pathway (2)). First reaction order in Pt/C (Fig. 4.4) suggests that the initial steps catalysed by Pt, probably the formation of 2-hexanol, are the rate-limiting steps in pathways (1) and (2). Furthermore, each pathway involves the dehydration of 2-hexanol on proton sites as an effective driving force for the HDO reaction to occur. This follows by the final step of hexene-to-hexane hydrogenation on Pt sites, which is probably fast as no hexene was observed among the reaction products.

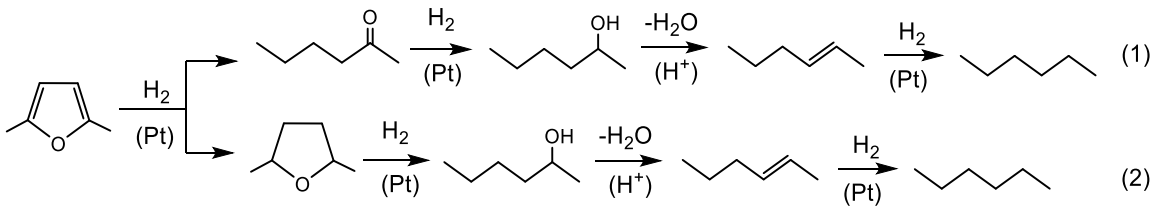

Scheme 4.1 Reaction network for hydrodeoxygenation of DMF over Pt-CsPW.

To support this reaction network, additional qualitative tests were carried out by passing 2-hexanone and 2-hexanol over CsPW, 9.6%Pt/C and Pt-CsPW at conditions comparable to those in Table 4.2 (90 °C, 2% substrate partial pressure, 20 mL min^{-1} H_2 flow rate, 1% Pt loading). The reaction of 2-hexanone over Pt/C gave 91% selectivity to 2-hexanol at 87% conversion; only 6% of hexane was formed. Complete deoxygenation of ketones to alkanes on 10%Pt/C has been reported to occur at >300 °C [18,19]. When 2-hexanone was passed over CsPW in the absence of Pt/C, practically no reaction was observed, whereas 100% hexane yield was obtained over Pt-CsPW in agreement with the previous report [19]. The reaction of 2-hexanol over Pt/C gave only hexane, but at a very small alcohol conversion (~5%). Interaction of 2-hexanol with CsPW, both in H_2 and in N_2, yielded a mixture of 1-hexene and 2-hexene (*cis* and *trans* isomers) at >99% alcohol conversion. The reaction of 2-hexanol over Pt–CsPW in H_2 produced n-hexane in >99 yields as expected. These tests confirm the hydrogenation-dehydration-hydrogenation sequence of reaction steps in Scheme 4.1 and demonstrate the importance of both Pt and H^+ sites for the HDO reaction. In more detail, pathway (1) for DMF ring hydrogenolysis is presented in Scheme 4.2.

Previous reports [6,13,15], as well as this study, show that the initial hydroconversion of DMF on Pt sites strongly favours the ring opening over the ring saturation, with the molar ratio of primary reaction products [2-hexanone]/[DMTHF] ≈ 10. Moreover, the turnover rate of DMF hydroconversion in the gas phase on monofunctional Pt/C is 2400 times greater than that of DMTHF at 80 °C and 1 bar H_2 [15] (Chapter 3). This indicates that reaction pathway (1) should dominate by far over pathway (2).

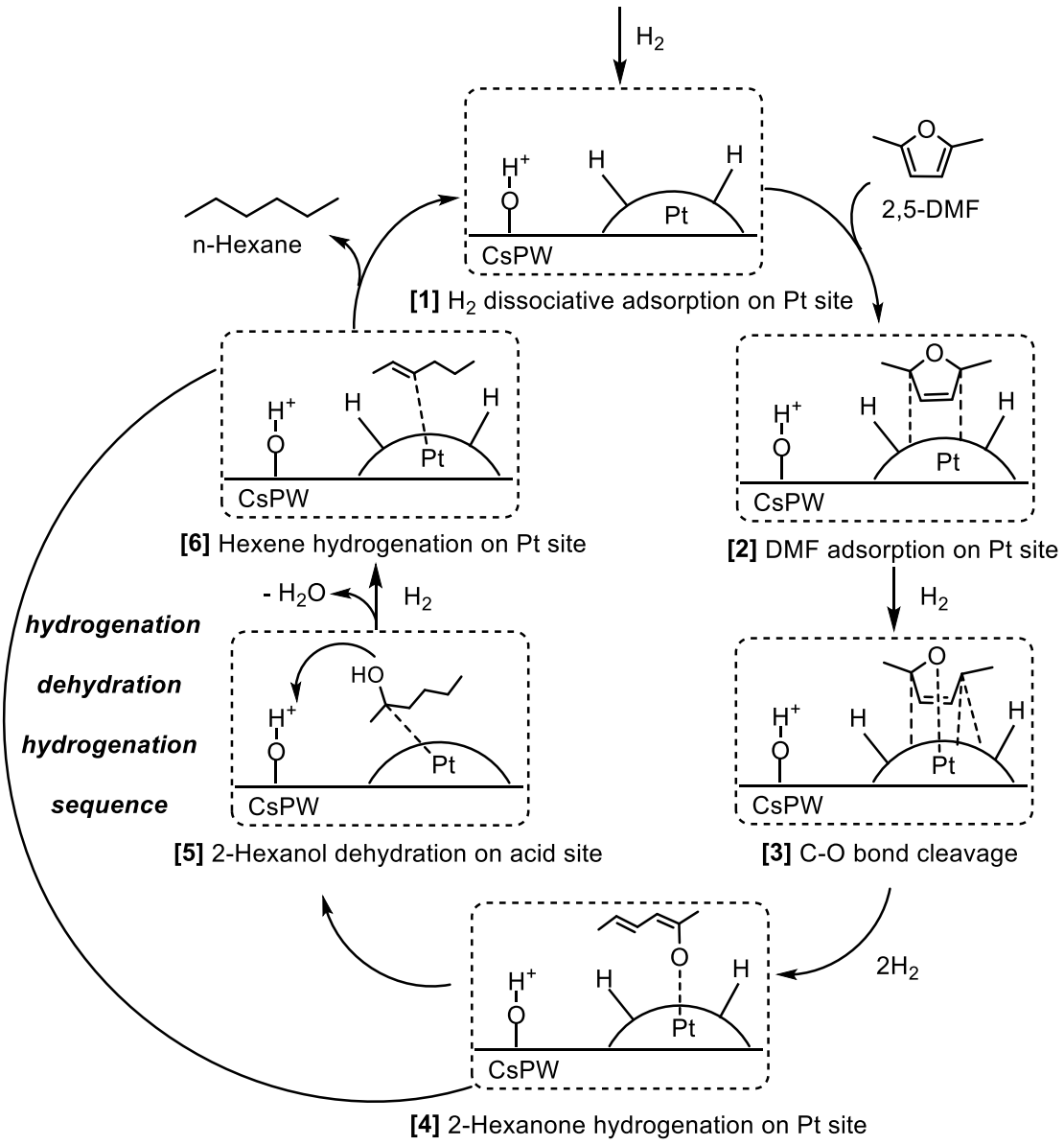

Scheme 4.2 Proposed mechanism for HDO of DMF (pathway (1)) over Pt-CsPW bifunctional catalyst (adapted from [35]).

4.3. Conclusions

The Pt-CsPW catalyst deoxygenates DMF to n-hexane with 100% yield under very mild conditions (90 °C, 1 bar H_2 pressure) in one step on a single catalyst bed composed of a Pt/C+CsPW mixture. Mild reaction conditions exclude n-hexane isomerisation allowing the complete transformation of DMF to alkane without carbon backbone alteration. The bifunctional Pt-CsPW catalyst is much more efficient than the previously reported monofunctional Pt catalysts operating at 200−400 °C and 7–20 MPa H_2 pressure [11,12,14]. The gas phase HDO in the flow system over Pt-CsPW is more efficient than the corresponding liquid phase batch reaction. Pd, Rh and Ru combined with CsPW are much less active than Pt-CsPW, giving 2,5-dimethyltetrahydrofuran (DMTHF) as the main product rather than hexane. The proposed reaction network for the HDO of DMF includes a sequence of hydrogenolysis, hydrogenation and dehydration steps catalysed by Pt and proton sites in the bifunctional catalyst. The combined action of the metal and acid sites is essential for the effectiveness of this process. Facile dehydration of secondary alcohol intermediate, 2-hexanol, on proton sites is an effective driving force for the HDO process by bifunctional metal-acid catalysis. A further insight into the reaction mechanism is gained in Chapter 5 from investigating the HDO of reaction intermediates, in particular DMTHF, over Pt-CsPW.

References

[1] A. Corma, S. Iborra, A. Velty, Chemical routes for the transformation of biomass into chemicals, Chem. Rev. 107 (2007) 2411−2502.

[2] Y. Román-Leshkov, J.N. Chheda, J.A. Dumesic, Phase modifiers promote efficient production of hydroxymethylfurfural from fructose, Science 312 (2006) 1933−1937.

[3] R.M. West, Z.Y. Liu, M. Peter, J.A. Dumesic, Liquid alkanes with targeted molecular weights from biomass-derived carbohydrates, ChemSusChem 1 (2008) 417−424.

[4] G.W. Huber, J.N. Chheda, C.J. Barrett, J.A. Dumesic, Production of liquid alkanes by aqueous-phase processing of biomass-derived carbohydrates, Science 308 (2005) 1446−1450.

[5] Z.J. Brentzel, K.J. Barnett, K. Huang, C.T. Maravelias, J.A. Dumesic, G.W. Huber, Conversion of furfural to 1,5-pentanediol: process synthesis and analysis, ChemSusChem 10 (2017) 1351−1355.

[6] Y.L. Louie, J. Tang, A.M.L. Hell, A.T. Bell, Kinetics of hydrogenation and hydrogenolysis of 2,5-dimethylfuran over noble metals catalysts under mild conditions, Appl. Catal. B 202 (2017) 557−568.

[7] V. Vorotnikov, D.G. Vlachos, Group additivity and modified linear scaling relations for estimating surface thermochemistry on transition metal surfaces: Application to furanics, J. Phys. Chem. C 119 (2015) 10417−10426.

[8] J. Kang, A. Vonderheide, V.V. Guliants, Deuterium-labeling study of the hydrogenation of 2-methylfuran and 2,5-dimethylfuran over carbon-supported noble metal catalysts, ChemSusChem 8 (2015) 3044−3047.

[9] R.C. Runnebaum, T. Nimmanwudipong, J. Doan, D.E. Block, B.C. Gates, Catalytic conversion of furan to gasoline-range aliphatic hydrocarbons via ring opening and decarbonylation reactions catalyzed by Pt/γ-Al_2O_3, Catal. Lett. 142 (2012) 664−666.

[10] J. Kang, X. Liang, V.V. Guliants, Selective hydrogenation of 2-methylfuran and 2,5-dimethylfuran over atomic layer deposited platinum catalysts on multiwalled carbon nanotube and alumina supports, ChemCatChem 9 (2017) 282−286.

[11] A. Corma, O. de la Torre, M. Renz, N. Villandier, Production of high-quality diesel from biomass waste products, Angew. Chem. Int. Ed. 50 (2011) 2375−2378.

[12] J. Yang, S. Li, L. Zhang, X. Liu, J. Wang, X. Pan, N. Li, A. Wang, Y. Cong, X. Wang, T. Zhang, Hydrodeoxygenation of furans over Pd-FeOx/SiO_2 catalyst under atmospheric pressure, Appl. Catal. B 201 (2017) 266−277.

[13] H. Goto, A. Takagaki, R. Kikuchi, S.T. Oyama, Hydrogenation of 2,5-dimethylfuran on hexagonal-boron nitride- and silica-supported platinum catalysts, Appl. Catal. A 548 (2017) 122–127.

[14] F. Xue, D. Ma, T. Tong, X. Liu, Y. Hu, Y. Guo, Y. Wang, Contribution of different NbOx species in the hydrodeoxygenation of 2,5-dimethyltetrahydrofuran to hexane, Sustainable Chem. Eng. 6 (2018) 13107−13113.

[15] H. Althikrallah, C. Kunstmann-Olsen, E.F. Kozhevnikova, I.V. Kozhevnikov, Turnover rate of metal-catalysed hydroconversion of 2,5-dimethylfuran: gas-phase versus liquid-phase, Catalysts 10 (2020) 1171.

[16] D.M. Alonso, J.Q. Bond, J.A. Dumesic, Catalytic conversion of biomass to biofuels, Green Chem. 12 (2010) 1493–1513.

[17] M.A. Alotaibi, E.F. Kozhevnikova, I.V. Kozhevnikov, Deoxygenation of propionic acid on heteropoly acid and bifunctional metal-loaded heteropoly acid

catalysts: Reaction pathways and turnover rates, Appl. Catal. A 447 (2012) 32–40.

[18] M.A. Alotaibi, E.F. Kozhevnikova, I.V. Kozhevnikov, Efficient hydrodeoxygenation of biomass-derived ketones over bifunctional Pt-polyoxometalate catalyst, Chem. Commun. 48 (2012) 7194−7196.

[19] K. Alharbi, E.F. Kozhevnikova, I.V. Kozhevnikov, Hydrogenation of ketones over bifunctional Pt-heteropoly acid catalyst in the gas phase, Appl. Catal. A 504 (2015) 457−462.

[20] S. Itagaki, N. Matsuhashi, K. Taniguchi, K. Yamaguchi, N. Mizuno, Efficient hydrodeoxygenation of ketones, phenols and ethers promoted by platinum–heteropolyacid bifunctional catalysts, Chem. Lett. 43 (2014) 1086−1088.

[21] K. Alharbi, W. Alharbi, E.F. Kozhevnikova, I.V. Kozhevnikov, Deoxygenation of ethers and esters over bifunctional Pt–heteropoly acid catalyst in the gas phase, ACS Catal. 6 (2016) 2067−2075.

[22] T. Okuhara, N. Mizuno, M. Misono, Catalytic chemistry of heteropoly compounds, Adv. Catal. 41 (1996) 113−252.

[23] I.V. Kozhevnikov, Catalysis by heteropoly acids and multicomponent polyoxometalates in liquid-phase reactions, Chem. Rev. 98 (1998) 171−198.

[24] I.V. Kozhevnikov, Catalysts for fine chemical synthesis: Catalysis by polyoxometalates, Wiley, West Sussex, 2002.

[25] J.B. Moffat, Metal-oxygen clusters. The surface and catalytic properties of heteropoly oxometalates, Kluwer: New York, 2001.

[26] P.Canton, G. Fagherazzi, M. Battagliarin, F. Menegazzo, F. Pinna, N. Pernicone, Pd/CO average chemisorption stoichiometry in highly dispersed supported Pd/γ-Al_2O_3 catalysts, Langmuir 18 (2002) 6530−6535.

[27] J.E. Benson, H.S. Hwang, M. Boudart, Hydrogen-oxygen titration and carbon monoxide chemisorption for the measurement of supported palladium surface areas, J. Catal. 30 (1973) 146−153.

[28] J.E. Benson, M. Boudart, Hydrogen-oxygen titration method for the measurement of supported platinum surface areas, J. Catal. 4 (1965) 704−710.

[29] A. Alazman, D. Belic, E.F. Kozhevnikova, I.V. Kozhevnikov, Isomerization of n-hexane over bifunctional pt-heteropoly acid catalyst: Enhancing effect of gold, J. Catal. 357 (2018) 80−89.

[30] P.B. Weisz, Polyfunctional heterogeneous catalysis, Adv. Catal. 13 (1962) 137−190.

[31] W. Alharbi, E.F. Kozhevnikova, I.V. Kozhevnikov, Dehydration of MeOH to dimethyl ether over heteropoly acid catalysts: The relationship between reaction rate and catalyst acid strength, ACS Catal. 5 (2015) 7186−7193.

[32] R. Al-Faze, A. Finch, E.F. Kozhevnikova, I.V. Kozhevnikov, Dehydration of methanol and ethanol over silica-supported heteropoly acids in the gas phase: surface-type versus bulk-type catalysis mechanism, Appl. Catal. A 597 (2020) 117549.

[33] L.J. Florusse, C.J. Peters, J.C. Pamies, L.F. Vega, H. Meijer, Solubility of hydrogen in heavy n-alkanes: experiments and SAFT modeling, AIChE 49 (2003) 3260−3269.

[34] M. Boudart, Turnover rates in heterogeneous catalysis, Chem. Rev. 95 (1995) 661−666.

[35] M.J. Gilkey, A.V. Mironenko, L. Yang, D.G. Vlachos, B. Xu, Insights into the ring-opening of biomass-derived furanics over carbon-supported ruthenium. ChemSusChem 9 (2016) 3113−3121.

Chapter 5. Hydrodeoxygenation of 2,5-DMTHF over Bifunctional Catalysts Pt-$Cs_{2.5}H_{0.5}PW_{12}O_{40}$ in the Gas–Solid System: Kinetics and Mechanism

5

5.1. Introduction

Hydroconversion of bio-furanic compounds using heterogeneous catalysis is an effective strategy to produce green fuels and value-added chemicals ([1–22] and references therein). In Chapter 4, Pt–CsPW comprising Pt and strongly acidic heteropoly salt $Cs_{2.5}H_{0.5}PW_{12}O_{40}$ (CsPW) has been demonstrated to be a highly active catalyst for the gas phase HDO of 2,5-dimethylfuran (DMF) to produce n-hexane with 100% yield at 90 °C and ambient pressure [21] (Chapter 4). Among the platinum group metals, Pt is the most active catalyst for HDO of DMF due to its high activity in the hydrogenolysis of the furan ring (Chapter 3). In contrast, Pd, Rh and Ru, which have high selectivity to ring-saturated tetrahydrofuran derivatives rather than furan ring hydrogenolysis [6,13,15], have low activities in HDO of DMF [21].

The HDO of DMF over Pt–CsPW can be represented by Scheme 5.1 including two parallel pathways: ring hydrogenolysis (1) and ring hydrogenation (2) [21]. The primary ring-opened and ring-saturated products – 2-hexanone and 2,5-dimethyltetrahydrofuran (DMTHF) – are formed in parallel on Pt sites directly from DMF [6,13,15]. Further, on Pt sites, 2-hexanone is hydrogenated and DMTHF undergoes ring opening, both giving 2-hexanol, which is dehydrated to hexene on proton sites. Finally, the hexene is hydrogenated to n-hexane on Pt

sites to form n-hexane [21]. The HDO of ketones, including 2-hexanone (pathway 1), over Pt-CsPW has been studied in detail previously [19,20]. In contrast, the HDO of DMTHF (pathway 2) has not been reported yet, to the best of our knowledge. Since the HDO of furanic compounds involves tetrahydrofuran derivatives as intermediates, it would be interesting to investigate the HDO of DMTHF in the presence of bifunctional metal-acid catalysts.

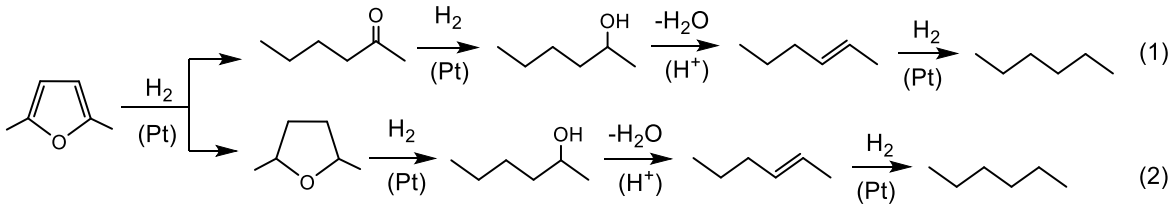

Scheme 5.1 Reaction network for hydrodeoxygenation of DMF over Pt–CsPW.

Here, the HDO of DMTHF is investigated at a gas solid interface in the presence of bifunctional metal-acid catalyst Pt-CsPW. The strongly acidic CsPW heteropoly salt is a well documented solid Brønsted acid catalyst [17,23–25]. It is demonstrated that Pt–CsPW deoxygenates DMTHF to n-hexane with >99% selectivity under mild conditions and an insight into the reaction mechanism is gained from the kinetic investigation.

The reactions were carried out in a fixed-bed continuous flow reactor in the temperature range of 60–100 °C using H_2 as a carrier gas at ambient pressure (1 bar). The catalyst bed (0.20 g total weight) contained a uniform physical mixture of powdered catalyst comprising M/support + acid co-catalyst or SiO_2 prepared by grinding a mixture of the corresponding components. The catalysts were characterised by BET, XRD, TEM, ICP-OES and pulse chemisorption of CO or H_2/O_2 titration. Information about catalyst preparation, reaction procedure and characterisation techniques is presented in Chapter 2. Information about the catalysts studied is given in Table 4.1, Chapter 4.

5.2. Results and Discussion

5.2.1. Hydrodeoxygenation of DMTHF over bifunctional Pt-CsPW catalyst

The Pt–CsPW catalyst exhibited stable performance in HDO of DMTHF; no deactivation was observed at least during 4 h on stream (Fig. 5.1). The previous H_2-TPR, XRD and FTIR studies have shown that CsPW in Pt/CsPW and Pd/CsPW catalysts is resistant toward reduction by H_2 below 600 °C and the Keggin structure of CsPW is retained in CsPW-supported Pt and Pd catalysts after H_2 treatment at 400 °C [26].

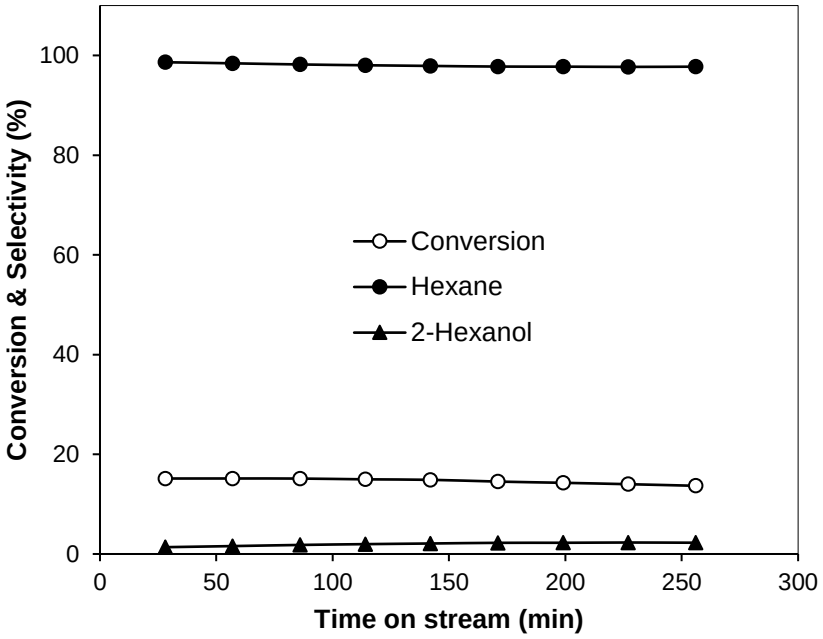

Fig. 5.1 Time course for HDO of DMTHF: 9.6%Pt/C+CsPW (1:9 w/w, 0.10 g, 10 mg Pt/C, diluted by 0.10 g SiO_2), 90 °C, 2.3 kPa DMTHF partial pressure, 40 mL min^{-1} H_2 flow rate.

Table 5.1 shows the representative results on the HDO of DMTHF. CsPW alone had a low activity to form mainly cracking products at 2.0% DMTHF conversion (entry 1). The monofunctional Pt/C catalyst in the absence of CsPW had a very low HDO activity to form 2-hexanol in 88% selectivity at 1.6–3.0% DMTHF conversion, with only 7–8% of n-hexane being formed at 90–100 °C (entries 2 and 3). Bifunctional Pt/C + CsPW catalyst had a fairly good deoxygenation activity starting from 60 °C with 74% n-hexane selectivity (entry 4). It gave >99% n-hexane selectivity at 44% DMTHF conversion at 90 °C (entry 6) and 71% conversion at 100 °C (entry 7). 100% DMTHF conversion at >99% n-hexane selectivity was obtained at 120 °C (entry 8).

Table 5.1 Hydrodeoxygenation of DMTHF.[a]

Entry	Catalyst	Temp. (°C)	Conv.[b] (%)	Product selectivity [b] (mol %)			
				Hexane	2-Hexanone	2-Hexanol	Other
1	CsPW	90	2.0				
2	9.6%Pt/C+SiO_2 (1:9 w/w)	90	1.6	8.1	1.4	87.6	2.9
3	9.6%Pt/C+SiO_2 (1:9 w/w)	100	3.0	7.4	2.7	88.3	1.7
4	9.6%Pt/C+CsPW (1:9 w/w)	60	4.0	73.7	0.0	25.7	0.0
5	9.6%Pt/C+CsPW (1:9 w/w)	80	29	96.4	0.0	3.4	0.0
6	9.6%Pt/C+CsPW (1:9 w/w)	90	44	99.6	0.0	0.4	0.0
7	9.6%Pt/C+CsPW (1:9 w/w)	100	71	99.9	0.0	0.1	0.0
8	9.6%Pt/C+CsPW (1:9 w/w)	120	>99	100	0.0	0.0	0.0
9	7.8%Pd/C+CsPW (1:7 w/w)	80	0.9	89.9	3.0	2.0	5.5
10	7.8%Pd/C+CsPW (1:7 w/w)	100	5.1	91.0	3.8	0.2	5.0

[a]0.20 g catalyst (1% metal loading per total catalyst weight, 20 mg Pt/C or 30 mg Pd/C), 2.3 kPa DMTHF, 20 mL min^{-1} H_2 flow, 4 h TOS. [b]Average conversion and product selectivity over 4 h TOS.

At such conditions, no n-hexane isomerisation occurred allowing complete conversion of DMTHF to alkane without carbon chain alteration. The isomerisation of n-hexane on Pt-CsPW occurs at higher temperatures >150 °C [27]. These results clearly show that for the efficient HDO of DMTHF both Pt and H^+ sites are required, like in the case of HDO of DMF [21]. As expected, Pd-CsPW bifunctional catalyst had a much lower HDO activity compared to Pt-CsPW; Pd/C + CsPW gave only 1–5% DMTHF conversion at 90–91% n-hexane selectivity at 80–100 °C (entries 9 and 10).

While Pt is the key to the HDO of furanic compounds, the acid co-catalyst can also have a significant effect on the performance of bifunctional metal-acid catalysts [21]. In HDO of DMTHF, the acid co-catalyst will enhance the rate of dehydration of 2-hexanol (Scheme 5.1), thus affecting the selectivity to hexane. It has been demonstrated that the rate of alcohol dehydration over HPA catalysts correlates with the HPA acid strength [28]. Acid co-catalysts may also enhance the rate of the preceding step of DMTHF hydrogenolysis on Pt sites through kinetic coupling (see sect. 5.2.2 below). Table 5.2 shows the effect of Brønsted acid co-catalyst by comparing CsPW with zeolite HZSM-5 at the same Pt/C amount at 80 °C under kinetic control (DMTHF conversion 2.4–11%).

Table 5.2 Effect of acid co-catalyst on HDO of DMTHF in the gas phase.[a]

Catalyst	H^{+} [b] (mmol g^{-1})	Conversion [c] (%)	Product selectivity [c] (mol %)	
			Hexane	2-Hexanol
Pt/C+CsPW	0.080	11	95.9	3.6
Pt/C+HZSM-5-47	0.35	2.4	87.6	12.4

[a]80 °C, 2.3 kPa DMTHF, 20 mL min^{-1} H_2 flow rate, 1 h TOS, 0.10 g catalyst 9.6%Pt/C + solid acid (1:9 w/w, 10 mg Pt/C, 1% Pt loading) diluted with SiO_2 (0.10 g). [b]Proton site density per gram of acid co-catalyst; for CsPW calculated from the Keggin unit cross section of 144 $Å^2$ and CsPW surface area of 139 cm^2g^{-1} (Table 4.1); for zeolite calculated from Si/Al ratio. [c]Average conversion and product selectivity over 1 h TOS.

These acids differ significantly both in their strength and proton site density. CsPW has strong proton sites with an initial enthalpy of ammonia adsorption ΔH = –164 kJ mol^{-1} [29], but it has a low proton site density of 0.080 mmol g^{-1}. The zeolite has weaker proton sites, ΔH = –130 kJ mol^{-1} [28], however with a much greater proton site density of 0.35 mmol g^{-1}. The stronger acid, CsPW, despite its low proton site density, gives a higher hexane selectivity of 95.9% as compared to 87.6% for the zeolite (Table 5.2). Similar results have been reported for the HDO of DMF on Pt/C + CsPW [21]. This shows that the acid strength of the co-catalyst has a major effect on HDO efficiency, whereas the acid site density is less important. Furthermore, the HDO reaction on Pt/C + CsPW occurs with a significantly higher rate compared to Pt/C + HZSM-5 (11 and 2.4% DMTHF conversion, respectively, Table 5.2). This can be explained by the kinetic coupling between DMTHF hydrogenolysis and 2-hexanol dehydration steps (see sect. 5.2.2 below). It may also be due to diffusion limitations in zeolite micropores.

Next, we looked at the effect of Pt dispersion (D) on turnover frequency (TOF) for HDO of DMTHF over Pt-CsPW. In this study, physical mixtures of 9.6%Pt/C, 6.4%Pt/SiO_2 and 1%Pt/γ-Al_2O_3 with CsPW were used as catalysts, in which Pt dispersion varied from 0.039 to 0.63 (Table 4.1, Chapter 4). This corresponds to Pt particle size (d) variation from 26 to 1.6 nm as estimated from the conversion formula $d = (1/D)$ nm [29]. The reactions were carried out at 90 °C under kinetic control (DMTHF conversion 3.6–64%); in all cases, the amount of Pt in the catalyst bed was the same (0.6% per total catalyst weight). The results are shown in Table 5.3. With all catalysts, the selectivity to n-hexane was above 95%, which suggests the rate-limiting step being DMTHF hydrogenolysis on Pt sites (Scheme 5.2).

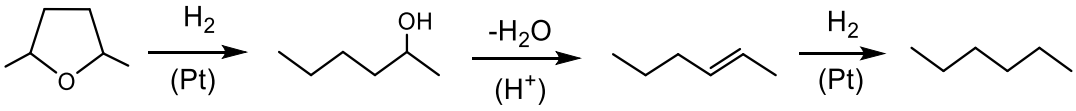

Scheme 5.2 Hydrodeoxygenation of DMTHF over Pt-CsPW catalyst.

From these results, TOF values per Pt site were calculated using the data on Pt dispersion (Table 4.1, Chapter 4). As can be seen, the TOF values increase two orders of magnitude with increasing Pt particle size from 1.6 to 26 nm in the series of supports (s^{-1}): γ-Al_2O_3 (0.0031) < SiO_2 (0.12) < C (0.40). Previously, the same order of TOF has been reported for HDO of DMF on the same Pt-CsPW catalysts (s^{-1}, at 70 °C): γ-Al_2O_3 (0.42) < SiO_2 (2.3) < C (9.3) [21] (Chapter 4). This suggests that the hydrogenolysis of C–O bond in furanic compounds on supported Pt catalysts is a structure-sensitive reaction occurring on active sites comprising ensembles of Pt atoms rather than single Pt atoms [29,30]. This is in agreement with Boudart's concept of structure sensitivity [29,31] classifying the metal-catalysed reactions involving breaking or making C–C, N–N and C–O bonds as the structure-sensitive reactions. A further in-depth investigation is required to characterise the size and symmetry of active Pt ensembles for the HDO of furanic compounds.

Table 5.3 Effect of support on Pt dispersion in HDO of DMTHF over Pt-CsPW.[a]

Catalyst	D[b]	d[c]	Conversion	TOF	Product selectivity (%)	
		(nm)	(%)	(s^{-1})	Hexane	2-Hexanol
Pt/C + CsPW	0.039	26	31	0.40	99.5	0.5
Pt/SiO_2 + CsPW	0.28	3.6	64	0.12	99.4	0.5
Pt-Al_2O_3 + CsPW	0.63	1.6	3.6	0.0031	95.8	1.1

[a]0.2 g total catalyst weight, 0.6% Pt loading, 90 °C, 2.3 kPa DMTHF, 20 mL min^{-1} H_2 flow rate, 3 h TOS. [b]Pt dispersion (from Table 4.1, Chapter 4). [c]Pt particle size (d = 1/D nm).

The results above show that the turnover rate HDO of DMTHF is much lower compared to the HDO of DMF. For 9.6%Pt/C + CsPW, it is 80 times lower given the activation energy of 65 kJ mol^{-1} for the HDO of DMF on 9.6%Pt/C + CsPW [21] (Chapter 4). This is not unexpected, as DMTHF hydrogenolysis on Pt/C is three orders of magnitude slower compared to DMF hydrogenolysis [15] (Chapter 3).

5.2.2. Kinetics and Mechanism of DMTHF Hydrodeoxygenation

Hydrodeoxygenation of DMTHF over Pt-CsPW can be represented by Scheme 5.2, which includes DMTHF ring opening on Pt sites to form 2-hexanol followed by 2-hexanol dehydration to hexene on proton sites and finally hexene hydrogenation to n-hexane on Pt sites [21]. Since no hexene was observed among the reaction products, the last step can be assumed to be fast and kinetically irrelevant. The rate-limiting step (first or second step in Scheme 5.2) is likely to be determined by the balance between metal and acid functionalities in bifunctional catalyst, i.e., by the ratio of accessible surface metal and acid sites Pt_s/H^+.

Fig. 5.2 shows the dependence of DMTHF conversion and reaction selectivity on the relative number of surface Pt and H^+ sites in the catalyst mixture Pt/C + CsPW. The density of Pt surface sites was calculated from the Pt dispersion (Table 4.1, Chapter 4), the density of H^+ surface sites in CsPW was 0.080 mmol g^{-1}, as calculated from the $PW_{12}O_{40}^{3-}$ Keggin unit cross section of 144 $Å^2$ [24,28] and CsPW surface area of 139 m^2g^{-1} (Table 4.1, Chapter 4). In Fig. 5.2A, the amount of CsPW was kept constant (0.18 g) at a sufficiently high level to effectively convert 2-hexanol to hexene. The amount of Pt/C was varied from zero to 0.06 g. As can be seen, the DMTHF conversion increases with Pt_s/H^+ ratio and reaches a plateau (22%) at $Pt_s/H^+ \approx 0.05$. The selectivity to hexane was ~100% throughout this series. These results indicate the change of rate-limiting step from the first step (DMTHF hydrogenolysis) at low Pt_s/H^+ to the second step (2-hexanol dehydration) at high Pt_s/H^+, with the first step reaching equilibrium.

In Fig. 5.2B, the experiment was carried out the other way around. The amount of Pt/C was kept constant at a typical level of 0.020 g, whereas the amount of CsPW was varied from zero to 0.22 g. As seen, the DMTHF conversion increases with the H^+/Pt_s ratio to reach a plateau (18%) at $H^+/Pt_s \approx 30$ or $Pt_s/H^+ \approx 0.03$. At such conditions, the first step is not

equilibrated, being the rate-limiting step throughout this series. The levelling-off of DMTHF conversion can be explained by kinetic coupling [32] between the first and the second step in Scheme 5.2. As the H^+/Pt_s ratio increases, the rate of the second (dehydration) step in the forward direction becomes greater than the rate of the first step in a reverse direction, which drives the HDO reaction forward. An important outcome of the kinetic coupling is a dramatic increase in reaction selectivity (Fig. 5.2B). In the absence of CsPW, the reaction over Pt/C gave 85% of 2-hexanol and 15% of hexane at ~1% DMTHF conversion. Increasing the amount of CsPW greatly affected the selectivity, with hexane becoming the main and then the only product at the expense of 2-hexanol. The acid-catalysed dehydration of secondary alcohol intermediate, 2-hexanol, is known to occur readily in the presence of CsPW [19], which greatly enhances the HDO process.

Kinetics of the gas phase HDO of DMTHF was examined at 60–100 °C and DMTHF conversion $X < 20\%$. The HDO reaction was carried out at $Pt_s/H^+ = 0.026$ with the catalyst mixture 9.6%Pt/C + CsPW (1:9 w/w), which was diluted with SiO_2 whenever required to keep the conversion low. In this system, the HDO reaction was under the impact of kinetic coupling, with the first (hydrogenolysis) step being rate-limiting (see above) and hexane selectivity >90%. The kinetic parameters obtained at such conditions are therefore attributable to the first step. The rate based on Pt/C was determined as $R = XF/W$, where X is the DMTHF conversion, F is the inlet molar flow rate of DMTHF and W is the weight of the Pt/C catalyst. In most cases, catalyst performance was stable, practically no deactivation was observed (Fig. 5.1).

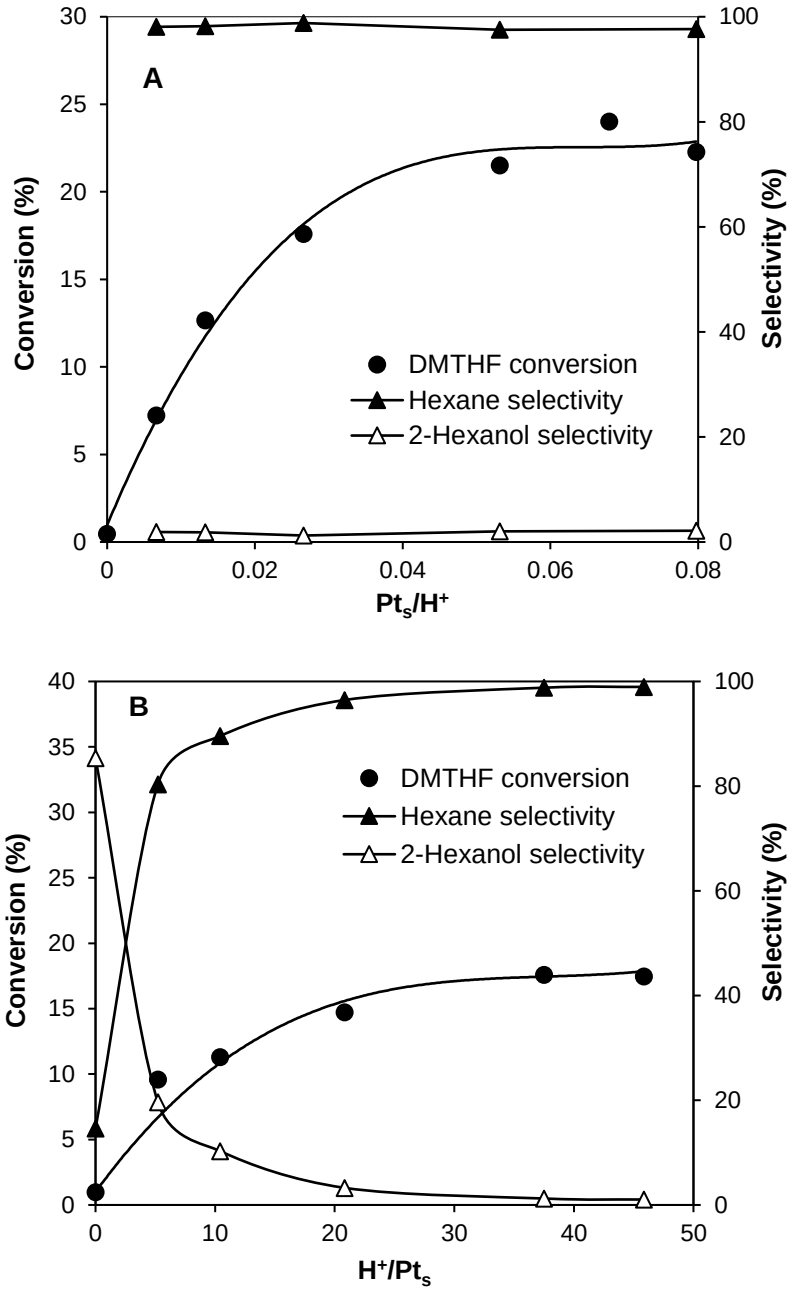

Fig. 5.2 Effect of molar ratio of surface Pt and H^+ sites on DMTHF conversion and reaction selectivity at 80 °C, 2.3 kPa DMTHF partial pressure, 20 mL min^{-1} H_2 flow rate: (A) 9.6%Pt/C (varied from 0 to 0.060 g), CsPW (0.18 g), catalyst diluted by 0.10 g SiO_2; (B) 9.6%Pt/C (0.020 g), CsPW (varied from 0 to 0.22 g), catalyst diluted by 0.10 g SiO_2.

The reaction order in DMTHF was close to zero (0.11) (Fig. 5.3), which indicates the saturation of catalyst surface sites by the substrate. To measure the reaction order in H_2, the partial pressure of H_2 was varied by changing the composition of H_2 + N_2 gas mixture at ambient pressure. This did not affect the selectivity to hexane, which was 92–93%

throughout the measurement. The order in H_2 was found to be negative, –0.45 (Fig. 5.4), which indicates competitive adsorption of DMTHF and H_2 on the Pt sites. The order in Pt–CsPW catalyst was close to 1 (Fig. 5.5), which confirms that the DMTHF ring opening is the rate-limiting step.

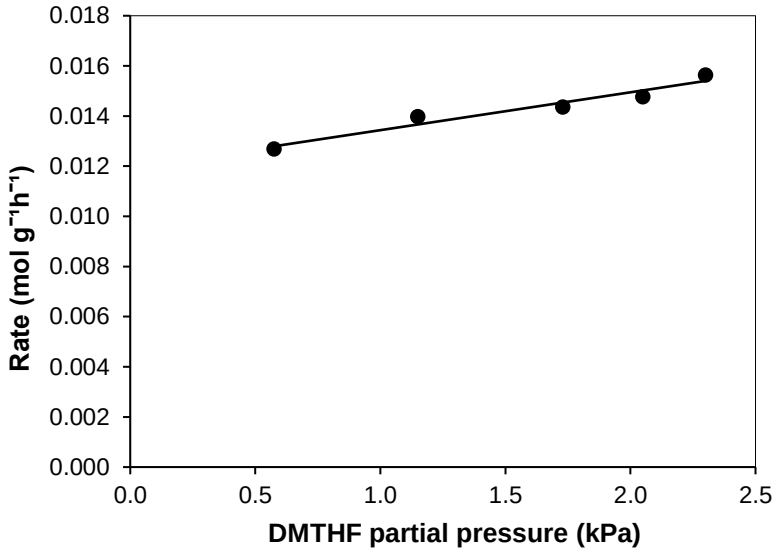

Fig. 5.3 Effect of DMTHF partial pressure on reaction rate (based on Pt/C): 9.6%Pt/C+CsPW (1:9 w/w, 0.10 g, 10 mg Pt/C, diluted by 0.10 g SiO_2), 80 °C, 40 mL min^{-1} H_2 flow rate; reaction order in DMTHF 0.11.

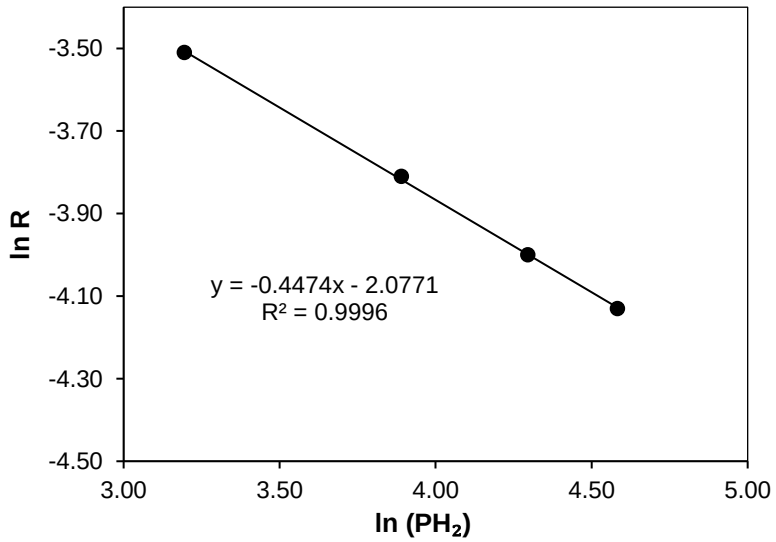

Fig. 5.4 Effect of hydrogen partial pressure (P_{H_2}, kPa) on reaction rate (mol $g^{-1}h^{-1}$ based on Pt/C): 9.6%Pt/C+CsPW (1:9 w/w, 0.10 g, 10 mg Pt/C, diluted by 0.10 g SiO_2), 80 °C, 2.3 kPa DMTHF partial pressure, 40 mL min^{-1} H_2 + N_2 flow rate; reaction order in H_2 –0.45.

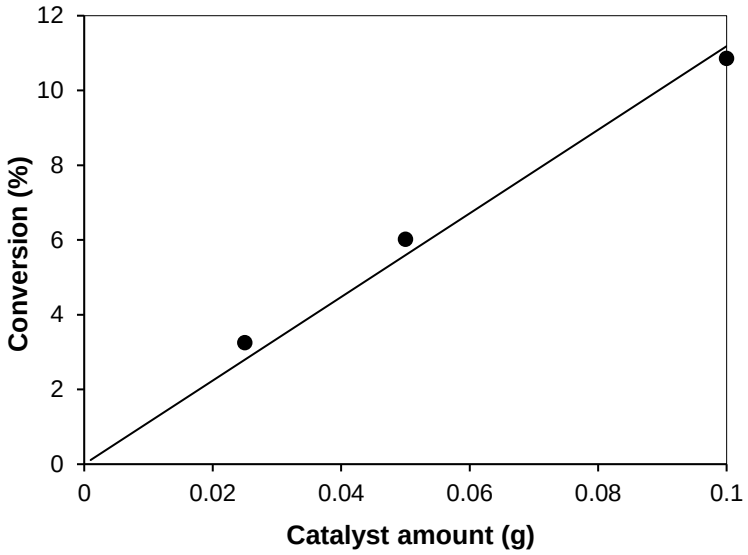

Fig. 5.5 Effect of catalyst amount on DMTHF conversion: 9.6%Pt/C+CsPW (1:9 w/w, 1% Pt loading, varied amount, diluted by 0.10 g SiO_2), 80 °C, 2.3 kPa DMTHF partial pressure, 20 mL min^{-1} H_2 flow rate.

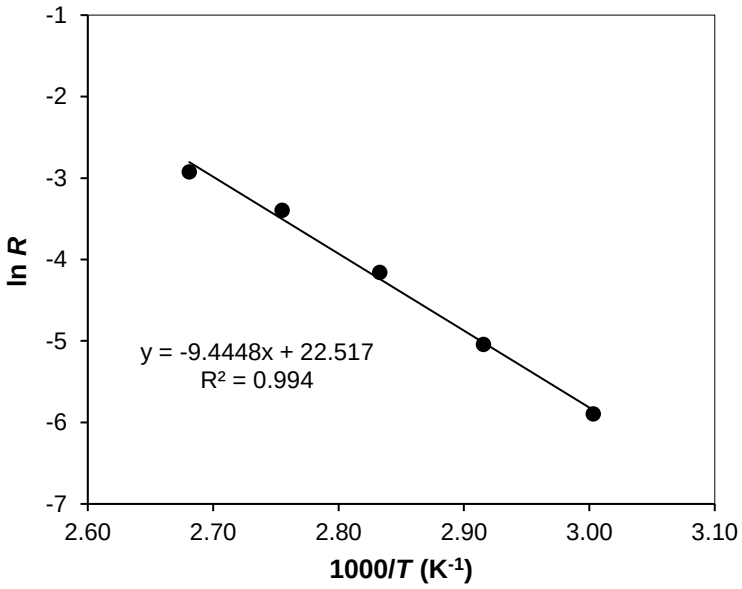

Fig. 5.6 Arrhenius plot for HDO of DMTHF: 9.6%Pt/C+CsPW (1:9 w/w, 0.10 g, 10 mg Pt/C, diluted by 0.10 g SiO_2), 2.3 kPa DMTHF partial pressure, 40 mL min^{-1} H_2 flow rate; R is the reaction rate (mol $h^{-1}g^{-1}$) per Pt/C weight; E = 78.5 kJ mol^{-1}.

The reaction was found to have an activation energy E = 78.5 kJ mol^{-1} (the Arrhenius plot is shown in Fig. 5.6). Given zero order in DMTHF, this is the true value E. The high E value and zero reaction order in DMTHF indicate no diffusion limitations in this reaction. As specified above, the E value can be attributed to the DMTHF hydrogenolysis step. The

activation energy for the dehydration step is expected to be higher. This is indicated by the increase in hexane selectivity with reaction temperature (64% at 60 °C, 94% at 80 °C and >99% at 100 °C). The gas phase dehydration of similar secondary alcohol, 2-methyl-4-pentanol, over CsPW has been reported to have E = 130 kJ mol^{-1} at 60–80 °C [19].

The rate equation (Eq. 5.13) was derived for the HDO reaction (Scheme 5.2) using reaction steps (5.1) – (5.4), where S is the substrate DMTHF, S* is the primary ring-opened product after addition of the first H atom to DMTHF, HXL is 2-hexanol, [ ] is the vacant Pt surface site, [H] is the H atom adsorbed on the Pt site, [S], [S*] and [HXL] are the corresponding species adsorbed on Pt. It was assumed that the reaction proceeds through equilibrated competitive adsorption of DMTHF (equilibrium constant K_1) and dissociative adsorption of H_2 (K_2) on Pt sites, followed by the rate-limiting hydrogenolysis of the adsorbed DMTHF by addition of the first hydrogen atom (rate constant k). Then the second H atom adds to form 2-hexanol. The latter step and subsequent steps of 2-hexanol dehydration to hexene on acid sites and hexene hydrogenation to hexane on Pt sites (not shown) were assumed to be fast, hence kinetically irrelevant.

$$S + [\ ] \overset{K_1}{\rightleftharpoons} [S] \tag{5.1}$$

$$H_2 + 2[\ ] \overset{K_2}{\rightleftharpoons} 2[H] \tag{5.2}$$

$$[S] + [H] \xrightarrow[\text{slow}]{k} [S^*] + [\ ] \tag{5.3}$$

$$[S^*] + [H] \xrightarrow[\text{fast}]{} [HXL] + [\ ] \tag{5.4}$$

The balance of Pt sites in the catalyst is represented by:

$$[Pt]_t = [\ ] + [H] + [S] + [S^*] + [HXL] \tag{5.5}$$

Where $[Pt]_t$ is the total density of surface Pt sites. At low DMTHF pressure and low conversion, the number of adsorbed [S^*] and [HXL] species could be assumed to be small compared to [H] and [S], then

$$[Pt]_t \approx [\ ] + [H] + [S] \tag{5.6}$$

From adsorption equilibria (5.1) and (5.2)

$$[S] = K_1 P_s [\ ] \tag{5.7}$$

$$[H] = \sqrt{K_2 P_{H_2}}\ [\ ] \tag{5.8}$$

where P_S is the partial pressure of DMTHF and P_{H2} is the partial pressure of H_2.

Combining (5.6), (5.7) and (5.8) gives:

$$[Pt]_t = [\ ] + \sqrt{K_2 P_{H_2}}\ [\ ] + K_1 P_s [\ ] = [\ ]\left(1 + K_1 P_s + \sqrt{K_2 P_{H_2}}\right) \tag{5.9}$$

From step (5.3), the HDO reaction rate is given by Eq. 5.10

$$R = k\theta_S \theta_H \tag{5.10}$$

where θ_S and θ_H are the surface coverages of S and H, respectively:

$$\theta_S = \frac{K_1 P_S}{1 + K_1 P_S + \sqrt{K_2 P_{H_2}}} \tag{5.11}$$

$$\theta_H = \frac{\sqrt{K_2 P_{H_2}}}{1 + K_1 P_S + \sqrt{K_2 P_{H_2}}} \tag{5.12}$$

Combining (5.10) with (5.11) and (5.12) gives (5.13), where $P_{DMTHF} = P_S$

$$R = \frac{k K_1 P_{DMTHF} \sqrt{K_2 P_{H_2}}}{\left(1 + K_1 P_{DMTHF} + \sqrt{K_2 P_{H_2}}\right)^2} \tag{5.13}$$

Eq. 5.13 is consistent with the kinetics observed for hydrodeoxygenation of DMTHF. It accounts for zero order in DMTHF pressure (P_{DMTHF}) at sufficiently high P_{DMTHF} and –0.45

order in H_2 pressure (P_{H2}). It also accounts for the first order in Pt/C catalyst since the rate constant *k* is proportional to the density of Pt sites.

5.3. Conclusion

In Chapter 5, we demonstrate the high effectiveness of metal-acid bifunctional heterogeneous catalysis for the gas phase HDO of a saturated furan derivative 2,5-dimethyltetrahydrofuran (DMTHF). The Pt–CsPW bifunctional catalyst comprising a mixture of Pt/C and strongly acidic heteropoly salt CsPW deoxygenates DMTHF to n-hexane with >99% selectivity under mild conditions (90–100 °C, ambient pressure) and is much more efficient than monofunctional Pt/C. At such conditions, no n-hexane isomerisation takes place allowing complete conversion of DMTHF to alkane without carbon chain alteration. The proposed reaction mechanism includes a sequence of hydrogenolysis, dehydration and hydrogenation steps catalysed by Pt and proton sites in the bifunctional catalyst. The results suggest that the HDO of furanic compounds on Pt–CsPW is a structure-sensitive reaction occurring on active sites that are complex ensembles of Pt atoms. Synergistic action of the metal and acid sites is essential for the effectiveness of the HDO process. Easy dehydration of secondary alcohol intermediate, 2-hexanol, on strong proton sites of CsPW is an effective driving force of the HDO process by bifunctional metal-acid catalysis through kinetic coupling between DMTHF hydrogenolysis and 2-hexanol dehydration steps.

References

[1] A. Corma, S. Iborra, A. Velty, Chemical routes for the transformation of biomass into chemicals, Chem. Rev. 107 (2007) 2411–2502.

[2] Y. Román-Leshkov, J.N. Chheda, J.A. Dumesic, Phase modifiers promote efficient production of hydroxymethylfurfural from fructose, Science 312 (2006) 1933–1937.

[3] R.M. West, Z.Y. Liu, M. Peter, J.A. Dumesic, Liquid alkanes with targeted molecular weights from biomass-derived carbohydrates, ChemSusChem 1 (2008) 417–424.

[4] G.W. Huber, J.N. Chheda, C.J. Barrett, J.A. Dumesic, Production of liquid alkanes by aqueous-phase processing of biomass-derived carbohydrates, Science 308 (2005) 1446–1450.

[5] Z. J. Brentzel, K.J. Barnett, K. Huang, C.T. Maravelias, J.A. Dumesic, G.W. Huber, Conversion of furfural to 1,5-pentanediol: process synthesis and analysis, ChemSusChem 10 (2017) 1351–1355.

[6] Y.L. Louie, J. Tang, A.M.L. Hell, A.T. Bell, Kinetics of hydrogenation and hydrogenolysis of 2,5-dimethylfuran over noble metals catalysts under mild conditions, Appl. Catal. B 202 (2017) 557–568.

[7] V. Vorotnikov, D.G. Vlachos, Group additivity and modified linear scaling relations for estimating surface thermochemistry on transition metal surfaces: Application to furanics, J. Phys. Chem. C 119 (2015) 10417–10426.

[8] J. Kang, A. Vonderheide, V.V. Guliants, Deuterium-labeling study of the hydrogenation of 2-methylfuran and 2,5-dimethylfuran over carbon-supported noble metal catalysts, ChemSusChem 8 (2015) 3044–3047.

[9] R.C. Runnebaum, T. Nimmanwudipong, J. Doan, D.E. Block, B.C. Gates, Catalytic conversion of furan to gasoline-range aliphatic hydrocarbons via ring opening and decarbonylation reactions catalyzed by Pt/γ-Al_2O_3, Catal. Lett. 142 (2012) 664–666.

[10] J. Kang, X. Liang, V.V. Guliants, Selective hydrogenation of 2-methylfuran and 2,5-dimethylfuran over atomic layer deposited platinum catalysts on multiwalled carbon nanotube and alumina supports, ChemCatChem 9 (2017) 282–286.

[11] A. Corma, O. de la Torre, M. Renz, N. Villandier, Production of high-quality diesel from biomass waste products, Angew. Chem. Int. Ed. 50 (2011) 2375–2378.

[12] J. Yang, S. Li, L. Zhang, X. Liu, J. Wang, X. Pan, N. Li, A. Wang, Y. Cong, X. Wang, T. Zhang, Hydrodeoxygenation of furans over Pd-FeOx/SiO_2 catalyst under atmospheric pressure, Appl. Catal. B 201 (2017) 266–277.

[13] H. Goto, A. Takagaki, R. Kikuchi, S.T. Oyama, Hydrogenation of 2,5-dimethylfuran on hexagonal-boron nitride- and silica-supported platinum catalysts, Appl. Catal. A 548 (2017) 122–127.

[14] F. Xue, D. Ma, T. Tong, X. Liu, Y. Hu, Y. Guo, Y. Wang, Contribution of different NbOx species in the hydrodeoxygenation of 2,5-dimethyltetrahydrofuran to hexane, Sustainable Chem. Eng. 6 (2018) 13107−13113.

[15] H. Althikrallah, C. Kunstmann-Olsen, E.F. Kozhevnikova, I.V. Kozhevnikov, Turnover rate of metal-catalysed hydroconversion of 2,5-dimethylfuran: gas-phase versus liquid-phase, Catalysts 10 (2020) 1171.

[16] D.M. Alonso, J.Q. Bond, J.A. Dumesic, Catalytic conversion of biomass to biofuels, Green Chem. 12 (2010) 1493–1513.

[17] J. Zhong, J. Pérez-Ramírez, N. Yan, Biomass valorisation over polyoxometalate-based catalysts, Green Chem. 23 (2021) 18–36.

[18] S. Itagaki, N. Matsuhashi, K. Taniguchi, K. Yamaguchi, N. Mizuno, Efficient hydrodeoxygenation of ketones, phenols and ethers promoted by platinum–heteropolyacid bifunctional catalysts, Chem. Lett. 43 (2014) 1086–1088.

[19] K. Alharbi, E.F. Kozhevnikova, I.V. Kozhevnikov, Hydrogenation of ketones over bifunctional Pt-heteropoly acid catalyst in the gas phase, Appl. Catal. A 504 (2015) 457–462.

[20] K. Alharbi, W. Alharbi, E.F. Kozhevnikova, I.V. Kozhevnikov, Deoxygenation of ethers and esters over bifunctional Pt–heteropoly acid catalyst in the gas phase, ACS Catal. 6 (2016) 2067–2075.

[21] H. Althikrallah, E. F. Kozhevnikova, I. V. Kozhevnikov, Facile gas phase hydrodeoxygenation of 2,5-dimethylfuran over bifunctional metal-acid catalyst Pt-$Cs_{2.5}H_{0.5}PW_{12}O_{40}$, Chem. Commun. 57 (2021) 227–230.

[22] S. Li, L. Yan, Q. Liu, J. Liu, Q. Liu, W. Fan, X. Zhao, X. Zhang, C. Wang, L. Maa, Q. Zhang, One-pot hydrodeoxygenation of biomass furan derivatives into decane under mild conditions over Pd/C combined with phosphotungstic acid, Green Chem. 22 (2020) 2889–2900.

[23] T. Okuhara, N. Mizuno, M. Misono, Catalytic chemistry of heteropoly compounds, Adv. Catal. 41 (1996) 113–252.

[24] I.V. Kozhevnikov, Catalysis by heteropoly acids and multicomponent polyoxometalates in liquid-phase reactions, Chem. Rev. 98 (1998) 171–198.

[25] J.B. Moffat, Metal-oxygen clusters. The surface and catalytic properties of heteropoly oxometalates, Kluwer: New York, 2001.

[26] M.A. Alotaibi, E.F. Kozhevnikova, I.V. Kozhevnikov, Deoxygenation of propionic acid on heteropoly acid and bifunctional metal-loaded heteropoly acid catalysts: Reaction pathways and turnover rates, Appl. Catal. A 447 (2012) 32–40.

[27] A. Alazman, D. Belic, E.F. Kozhevnikova, I.V. Kozhevnikov, Isomerization of n-hexane over bifunctional Pt-heteropoly acid catalyst: Enhancing effect of gold. J. Catal. 357 (2018) 80–89.

[28] W. Alharbi, E.F. Kozhevnikova, I.V. Kozhevnikov, Dehydration of MeOH to dimethyl ether over heteropoly acid catalysts: The relationship between reaction rate and catalyst acid strength, ACS Catal. 5 (2015) 7186−7193.

[29] M. Boudart, Catalysis by supported metals, Adv. Catal. 20 (1969) 153–166.

[30] G.C. Bond, Metal-catalysed reactions of hydrocarbons, Springer, New York, 2005.

[31] M. Boudart, Heterogeneous catalysis by metals, J. Mol. Catal. 30 (1985) 27–38.

[32] M. Boudart, Turnover rates in heterogeneous catalysis, Chem. Rev. 95 (1995) 661–666.

Chapter 6. Hydrodeoxygenation of 2,5-Dimethyltetrahydrofuran over Bifunctional Pt-$Cs_{2.5}H_{0.5}PW_{12}O_{40}$ Catalyst In the Gas Phase: Enhancing Effect of Gold

6

6.1. Introduction

As stated earlier, biomass-derived furanic compounds are of interest as a renewable feedstock, which can be processed into a range of value-added chemicals and green fuels via catalytic hydroconversion [1–8]. Hydrodeoxygenation (HDO) of furanic compounds using bifunctional metal–acid catalysis has been demonstrated to be an effective strategy to produce green fuels under mild conditions ([3,4,6,8–12] and references therein). Previously, we have reported HDO of a wide range of oxygenates in the gas phase to produce alkanes in the presence of bifunctional catalysts comprising Pt, Ru, Ni and Cu as metal components and Keggin-type heteropoly acids, with their activity decreasing in the order Pt > Ru > Ni > Cu [13-14]. In Chapters 4 and 5, Pt-CsPW comprising Pt and strongly acidic heteropoly salt $Cs_{2.5}H_{0.5}PW_{12}O_{40}$ (CsPW) has been reported to be a highly efficient catalyst for the HDO of 2,5-dimethylfuran (DMF) and 2,5 dimethyltetrahydrofuran (DMTHF) to produce n-hexane with 100% yield at 90–120 °C and ambient pressure [11,12]. The HDO of DMTHF over Pt-CsPW occurs through a sequence of hydrogenolysis, dehydration and hydrogenation steps catalysed by Pt and proton sites of the bifunctional catalyst (Scheme 6.1).

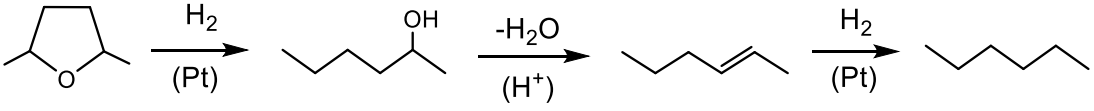

Scheme 6.1 Hydrodeoxygenation of DMTHF over Pt-CsPW catalyst.

There has been a continued interest in bimetallic catalysis since the discovery of superior properties of bimetallic catalysts in petrochemistry and petroleum reforming ([15-17] and references therein). Bimetallic PtAu and PdAu catalysts have an enhanced performance in comparison to monometallic Pt and Pd catalysts [18−34], for example, in hydrogenation [19,24,30], hydrodesulphurisation [28,29], oxidation [25,27], isomerisation [18,22,31,32] and other reactions [20,21,23,33,34]. The enhancement of catalyst performance by addition of gold can be attributed to geometric (ensemble) and electronic (ligand) effects of the constituent elements in PtAu and PdAu bimetallic species [33−38]. Here we looked at the effect of Au on the performance of Pt-CsPW catalysts in the HDO of DMTHF in the gas phase.

6.2. Results and Discussion

Supported bimetallic catalysts PtAu/SiO_2 and PtAu/CsPW were prepared by co-impregnation of H_2PtCl_6 and $HAuCl_3$ (with a 1:1 atomic ratio) onto SiO_2 and CsPW followed by reduction with H_2 at 250 °C, as explained in detail in Chapter 2. This method gives supported bimetallic PtAu nanoparticles of a random composition together with various Pt and Au nanoparticles [18,19,32,36]. The bimetallic PtAu catalysts were characterised by XRD and STEM-EDX. Powder X-ray diffraction patterns of catalysts were recorded on a PANalytical Xpert diffractometer with CuKα radiation (λ = 1.542 Å) and attributed using the JCPDS database. High-angle annular dark-field scanning transmission electron microscopy (HAADF-STEM) images were obtained on a spherical aberration-corrected JEOL 2100 F microscope at an accelerating voltage of 200 kV. Energy dispersive X-ray spectroscopy (EDX) mapping was performed using JEOL Silicon Drift Detector DrySD100GV with a solid angle of up to 0.98 steradians from a detection area of 100 mm^2.

Platinum dispersion, *D*, in supported Pt and PtAu catalysts defined as the Pt fraction at the surface of platinum particles, $D = Pt_s/Pt_{total}$, was measured on a Micromeritics TPD/TPR 2900 instrument using H_2/O_2 titration pulse method in a flow system at room temperature as described in Chapter 2. The *D* values were obtained assuming the stoichiometry of H_2 adsorption $Pt_sO + 1.5\ H_2 \rightarrow Pt_sH + H_2O$. Adsorption of H_2 on PtAu catalysts was attributed entirely to platinum as Au did not adsorb H_2 under such conditions. The average diameter of Pt particles, *d*, was obtained from the empirical conversion equation *d* (nm) = 1/*D*. The size of Pt and Au particles was also estimated from STEM images and XRD using the Scherrer equation. Information about the catalysts studied is given in Table 6.1.

Table 6.1 Catalysts characterisation.

Catalyst	Surface area[a] (m^2g^{-1})	Pore volume[b] (cm^3g^{-1})	Pore diameter[c] (Å)	D[d]	d[e] (nm)
$Cs_{2.5}H_{0.5}PW_{12}O_{40}$ (CsPW)	135	0.089	27		
SiO_2 (Aerosil 300 silica)	283	1.2	164		
6.5% Au/SiO_2	257	1.01	157	0.019[f]	46[g], 38[i]
4.7%Au/CsPW	103	0.048	33	0.016[f]	60[g]
6.4%Pt/SiO_2	266	1.06	159	0.28±0.04[h]	3.2[f], 8.0[g], 5[i]
6.0%Pt%/CsPW	84	0.052	25	0.17±0.03[h]	5.3[f]
6.6%Pt/5.9%Au/SiO_2	240	1.08	179	0.29±0.05[h]	3.1[f]
5.9%Pt/4.4%Au/CsPW	91	0.082	36	0.17±0.04[h]	5.3[f]

[a]BET surface area. [b]Single point total pore volume. [c]Average BET pore diameter. [d]Metal dispersion. [e]Metal particle size. [f]Calculated from the equation *d* (nm) = 1/*D*. [g]Metal particle diameter from powder XRD (Scherrer equation). [h]Pt dispersion determined by H_2/O_2 titration (average from three measurements); for PtAu catalysts, assumed negligible H_2 adsorption on gold. [i]From STEM.

The HDO of DMTHF was carried out in a gas solid system at 90 °C in flowing H_2 at ambient pressure using a down-flow fixed-bed microreactor (9 mm internal diameter) fitted with an on-line GC analysis as described in Chapter 2. The initial reaction rate (R) based on total Pt weight in the catalyst was calculated as $R = XF/W$ (mol $h^{-1}g^{-1}$), where X is the fractional conversion at 1 h TOS, F (mol h^{-1}) is the inlet molar flow rate of DMTHF and W is the weight of Pt (g) in the catalyst. The initial turnover frequency (TOF) was calculated from the initial reaction rate per surface Pt site, TOF = R/M_s (h^{-1}), using the values of Pt dispersion D from Table 6.1.

6.2.1. XRD analysis of bimetallic PtAu catalysts

Powder X-ray diffraction (XRD) has been widely used for the characterisation of supported Au alloy catalysts [34]. The XRD patterns for the silica-supported catalysts 6.4%Pt/SiO_2, 6.5%Au/SiO_2 and 6.6%Pt/5.9%Au/SiO_2 are shown in Fig. 6.1. As expected, the 6.4%Pt/SiO_2 and 6.5%Au/SiO_2 catalysts display the fcc pattern of Pt and Au metal nanoparticles. The Pt peaks are broader than the Au peaks, which indicates a higher dispersion of Pt particles, with an average particle size of 8.0 nm for Pt and 46 nm for Au, which is in agreement with the STEM values (Table 6.1). The pattern for the 6.6%Pt/5.9%Au/SiO_2 catalyst clearly shows the presence of PtAu bimetallic particles with broad [111], [200], [220] and [311] diffraction peaks of the fcc PtAu alloy between the corresponding diffractions of the pure metals in the range 38–40°, 44–48°, 65–68° and 78–81°, respectively.

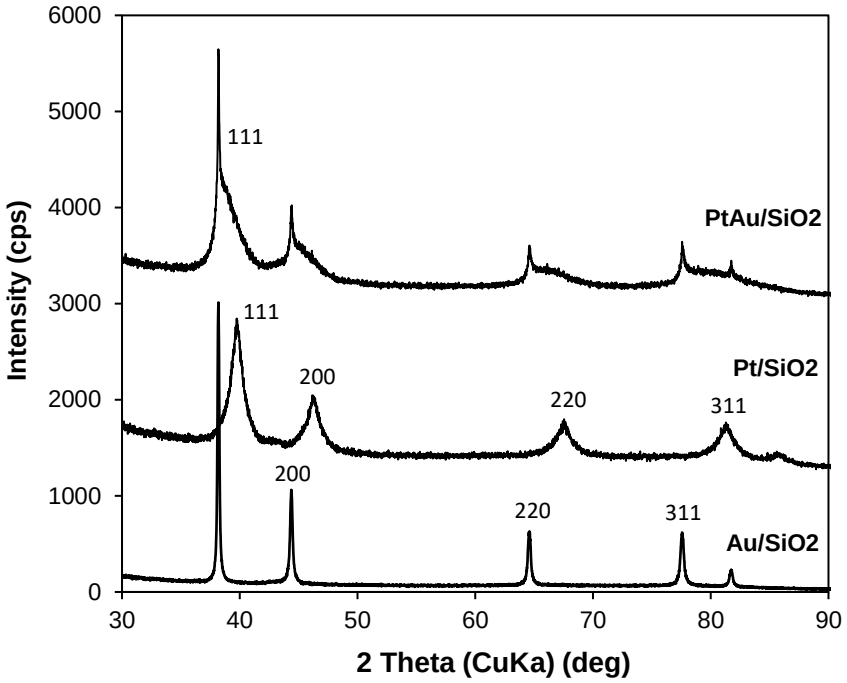

Fig. 6.1 Powder XRD patterns of 6.4%Pt/SiO_2, 6.5%Au/SiO_2 and 6.6%Pt/5.9%Au/SiO_2; the pattern for 6.6%Pt/5.9%Au/SiO_2 shows broad [111], [200], [220] and [311] fcc PtAu alloy peaks in the range 38–40°, 44–48°, 65–68° and 78–81°, respectively.

6.2.2. STEM-EDX analysis of PtAu catalysts

Fig. 6.2 shows the high-angle annular dark field (HAADF) TEM images of the three silica-supported catalysts 6.4%Pt/SiO_2, 6.5%Au/SiO_2 and 6.6%Pt/5.9%Au/SiO_2 with metal nanoparticles indicated as bright spots on the darker background. In the Pt/SiO_2 catalyst, there are two populations: small Pt particles of 5 nm size and coalesced Pt particles of a larger size. The Au/SiO_2 catalyst displays Au particles of spherical, rectangular and triangular morphology, with an average size of 38 nm. The bimetallic PtAu/SiO_2 catalyst shows a high agglomeration and different kinds of morphology of metal particles.

The energy dispersive X-ray spectroscopic analysis (EDX) of metal particles in the PtAu/SiO_2 catalyst shows that these particles contain both platinum and gold. EDX elemental mapping clearly demonstrates that Pt and Au maps cover the same areas of

$PtAu/SiO_2$ catalyst (Fig. 6.3), indicating PtAu alloying with formation of a non-uniform bimetallic PtAu particles.

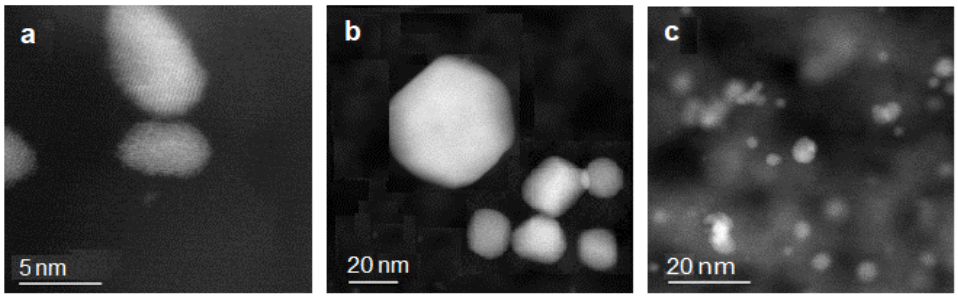

Fig. 6.2 HAADF-STEM images of (a) 6.4% Pt/SiO_2, (b) 6.5% Au/SiO_2 and (c) 6.6% Pt/5.9% Au/SiO_2 catalysts, showing noble metal nanoparticles as bright spots.

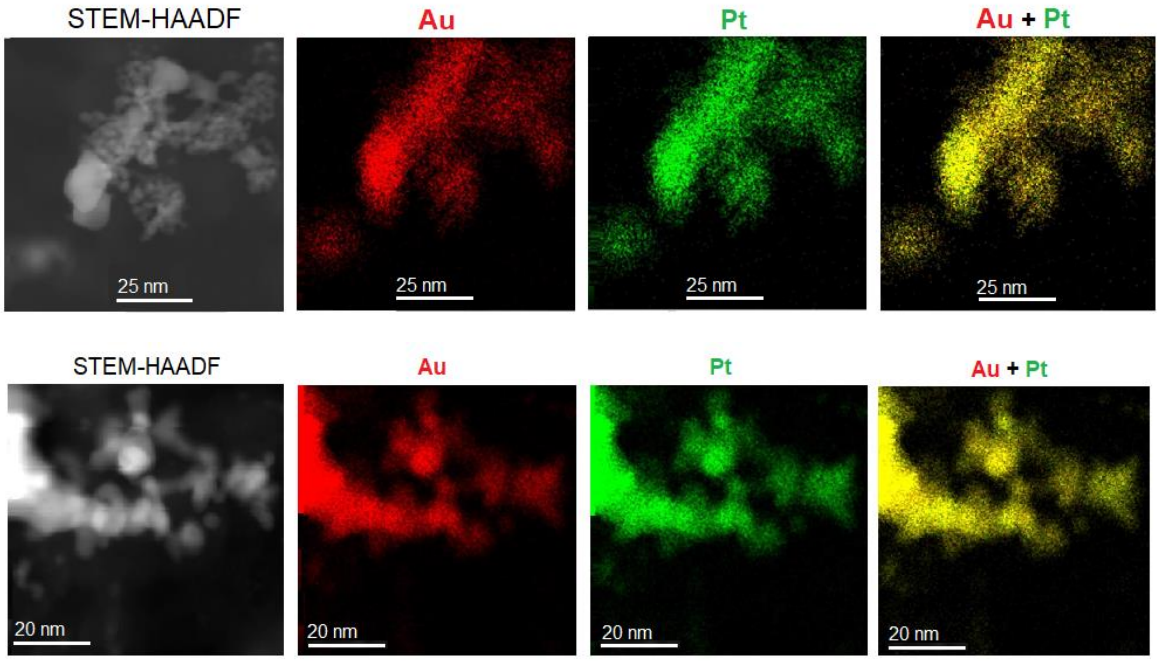

Fig. 6.3 HAADF-STEM image of 6.6% Pt/5.9% Au/SiO_2 catalyst and the corresponding STEM-EDX elemental maps showing the spatial distribution of Au (red) and Pt (green) in the sample.

STEM–EDX for CsPW-supported Pt, Au and PtAu catalysts has been reported elsewhere [19]. These STEM images are difficult to analyse due to W, Pt and Au having similar large atomic numbers Z (74, 78 and 79, respectively). Crystalline CsPW containing 70 wt% of W displays a strong background which makes it difficult to discern smaller Pt and Au particles from the Z-contrast HAADF images and determine accurately metal particle size.

Nevertheless, the STEM-EDX analysis indicates the presence of bimetallic PtAu particles in the PtAu/CsPW catalyst with a wide range of Pt/Au atomic ratios [19].

6.2.3. Effect of Au on the performance of Pt-CsPW catalyst

The HDO reaction was carried out in flowing hydrogen at 90 °C and ambient pressure in a fixed-bed reactor. The molar ratio of surface metal and proton sites in the catalysts was chosen low enough (Pt/H^+ = 0.03–0.1) to ensure the reaction being limited by the DMTHF ring opening step [12]. The density of surface Pt sites was estimated from the Pt dispersion (Table 6.1), the density of surface proton sites in CsPW was calculated assuming a cross section of the $PW_{12}O_{40}^{3-}$ Keggin unit of 144 Å 32,33 and the CsPW surface area of 135 cm^2g^{-1} (Table 6.1). Representative results for HDO of DMTHF in the presence of bifunctional metal-acid catalysts Pt-CsPW and PtAu-CsPW, which were used as physical mixtures of metal and acid components at similar Pt loadings, are shown in Table 6.2.

In the absence of Pt, the CsPW alone (entry 1) and Au–CsPW (entries 2 and 5) showed a negligible activity (1.9–2.2% DMTHF conversion with practically no 2-hexanol and n-hexane formed). Physically mixed Pt–CsPW catalysts, Pt/CsPW + CsPW and Pt/SiO_2 + CsPW (1:9 w/w), exhibited a high activity giving >99% n-hexane selectivity at 8.0 to 85% DMTHF conversion depending on the catalyst and reaction conditions, in agreement with the previous report [12]. It should be noted that the catalyst based on Pt/SiO_2 had almost 6-fold greater activity than the one based on Pt/CsPW in terms of turnover frequency (TOF) per surface Pt site (cf. entries 3 and 6), thus demonstrating a strong effect of Pt support.

Table 6.2 Hydrodeoxygenation of DMTHF over bifunctional metal-acid catalysts.[a]

Entry	Catalyst	Conv. (%)	TOF[b] (h^{-1})	Product selectivity (% mol)	
				n-Hexane	2-Hexanol
1	CsPW	2.1			
2	4.7%Au/CsPW + CsPW	2.2			
3	6.0%Pt/CsPW + CsPW	8.6	70	98.6	0.7
4	5.9%Pt/4.4%Au/CsPW + CsPW	17	170	98.6	0.8
5	6.5%Au/SiO_2 + CsPW	1.9			
6	6.4%Pt/SiO_2 + CsPW	64	390	99.4	0.5
7	6.6%Pt/5.9%Au/SiO_2 + CsPW	85	490	99.6	0.3
8	6.4%Pt/SiO_2+CsPW[c]	8.0	150	98.6	1.2
9	6.6%Pt/5.9%Au/SiO_2 + CsPW[c]	13	260	98.5	0.7
10	6.0% Pd/SiO_2 + CsPW	5.6	34	97.2	0.0
11	5.4%Pd/5.4%Au/SiO_2 + CsPW	3.7	37	91.7	0.0
12	6.9%Pt/6.0%Pd/SiO_2 + CsPW	54.9	-	99.4	0.0

[a]0.20 g total catalyst weight (physical mixture of 0.020 g metal catalyst + 0.18 g CsPW), 0.6% Pt, 90 °C, 2.3 kPa DMTHF, 20 ml min^{-1} H_2 flow rate, catalyst pre-treatment at 90 °C for 1 h in H_2 flow, 1 h TOS. [b]TOF values per Pt surface site, the contribution of Au and CsPW subtracted. [c]Catalyst bed contained 0.005 g metal catalyst + 0.18 g CsPW; catalyst pre-treatment at 250 °C for 1 h in H_2 flow.

As can be seen from Table 6.2, the addition of gold to Pt/CsPW and Pt/SiO_2 caused a significant enhancement of catalyst activity, with DMTHF conversion increasing 1.3–2 times compared to the corresponding Pt only catalysts (cf. entries 3 and 4, 6 and 7, 8 and 9). As the gold alone was practically inactive, the increase in catalyst activity can be attributed to an enhancement of the activity of the Pt sites. For the bimetallic PtAu catalysts, the TOF values at Pt sites increased 1.3–2.4 times as compared to the monometallic Pt catalysts

(Table 6.2). The results at lower DMTHF conversions of 8–17% give a more accurate estimate of the TOF enhancement reaching 1.7–2.4 times (cf. entry 3 with 4 and 8 with 9). Previously, the gold enhancement on a similar scale has been reported for alkane isomerisation on PtAu-CsPW catalysts [18,32].

The enhancement of catalyst activity by addition of gold has been attributed to geometric (ensemble) and electronic (ligand) effects of the constituent metals in PtAu bimetallic nanoparticles [34]. The XRD and STEM-EDX data shown above clearly demonstrate PtAu alloying in the PtAu/SiO2 catalyst leading to the formation of bimetallic PtAu species. The same has also been reported for the PtAu/CsPW catalyst [19]. Previously, it has been shown that the HDO of DMTHF on Pt–CsPW is a structure-sensitive reaction [12], hence the geometric effects may be expected to contribute to the gold enhancement. The description of the influence of the second metal on the overall catalytic activity is given in chapter 1, section 1.2.4. However, in order to prove the role of geometric and electronic effects as the cause of the gold enhancement, more accurate metal dispersion measurements complemented by spectroscopic characterisation will be required.

We also tested the performance of bifunctional PdAu/SiO_2+CsPW and PtPd/SiO2 + CsPW bimetallic catalysts under similar conditions in comparison to the corresponding monometallic Pd and Pt catalysts, (Table 6.2, cf. entry 11 and 12). However, no enhancement of activity was observed. This is in agreement with XRD analysis, which showed no distinct alloying in PdAu/SiO_2 (Fig. 6.4).

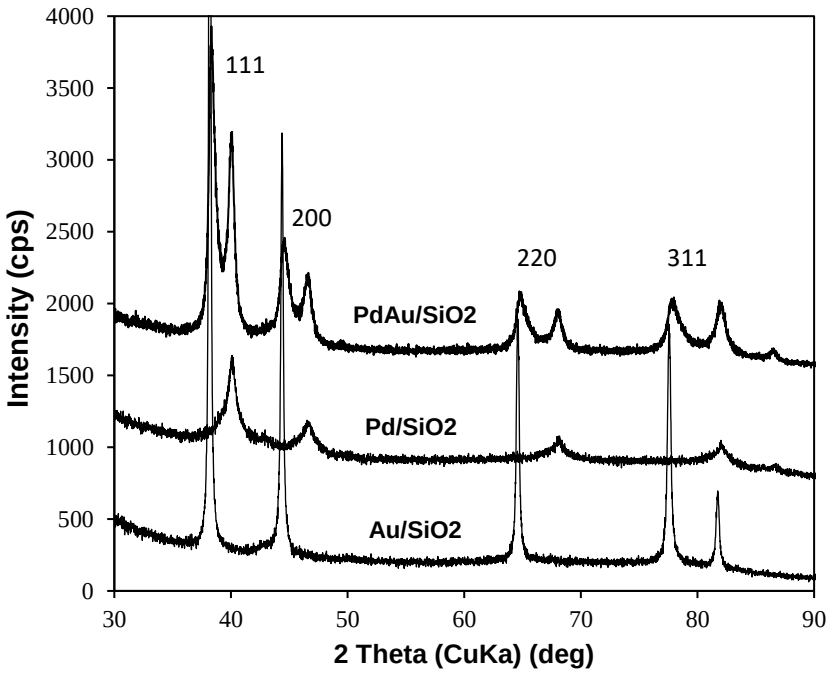

Fig. 6.4 Powder XRD patterns: 6.5%Au/SiO_2, 6.0 %Pd/SiO_2 and 5.6%Pd/5.9%Au/SiO_2.

6.3. Conclusion

In conclusion, we have demonstrated that the addition of gold to the Pt–CsPW catalyst has an enhancing effect on the HDO of DMTHF, increasing the turnover rate at Pt sites more than twofold. The enhancing effect is attributed to PtAu alloying. The formation of bimetallic PtAu nanoparticles in the PtAu–CsPW catalyst is confirmed by STEM-EDX and XRD.

References

[1] A. Corma, S. Iborra, A. Velty, Chemical routes for the transformation of biomass into chemicals, Chem. Rev. 107 (2007) 2411–2502.

[2] Y.L. Louie, J. Tang, A.M.L. Hell, A.T. Bell, Kinetics of hydrogenation and hydrogenolysis of 2,5-dimethylfuran over noble metals catalysts under mild conditions, Appl. Catal. B 202 (2017) 557–568.

[3] A. Corma, O. de la Torre, M. Renz, N. Villandier, Production of high-quality diesel from biomass waste products, Angew. Chem. Int. Ed. 50 (2011) 2375–2378.

[4] J. Yang, S. Li, L. Zhang, X. Liu, J. Wang, X. Pan, N. Li, A. Wang, Y. Cong, X. Wang, T. Zhang, Hydrodeoxygenation of furans over Pd-FeOx/SiO_2 catalyst under atmospheric pressure, Appl. Catal. B 201 (2017) 266–277.

[5] H. Goto, A. Takagaki, R. Kikuchi, S.T. Oyama, Hydrogenation of 2,5-dimethylfuran on hexagonal-boron nitride- and silica-supported platinum catalysts, Appl. Catal. A 548 (2017) 122–127.

[6] F. Xue, D. Ma, T. Tong, X. Liu, Y. Hu, Y. Guo, Y. Wang, Contribution of different NbOx species in the hydrodeoxygenation of 2,5-dimethyltetrahydrofuran to hexane, Sustainable Chem. Eng. 6 (2018) 13107−13113.

[7] H. Althikrallah, C. Kunstmann-Olsen, E.F. Kozhevnikova, I.V. Kozhevnikov, Turnover rate of metal-catalysed hydroconversion of 2,5-dimethylfuran: gas-phase versus liquid-phase, Catalysts 10 (2020) 1171.

[8] D.M. Alonso, J.Q. Bond, J.A. Dumesic, Catalytic conversion of biomass to biofuels, Green Chem. 12 (2010) 1493–1513.

[9] J. Zhong, J. Pérez-Ramírez, N. Yan, Biomass valorisation over polyoxometalate-based catalysts, Green Chem. 23 (2021) 18–36.

[10] S. Li, L. Yan, Q. Liu, J. Liu, Q. Liu, W. Fan, X. Zhao, X. Zhang, C. Wang, L. Maa, Q. Zhang, One-pot hydrodeoxygenation of biomass furan derivatives into decane under mild conditions over Pd/C combined with phosphotungstic acid, Green Chem. 22 (2020) 2889–2900.

[11] H. Althikrallah, E. F. Kozhevnikova, I. V. Kozhevnikov, Facile gas phase hydrodeoxygenation of 2,5-dimethylfuran over bifunctional metal-acid catalyst Pt–$Cs_{2.5}H_{0.5}PW_{12}O_{40}$, Chem. Commun. 57 (2021) 227–230.

[12] H. Althikrallah, E. F. Kozhevnikova, I. V. Kozhevnikov, Hydrodeoxygenation of 2,5-dimethyltetrahydrofuran over bifunctional metal-acid catalyst Pt $Cs_{2.5}H_{0.5}PW_{12}O_{40}$ in the gas phase: Kinetics and mechanism, Mol. Catal. 510 (2021) 111711.

[13] K. Alharbi, E.F. Kozhevnikova, I.V. Kozhevnikov, Hydrogenation of ketones over bifunctional Pt-heteropoly acid catalyst in the gas phase, Appl. Catal. A 504 (2015) 457–462.

[14] K. Alharbi, W. Alharbi, E.F. Kozhevnikova, I.V. Kozhevnikov, Deoxygenation of ethers and esters over bifunctional Pt–heteropoly acid catalyst in the gas phase, ACS Catal. 6 (2016) 2067–2075.

[15] D.M. Alonso, S.G. Wettstein, J.A. Dumesic, Bimetallic catalysts for upgrading of biomass to fuels and chemicals, Chem. Soc. Rev. 41(2012) 8075−8098.

[16] M. Sankar, Q. He, R.V. Engel, M.A. Sainna, A.J. Logsdail, A. Roldan, D.J. Willock, N. Agarwal, C.J. Kiely, G.J. Hutchings, Role of the support in gold-containing nanoparticles as heterogeneous catalysts, Chem. Rev. 120 (2020) 3890−3938.

[17] L. Guczi, Z. Schay, Role of bimetallic catalysts in catalytic hydrogenation and hydrogenolysis, Stud. Surf. Sci. Catal. 27 (1986) 313−335.

[18] A. Alazman, D. Belic, E.F. Kozhevnikova, I.V. Kozhevnikov, Isomerization of n-hexane over bifunctional Pt-heteropoly acid catalyst: Enhancing effect of gold. J. Catal. 357 (2018) 80–89.

[19] O. Poole, K. Alharbi, D. Belic, E.F. Kozhevnikova, I.V. Kozhevnikov, Hydrodeoxygenation of 3-pentanone over bifunctional Pt-heteropoly acid catalyst in the gas phase: Enhancing effect of gold, Appl. Catal. B 202 (2017) 446−453.

[20] L. Guczi, Z. Schay, Role of bimetallic catalysts in catalytic hydrogenation and hydrogenolysis, Stud. Surf. Sci. Catal. 27 (1986) 313−336.

[21] G.C. Bond, Metal-catalysed reactions of hydrocarbons, Springer, New York, 2005.

[22] G. Riahi, D. Guillemot, M. Polisset-Thfoin, A.A. Khodadadi, J. Fraissard, Preparation, characterization and catalytic activity of gold-based nanoparticles on HY zeolites, Catalysis Today 72 (2002) 115−121.

[23] G.J. Hutchings, Nanocrystalline gold and gold palladium alloy catalysts for chemical synthesis, Chem. Commun. (2008) 1148−1164.

[24] K. Sun, A.R. Wilson, S.T. Thompson, H.H. Lamb, Catalytic deoxygenation of octanoic acid over supported palladium: effects of particle size and alloying with gold, ACS Catal. 5 (2015) 1939−1948.

[25] Y.F. Han, J.H. Wang, D. Kumar, Z. Yan, D.W. Goodman, A kinetic study of vinyl acetate synthesis over Pd-based catalysts: kinetics of vinyl acetate synthesis over Pd–Au/SiO_2 and Pd/SiO_2 catalysts, J. Catal. 232 (2005) 467−475.

[26] E.K. Hanrieder, A. Jentys, J.A. Lercher, Impact of alkali acetate promoters on the dynamic ordering of PdAu catalysts during vinyl acetate synthesis, J. Catal. 333 (2016) 71−77.

[27] J. Xu, T. White, P. Li, C. He, J. Yu, W. Yuan, Y.F. Han, Biphasic Pd−Au alloy catalyst for low-temperature CO oxidation, J. Am. Chem. Soc. 132 (2010) 10398−10406

[28] A.M. Venezia, V. La Parola, V. Nicolı, G. Deganello, Effect of gold on the HDS activity of supported palladium catalysts, J. Catal. 212 (2002) 56−62.

[29] A.M. Venezia, V. La Parola, G. Deganello, B. Pawelec, J.L.G. Fierro, Synergetic effect of gold in Au/Pd catalysts during hydrodesulfurization reactions of model compounds, J. Catal. 215 (2003) 317−325.

[30] T.J. Schwartz, S.D. Lyman, A.H. Motagamwala, M.A. Mellmer, J.A. Dumesic, Selective hydrogenation of unsaturated carbon–carbon bonds in aromatic-containing platform molecules, ACS Catal. 6 (2016) 2047−2054.

[31] J. Fraissard, V. Gerda, K.I. Patrylak, Y.G. Voloshyna, Isomerization of hexane on PtAu nanoparticles supported on zeolites, Catalysis today. 122 (2007) 338-340.

[32] A. Alazman, D. Belic, A. Alotaibi, E.F. Kozhevnikova, I.V. Kozhevnikov, Isomerization of cyclohexane over bifunctional Pt-, Au- and PtAu-heteropoly acid Catalysts, ACS Catal. 9 (2019) 5063−5073.

[33] B. Coq, F. Figueras, Bimetallic palladium catalysts: influence of the co-metal on the catalyst performance, J. Mol. Catal. A 173 (2001) 117−134.

[34] F. Gao, D.W. Goodman, Pd–Au bimetallic catalysts: understanding alloy effects from planar models and (supported) nanoparticles, Chem. Soc. Rev. 41 (2012) 8009−8020

[35] A. Vazquez-Zavala, J. Garcıa-Gómez, A. Gomez-Cortes, Study of the structure and selectivity of Pt–Au catalysts supported on Al_2O_3, TiO_2 and SiO_2. Appl. Surf, Sci. 167 (2000) 177−183.

[36] K. Balakrishnan, A. Sachdev, J. Schwank, Chemisorption and FTIR study of bimetallic Pt-Au/SiO_2 catalysts, J. Catal. 121 (1990) 441−455.

[37] E. Bus, J.A. van Bokhoven, Electronic and geometric structures of supported platinum, gold and platinum−gold catalysts, J. Phys. Chem. C 111(2007) 9761−9768.

[38] H. Ren, M.P. Humbert, C.A. Menning, J.G. Chen, Y. Shu, U.G. Singh, W.C. Cheng, Inhibition of coking and CO poisoning of Pt catalysts by the formation of Au/Pt bimetallic surfaces, Appl. Catal. A 375 (2010) 303−309.

[39] T. Okuhara, N. Mizuno, M. Misono, Catalytic chemistry of heteropoly compounds, Adv. Catal. 41 (1996) 113–252.

[40] I.V. Kozhevnikov, Catalysis by heteropoly acids and multicomponent polyoxometalates in liquid-phase reactions, Chem. Rev. 98 (1998) 171–198.

[41] J.B. Moffat, Metal-oxygen clusters. The surface and catalytic properties of heteropoly oxometalates, Kluwer: New York, 2001.

Chapter 7. Conclusion and Future Perspectives

7

The changing global climate and depletion of fossil fuel reserves are pushing researchers to look for alternative ways to generate environmentally friendly sources of fuel and energy that are sustainable both to the economy and industry. Biomass-derived furanic compounds are an inexpensive abundant renewable feedstock, which can be converted to green fuels and a range of value-added chemicals by catalytic hydroconversion. However, these compounds accommodate a large number of oxygen-containing groups, hence cannot be directly applied in the existing industrial processes. Hydrodeoxygenation (HDO) is an effective strategy of oxygen removal from renewable feedstock to produce transportation fuels, lubricants and a wide range of chemicals. Much current research is focused on the HDO of furanic compounds using heterogeneous catalysis utilizing supported metal catalysts. Complete oxygen removal from furanic compounds over noble metals to produce hydrocarbons requires harsh conditions (200−400 °C, 7–20 MPa H_2 pressure). Bifunctional metal-acid catalysis has been found more efficient than monofunctional metal catalysis to eliminate oxygen from organic oxygenates such as ketones, alcohols, phenols, ethers and esters. Previously, highly efficient bifunctional catalysts comprising platinum on acidic supports such as zeolites and Keggin-type heteropoly acids have been reported for HDO of aliphatic and aromatic ketones in the gas phase. In our work, this approach was successfully applied to the HDO of furanic compounds.

The key objective in this thesis was to investigate the catalytic hydroconversion of 2,5-dimethylfuran (DMF) and 2,5-dimethyltetrahydrofuran (DMTHF) as the model furanic compounds. This included hydrogenation, hydrogenolysis and hydrodeoxygenation of DMF and DMTHF in the gas phase using bifunctional metal-acid catalysis. The main attention was focused on the Pt-CsPW catalyst due to Pt being the most active metal among the noble metals for furan ring hydrogenolysis. CsPW is well documented as a solid Brønsted acid catalyst. It has important advantages over the parent heteropoly acid $H_3PW_{12}O_{40}$ (HPW), having a much larger surface area, higher thermal stability (ca. 500 °C decomposition temperature) and higher tolerance to water than HPW. The proton sites in CsPW are almost as strong as those in HPW. All reactions were carried out in a fixed-bed continuous flow reactor using H_2 as a carrier gas at 60–100 °C and ambient pressure.

The hydrogenation and hydrogenolysis of DMF was investigated at a gas solid interface over carbon-supported Pt, Pd, Rh and Ru catalysts to determine the relative efficiency of noble metal catalysts and clarify the reaction network (Chapter 3). All noble metal catalysts were found to be very active for DMF hydroconversion which occurred with >99% conversion under very mild conditions at 90 °C and 1 bar H_2 pressure. The platinum catalyst was mainly active in the ring cleavage to produce 2-hexanone as the primary product, followed by its hydrogenation to 2-hexanol and hexane. The ring hydrogenation and ring cleavage of DMF on Pt/C were found to occur in parallel. In contrast, Pd/C, Rh/C and Ru/C catalysts were selective in DMF ring hydrogenation to form DMTHF under the same mild reaction conditions.

The total turnover frequency (TOF) of metal sites in the gas phase hydroconversion of DMF, including ring-opening and ring-saturation pathways, was determined from zero-order kinetics in the absence of diffusion limitations and catalyst deactivation. The TOF values were found to decrease in the sequence Pt > Rh > Pd >> Ru, similar to the liquid phase

reaction, albeit were one order of magnitude greater than those for the liquid phase reaction. This shows that the gas phase reaction is much more efficient than the corresponding liquid phase reaction. A possible explanation for these facts can be given considering the concentration of hydrogen, the effect of competitive adsorption of reaction products and the accessibility of metal sites in the two systems. The gas phase hydroconversion of ring-saturated furan derivatives such as THF and DMTHF occurred much slower in comparison to DMF on Pt/C catalyst, with the TOF values decreasing in the order: DMF >> DMTHF > THF. Much greater reactivity of DMF compared to DMTHF suggests the importance of π-bonding between DMF and Pt site and gives additional support to the formation of DMTHF and 2-hexanone directly from DMF via independent parallel pathways.

Next, in Chapter 4, the gas phase HDO of DMF was investigated to produce n-hexane at mild conditions over bifunctional catalysts comprising carbon-supported Pt together with the strongly acidic heteropoly salt $Cs_{2.5}H_{0.5}PW_{12}O_{40}$ (CsPW). The Pt/C–CsPW catalyst gave 100% yield of n-hexane at ≤ 90 °C and 1 bar H_2 pressure. Mild reaction conditions excluded n-hexane isomerisation allowing complete transformation of DMF to alkane without carbon backbone alteration. The gas phase HDO in the flow system over Pt-CsPW was found to be more efficient than the corresponding liquid phase batch reaction. On the other hand, Pd, Rh and Ru combined with CsPW were much less active in the HDO of DMF, giving DMTHF as the main product. The proposed reaction network for the HDO of DMF over Pt–CsPW includes two parallel pathways: ring hydrogenolysis to give 2-hexanone and ring hydrogenation to give DMTHF, both led to the formation of 2-hexanol which further dehydrated to hexene on proton sites. The latter is finally hydrogenated on Pt sites to form n-hexane.

In Chapter 5, the gas phase hydrodeoxygenation of DMTHF was studied in the presence of bifunctional metal-acid catalyst Pt-CsPW in order to gain a mechanistic insight into the HDO process. We demonstrated the high effectiveness of metal-acid bifunctional heterogeneous catalysis for the gas phase HDO of the saturated furan derivative DMTHF. The Pt-CsPW bifunctional catalyst comprising a mixture of Pt/C and CsPW deoxygenated DMTHF to n-hexane with >99% selectivity under mild conditions (90–100 °C, ambient pressure) and was much more efficient than monofunctional Pt/C. At such conditions, no n-hexane isomerisation took place allowing complete conversion of DMTHF to alkane without carbon chain alteration. The proposed reaction mechanism includes a sequence of hydrogenolysis, dehydration and hydrogenation steps catalysed by Pt and proton sites in the bifunctional catalyst. The results suggest that the HDO of furanic compounds on Pt-CsPW is a structure-sensitive reaction occurring on active sites that are complex ensembles of Pt atoms. Synergistic action of the metal and acid sites is essential for the effectiveness of the HDO process. The acid strength of the acid co-catalyst had a more significant impact on HDO efficiency than the acid site density. It was demonstrated that the easy dehydration of secondary alcohol intermediate, 2-hexanol, on strong proton sites of CsPW is an effective driving force of the HDO process by bifunctional metal-acid catalysis through kinetic coupling between DMTHF hydrogenolysis and 2-hexanol dehydration steps.

Finally, in Chapter 6, addition of gold to the Pt-CsPW catalyst was demonstrated to have an enhancing effect on the HDO of DMTHF, increasing the turnover rate at Pt sites more than twofold. The enhancing effect is attributed to PtAu alloying. The formation of bimetallic PtAu nanoparticles in the PtAu-CsPW catalyst was confirmed by STEM-EDX and XRD analysis.

Overall, our findings demonstrate that the gas phase hydrodeoxygenation of furan derivatives over bifunctional metal-acid catalysts can offer significant economic and environmental advantages in producing green fuel components and value-added chemicals under mild conditions.

In the future, it would be interesting to expand the range of furanic substrates to include other important platform chemicals such as furfural, 5-hydroxymethylfurfural, 2-methylfuran, etc. Further exploration of bimetallic catalysis including a wide range of co-metals, such as Re, base metals, etc., could result in new, more efficient catalysts for HDO reactions. This should be complemented by the investigation of the role of geometric (ensemble) and electronic (ligand) effects in the bimetallic HDO catalysis using in-situ spectroscopic techniques (e.g., in-situ DRIFT spectroscopy) and density functional theory (DFT) modelling. It would also be interesting to continue in-depth kinetic and mechanistic studies on model furanic molecules coupled with thorough characterisation of metal and acid active sites in the bifunctional catalysts in order to gain a better understanding of reaction mechanism.